Application of yeast surface display screening methods to antibody discovery and proteomics of the blood-brain barrier

by

Jason M. Lajoie

A dissertation submitted in partial fulfillment of the requirements for the degree of

Doctor of Philosophy

(Chemical and Biological Engineering)

at the

UNIVERSITY OF WISCONSIN-MADISON

2016

Date of final oral examination: June 29, 2016
The dissertation is approved by the following members of the Final Oral Committee:
Eric V. Shusta, Professor, Chemical and Biological Engineering
Sean P. Palecek, Professor, Chemical and Biological Engineering
Regina M. Murphy, Professor, Chemical and Biological Engineering
Jennifer L. Reed, Associate Professor, Chemical and Biological Engineering
Michael R. Taylor, Assistant Professor, School of Pharmacy

Application of yeast surface display screening methods to antibody discovery and proteomics of the blood-brain barrier

Jason M. Lajoie
Under the supervision of Professor Eric V. Shusta
at the University of Wisconsin-Madison

Abstract

The blood-brain barrier (BBB), comprised of tightly joined endothelial cells lining the brain vasculature, is substantially more impermeable to blood-borne constituents than peripheral vasculature. Continuous paracellular tight junctions between adjacent endothelial cells, expression of drug efflux transporters, and a low level of pinocytotic uptake combine to severely restrict the nonspecific uptake of blood-borne constituents into the brain. While these barrier functions are essential in health, they present a significant challenge when attempting to treat neurological disorders since the majority of small molecule therapeutics and essentially all gene and protein-based drugs do not appreciably cross the BBB. Therefore, effective non-invasive drug delivery strategies that can overcome this barrier are needed for the successful development of central nervous system therapeutics.

One such strategy is the coopting of endogenous receptor-mediated transport (RMT) which is employed by the brain endothelium to shuttle proteins such as transferrin and insulin into the brain through endocytosis and vesicular trafficking. Targeting RMT for brain drug delivery has proven successful in many animal disease models and there are currently a small handful of RMT-targeting molecules in the clinic

for delivery of anti-cancer and lysosomal storage disorder drugs. However, the current state-of-the-art RMT-targeting strategies suffer from inefficiencies that limit their efficacy motivating the search for novel antibody reagents that target alternative receptors or the host of accessory proteins that regulate the RMT process at the BBB. These types of reagents would be useful from both the brain drug delivery and basic research perspectives. Recently, screening of combinatorial antibody display libraries in various formats has been employed for the discovery of novel RMT-targeting antibodies. Within this field, our lab has recently developed novel platforms to screen yeast surface display (YSD) antibody libraries for the discovery of antibodies against BBB membrane proteins. To extend these basic approaches, the body of work laid out in this thesis was aimed at the development and application of innovative YSD screening methods for discovery of antibodies targeting the RMT machinery at the BBB.

First, we developed a yeast display immunoprecipitation (YDIP) platform capable of detection and enrichment of antibodies against BBB membrane protein complexes involved in RMT. YDIP is a modification on traditional YSD techniques whereby antibodies can be screened for binding to detergent-solubilized membrane proteins directly in cell and tissue lysates. An open question was whether membrane protein complexes of functional interest could be detected on the yeast surface. During development of the functional YDIP (fYDIP) method we chose to target BBB membrane protein complexes containing the endocytosis adaptor protein adaptin 2 (AP-2). After confirming that known membrane protein:AP-2 interactions could be captured and detected on the yeast surface, screening of a non-immune yeast display antibody library was carried out using detergent solubilized *ex vivo* brain capillary plasma membrane

fractions as the antigen. Characterization of isolated antibody clones confirmed that this fYDIP screen resulted in the enrichment of antibodies that bound BBB complexes containing membrane proteins and AP-2. Further characterization of two of the isolated antibodies confirmed targeting of proteins with known RMT function (Myh9 and AHNAK). The drawback of this screening campaign from a BBB-targeting perspective was that none of the isolated antibodies bound to cell surface epitopes and therefore could not be used for non-invasive delivery of drugs to the brain.

To circumvent this problem we next developed and implemented an innovative screening platform taking advantage of a novel class of antigen recognition molecules from lamprey, variable lymphocyte receptors. An immune variable lymphocyte receptor library was created by immunization of lamprey with brain capillary plasma membranes from mice and cloning of the resultant repertoire into the YSD format. The library was screened via a novel two-step workflow aimed at enriching clones that targeted extracellular epitopes of *in vivo*-relevant membrane proteins. First, the library was screened using the YDIP method for binders to detergent solubilized mouse brain capillary plasma membrane antigens. Then biopanning on a brain endothelial cell line was used to recover clones targeting extracellular epitopes. The lead candidates identified from this screening procedure, VLR-Fc-11, VLR-Fc-30, and VLR-Fc-46, were shown to target the brain vasculature after intravenous administration and were found to traffic within the brain capillary endothelial cells. Thus, these new brain targeting molecules are promising candidates for further optimization and characterization with potential applications in brain drug delivery.

Acknowledgements

No man is an island and that is especially true in my case. None of the work in this thesis would have been possible without the hard work and dedication of those who came before me as well as those who shared this graduate school journey with me. I would first like to thank my advisor Dr. Eric Shusta for his mentorship and guidance throughout my time here. Next, I would like to thank in no particular order all the members of the Shusta lab who I had the pelasure of working with over the past five years: Dr. Ben Tillotson, Dr. Carrie Mrashall, Dr. Chris Stuz, Dr. Thomas Malott, Dr. Hannah Wilson, Dr. Scott Cannfield, Matt Stebbins, Loukas Goulatis, Dr. Abraham Al-Ahmad, Dr. Xiaobin Zhang, Dr. Ben Umlauf, Dr. Brandon Kim, and Dr. Julia Georgieva. Your help in training me, troubleshooting, designing experiments, analyzing data, and discussing life in general has had an imeasurable impact on my work and life.

I would like to thank our collaborators in the UW School of Pharmacy, Dr. Dustin Frost and Dr. Lingjun Li, who provided expertise in mass spectormetry, ran samples, and analyzed data for the antigen identification work described in Chapter 3. In additon, Dr. Brantley Herrin from Emory University played and integral role in the variable lymphocyte receptor work described in Chapter 4. Thanks Brant for providing your expert insights into lamprey immunology and VLRs and for working with me to create the BBBVLR library.

Thanks are also in order for the staff at the various core facilities I've used at UW. Thanks to the entire staff at the UW Carbone Cancer Center Flow Lab for help with library sorting, Jackie Cooper of the Civil Engineering Department for maintaining the flow cytometer and microscope I used on a regular basis, Dr. Elle Grevestad at the

Biochemistry Optical Core for training and use of the confocal microscope, and Randy Massey at the UW Electron Microscopy lab for help with sample preparation and imaging.

I was fortunate enough to receive and take part in two training fellowships while at UW. Thanks to organizers, Professors, and fellow students who were part of the NIH funded Biotechnology Training Program and Geneomic Sciences Training Program during my time here.

Last and certainly not least I would like to thank my family and cloes friends who have provided love, support, and encouragement throughout my life. Thanks to my wife Anna Margolin for sharing life's journey with me, reminding me that the world exists outside the lab, and understanding when I've had to work long hours and weekends. I love you and can't wait to start our next adventure together! Thanks to my parent's John and Susan Lajoie for instilling in me a love of learning, teaching me the value of hard work and attention to detail, and always loving and supporting me no matter what. Thanks to my sisters Jessica and Jackie for your friendship, love, and support. Finally thanks to the many friends near and far who have been an important part of my life outside of the lab.

Table of Contents

List of Figures

List of Tables

Chapter 1 Recent advances in blood-brain barrier membrane proteomics and antibody discovery

1.1 Introduction

Treatment of central nervous system (CNS) disorders represents one of the major public health challenges of the 21st Century. According to the 2013 National Vital Statistics Report three out of the top 15 causes of death in America are stroke, Alzheimer's disease, and Parkinson's disease accounting for 9.3% of deaths [1]. Furthermore, a recent report from the World Health Organization concluded that CNS disorders are responsible for around 10% of deaths world-wide on an annual basis [2]. These percentages are expected to rise given the aging of the world population and the mid to late life onset of many neurological diseases [3, 4]. Therefore, development of effective treatments for disorders of the CNS is needed to address this significant global disease burden. While drug discovery and optimization are important in the development of new treatments, non-invasive delivery of therapeutics to the brain presents perhaps one of the biggest challenges facing researchers due to the presence of the blood-brain barrier (BBB).

The BBB, comprised of tightly joined endothelial cells (ECs) continuously lining the vasculature of the brain, severely limits transport of drugs from the blood to the brain as the majority of small molecule therapeutics and essentially all protein and gene therapies cannot penetrate the barrier [5]. The restrictive nature of the BBB is demonstrated in Figure 1-1 A which shows the inability of a small molecule dye (<500 Da) to access the brain parenchyma upon transcardial perfusion providing an example

of the challenge faced when attempting to deliver drugs to the brain [6]. Despite this challenge, efficient non-invasive drug delivery strategies that take advantage of endogenous transport mechanisms at the BBB have been long sought-after due to the high vascular density in the brain. There are approximately 100 billion capillaries in the human brain, with an inter-vessel distance of around 40 µm, and a total drug transport surface area of ~20 m^2 [7, 8]. Thus, if a drug can cross the BBB it gains access to essentially every neuron in the brain.

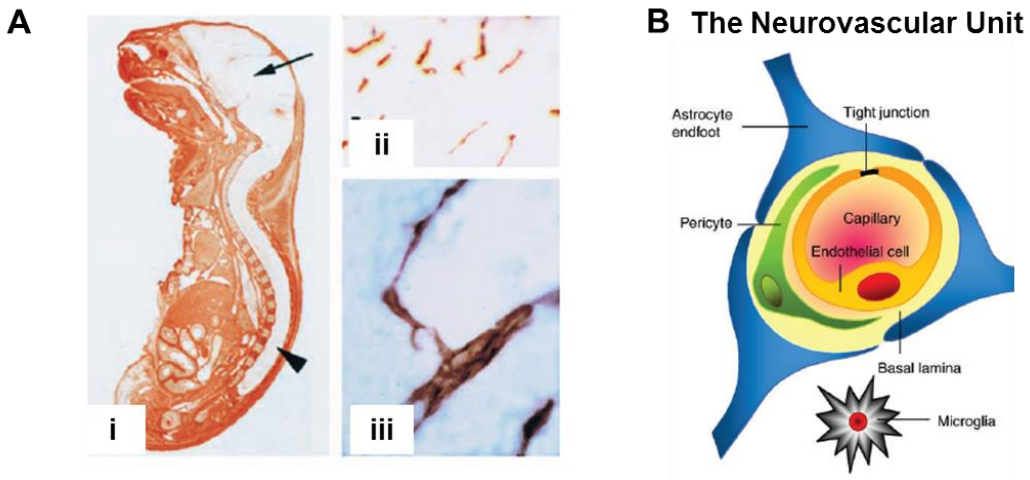

Figure 1-1. The blood-brain barrier. (A) The restrictive nature of the BBB is demonstrated when a small molecule dye (<500 Da) is perfused through the mouse vasculature. In the zoomed out image (i) the dye is seen to penetrate all the organs except the brain and spinal cord. Upon closer examination (ii-iii) the dye is found within the brain capillaries but is unable to extravasate into the parenchyma due to the presence of the BBB. Adapted from [6]. (B) A capillary cross section demonstrates the anatomy of the neurovascular unit. Endothelial cells form the wall of the brain vasculature and are welded together by continuous tight junctions. The endothelial cells and closely associated pericytes are encased by the basal lamina. Astrocyte endfeet surround the endothelial cells and pericytes. Adapted from [10].

The unique barrier established at the BBB arises due to continuous tight junctions between adjacent endothelial cells [9], limited non-specific pinocytotic uptake [10], and expression of drug efflux transporters [11]. These barrier properties as well as

the expression and regulation of endogenous transport systems needed to shuttle nutrients, proteins, metabolites, and cells between the blood and the brain are induced and maintained via close association and cross-talk between the BBB endothelial cells and other cell-types of the neurovascular unit [10, 12] (Figure 1-1 B). Figure 1-2 A depicts the various endogenous transport routes at the BBB. Active transport of molecules across the BBB can be divided into three categories: carrier-mediated, adsorptive-mediated, and receptor-mediated. The carrier-mediated route facilitates the transport of water soluble small molecules such as glucose, amino acids, and nucleotides across the BBB [13] (Figure 1-2 A ii). Transmembrane carrier proteins, such as the GLUT1 glucose transporter [14], which are located on both the apical (blood side) and basolateral (brain side) membranes of the endothelial cells are stereospecific and actively transport their cognate ligands into the brain. Another group of carrier proteins localized to the apical membrane are called efflux pumps. These proteins recognize a wide range of substrates and actively pump them out of the brain [15, 16]. Adsorptive-mediated transport (AMT) is a non-specific mechanism that mediates the endocytosis and vesicular trafficking of cationic serum proteins via interaction with negatively charged domains on the cell membrane [17] (Figure 1-2 A iv). Various strategies for non-invasive delivery of drugs to the brain that coopt the carrier-mediated and AMT routes have been pursued [18–20]. However, given the steric restrictions of carrier-mediated transport and the non-specific nature of AMT these strategies have met with limited success.

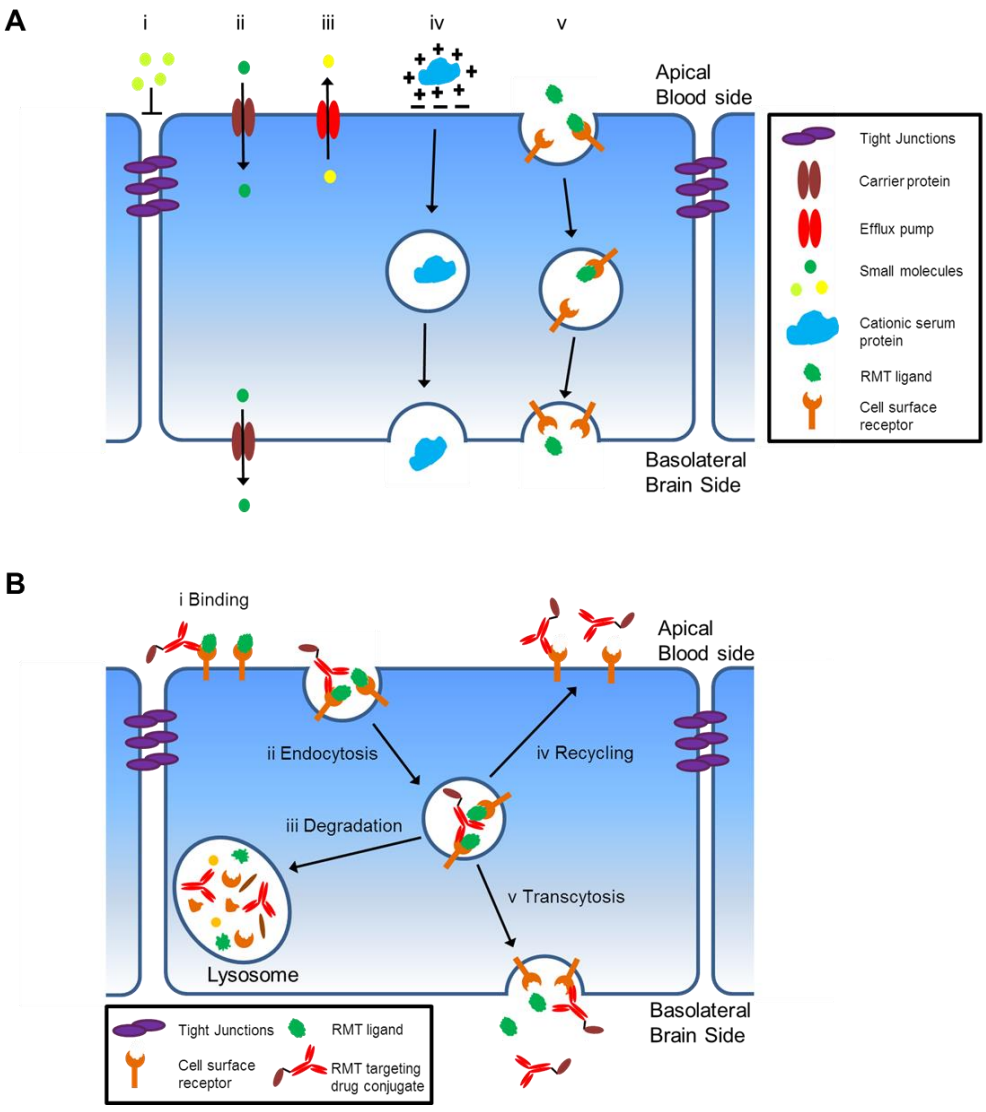

Figure 1-2. Nutrient and protein transport at the BBB. (A) Cartoon showing the various routes of endogenous transport at the BBB. (i) Paracellular diffusion of hydrophilic molecules is restricted by the tight junctions. (ii) Hydrophilic small molecules gain access to the brain via carrier-mediated transport (CMT). (iii) Drug efflux pumps contribute to the observed barrier properties of the BBB via recognition and removal of unwanted substances from the endothelial cells. (iv) Cationic serum proteins can gain access to the brain via adsorptive-mediated transport (AMT). (v) Several proteins gain access to the brain via receptor-mediated transport (RMT). (B) Schematic of the BBB RMT process. (i) Ligand binding to its receptor on the apical membrane is followed by (ii) endocytosis and (iii-v) vesicular trafficking within the cell which can lead to the (v) transcytosis and release of the ligand on the basolateral face of the endothelial cell. As a demonstration of the RMT-targeting strategy for brain drug delivery an RMT-targeting ADC is shown binding to and trafficking with the endogenous receptor. Adapted from [21].

The endogenous route which shows the most promise as a viable mechanism to non-invasively deliver a wide range of therapies to the brain is receptor-mediated transport (RMT) [21]. RMT facilitates the transport of proteins such as low-density lipoprotein [22], insulin [23], and transferrin [24] across the BBB as follows (Figure 1-2 B). Blood-borne ligands first bind to their cognate receptor at the apical cell membrane (Figure1-2 B i). Next, the complex is internalized into intracellular vesicles via one of several modes of endocytosis (Figure 1-2 B ii). Once internalized, the receptors and bound ligands are trafficked within the cell and can reach several destinations. Vesicle contents can be trafficked to the lysosome for degradation [25] (Figure 1-2 B iii). Alternatively, the receptors can be recycled back to the apical cell membrane [26] (Figure 1-2 B iv). Importantly for brain drug delivery, vesicles are also shuttled to the basolateral side of the cell where fusion with the cell membrane (termed exocytosis) leads to release of the vesicles contents into the brain parenchyma [27] (Figure 1-2 B v). The entire process of vesicular trafficking from the blood to the brain parenchyma is termed transcytosis. RMT is an attractive route for delivery of drugs to the brain since this vesicle-based mechanism allows for transport of a wide range of endogenous ligands; from uniform proteins like transferrin (~80 kDa) to large heterogeneous molecules such as lipoproteins (up to 80 nm in diameter) [28–31]. Theoretically, therapeutics that don't normally cross the BBB (e.g. antibodies, DNA, nanoparticles, etc) can gain improved access to the brain via tethering to appropriate RMT-targeting ligands (e.g. anti-receptor antibodies or peptides that mimic natural ligands) thereby piggybacking on the endogenous RMT process (Figure 1-2 B). In the case of anti-receptor antibodies, constructs comprised of a receptor-targeting antibody fused to a

therapeutic are called antibody-drug conjugates (ADC) and will be referred to as such throughout this chapter.

1.2 Targeting receptor-mediated transport for brain drug delivery

Demonstration of the feasibility to target RMT for the delivery of drug payloads to the brain was first achieved in the early 1990's using antibodies against the transferrin receptor (TfR) [32, 33]. Since that time, intensive work in the field has resulted in a host of viable brain drug delivery strategies. The most well studied and successful of these are antibodies and ligand mimics that coopt the TfR, insulin receptor (IR), and low density lipoprotein receptor family (LDLRf) endocytosis and vesicular trafficking pathways [34]. Chapter 2 provides significant detail on the multitude of studies that have demonstrated delivery of pharmacologic doses of therapeutics to the brain via targeting these pathways in various animal models so a detailed discussion will not be presented here. One point of significant note is that the promise of the RMT-targeting strategies demonstrated at the bench has recently been translated to the clinic. For example, AngioChem, Inc has developed an LDLRf-targeting peptide fused to the cancer drug paclitaxel (ANG1005) and this molecule has demonstrated the ability to significantly shrink brain tumors in Phase 1 clinical trials [35, 36]. In addition, ArmaGen, Inc has developed anti-IR ADCs for the treatment of rare lysosomal storage disorders which also show promise in the clinic [37].

Despite these exciting advances, the current state-of-the-art approaches targeting TfR, IR, and LDLRf face significant issues which limit their efficacy and motivate the search for novel RMT targets. Some of these issues stem from the ubiquitous

expression of these receptors throughout the body [38]. For example, safety liabilities resulting from off-target binding have been observed. In one study, dosing of mice with anti-TfR ADCs resulted in a decrease in circulating reticulocytes [39], immature red blood cells which express TfR at a high level. In another study, long-term dosing of parkinsonian monkeys with anti-IR ADCs resulted in the occurrence of pancreatic lesions and other adverse side effects [40]. The ubiquitous expression of these receptors throughout the body also leads to significant uptake and retention in peripheral organs limiting the dose reaching the brain. As a result, on average only between 0.5 and 1% of the injected dose of therapeutic reaches the brain parenchyma (see Chapter 2). Other factors limiting brain penetration include the trapping and degradation of RMT-targeting antibodies in the brain capillary endothelium which was highlighted by a series of recent studies with anti-TfR ADCs [41–43]. One theory is that high affinity anti-TfR binding antibodies, with characteristically slow dissociation rates, may simply not appreciably release from the receptor during the timeframe of typical TfR endocytosis, vesicle trafficking, and transcytosis (~15 minutes) [41, 44, 45]. Thus, the bulk of ADCs remain trapped in the endothelial cells and a negligible percentage escapes into the brain parenchyma. Second, it has been shown that high affinity and multivalent anti-TfR binding interactions promote trafficking of antibody:receptor complexes to the lysosome for degradation [42, 43]. To address these problems anti-TfR constructs with reduced affinity and avidity were engineered which enabled significant increases in brain penetration, target engagement, and therapeutic outcomes compared with their high affinity/multivalent parent molecules [41, 43]. Alternatively, engineering pH sensitivity into TfR-targeting constructs, enabling dissociation at

endosomal pH, has shown some success in altering intracellular trafficking and increasing brain penetration [46, 47]. Despite these optimization efforts the increases in brain penetration are marginal at best; e.g. in one study 0.22% injected dose/gram brain (ID/g) of anti-TfR antibodies having 1 nM affinity reached the mouse brain compared with 0.6% ID/g of antibodies with 100-fold weaker affinity [39, 41]. The limited brain access achieved after administration of anti-RMT ADCs resulting from the above detailed issues necessitates the administration of large doses (up to 50mg/kg) to achieve pharmacologically relevant concentrations in the brain parenchyma. For an average person of 75 kg, a 50 mg/kg dose corresponds to almost 4 grams of protein which raises concerns over the ultimate production feasibility and cost. Thus, researchers are continuously searching for new receptors and cognate targeting molecules which may provide alternative routes for RMT-based brain drug delivery with the potential to overcome the challenges discussed above.

1.3 Transcriptomics and proteomics of the BBB

Concerted efforts to profile the BBB transcriptome and proteome over the past 15 years have facilitated great insights into protein expression, regulation, and function at the BBB with common themes in the data serving to inform and motivate the search for novel RMT targets. One prominent theme is the fact that the uniquely restrictive nature of the BBB coupled with the necessity for transport of key nutrients, proteins, and metabolites between the blood and the brain endows the brain endothelium with a specialized profile of nutrient transporters and RMT proteins. Several studies used comparative transcriptomics techniques such as suppression subtractive hybridization

(SSH) [48–50], serial analysis of gene expression (SAGE) [51], transcriptome microarrays [52, 53], and RNAseq [54, 55] to elucidate mRNA expression upregulated at the BBB compared with both peripheral vasculature (e.g. lung, liver, and kidney) and other CNS cell types. Time and again these studies found expression of many solute carriers (SLC), ATP-binding cassette (ABC) transporters, and RMT proteins significantly upregulated in the BBB endothelium. For example, in a SAGE study of the rat BBB transcriptome Enerson and Drewes found that out of 864 genes upregulated in the endothelium versus the brain parenchyma 11% were SLC/ABC transporters, 5% were transmembrane receptors, and 4% were vesicular trafficking components [51]. It should be noted that increased mRNA transcript abundance does not necessarily correlate to increased protein expression given the existence of complex post-transcriptional regulatory networks [56, 57] and therefore direct proteomic profiling is needed to augment transcriptional studies. To this end data from proteomics studies has confirmed the protein-level expression of many of the transporters and receptors alluded to above [58–63]. For example, a shotgun proteomics analysis of the mouse BBB membrane proteome confirmed the expression of 62% of the SLC/ABC transporters identified in the SAGE work [61]. In a similar proteomics study it was found that 6.5% of identified proteins were SLC/ABC transporters, 4.8% were receptors, and 3.4% vesicular trafficking machinery which also matched well with the SAGE results [60]. Another common theme throughout the transcriptome and proteome profiling studies is the discovery of previously unknown or understudied transcripts and proteins. For example, in three transcriptome studies up to 30% of the identified upregulated genes were of unknown function [48, 50, 51] and in one proteome study approximately

22% of the identified proteins were also functionally unannotated [60]. Taken together with the proven high abundance expression of numerous transport-related proteins, the fact that a significant portion of the BBB proteome remains under-characterized suggests that several novel RMT systems with the ability to mediate brain drug delivery are yet to be discovered.

In a recent groundbreaking study, this hypothesis was confirmed through the identification of new RMT targets and subsequent development of antibodies with increased brain penetration compared with traditional anti-TfR antibodies. Zuchero and colleagues performed a quantitative proteomics analysis of primary brain endothelial cells isolated from mice and identified Basigin (Bsg) and CD98 heavy chain (CD98hc) as two novel targets with high protein expression [64]. While anti-Bsg antibodies performed similar to anti-TfR antibodies in brain uptake studies, anti-CD98hc antibodies had a 5-fold increase in the %ID/g compared with anti-TfR controls. One potential cause of this increased brain penetration is that, unlike the anti-TfR antibodies, high affinity binding to CD98hc did not trigger lysosomal degradation of the antibody:receptor pair. This finding is quite significant since it suggests that Zuchero's group discovered a novel RMT pathway at the BBB which overcomes one of the key challenges faced with anti-TfR targeting. With CD98hc-mediated BBB transport capacity confirmed, bispecific antibodies were produced for dual targeting of CD98hc and BACE (a popular target for Alzheimer's disease treatment). Administration of Anti-CD98hc/BACE bispecifics to a mouse model of Alzheimer's disease resulted in a reduction in brain amyloid β demonstrating the therapeutic applicability of CD98hc targeting. This work highlights the significant potential of rationally mining –omics datasets to discover novel BBB RMT

targets. However, while transcriptomics, proteomics, and related database searching can result in novel target identification, sequence and annotation data alone do not always properly predict protein function. Thus, some promising RMT targets may be overlooked. In addition, this approach is inherently low throughput as antibodies or other targeting molecules must be generated for each specific target after its identification. Furthermore, the possibility that not all identified targets have the desired functionality increases the inefficiency of this approach (e.g. in this study anti-Bsg showed no advantage over anti-TfR [64]). Therefore, phenotypic screening of displayed antibody and peptide libraries has been pursued as an alternative method to identify new brain drug delivery reagents.

1.4 High throughput screening of ligand display libraries

In recent years, high throughput screening of large antibody and peptide libraries has been pursued for the identification of novel RMT-targeting reagents capable of traversing the BBB. This section presents an overview of this body of work by first summarizing the general approaches taken and then discussing several illustrative examples.

1.4.1 General approaches for screening combinatorial ligand libraries

The typical screening campaign combines a handful of key parameters (Figure1-3 A) which can be tuned as necessary to achieve the desired outcomes. In most cases, a large (e.g. 10^7-10^{10} variants) ligand library (e.g. antibodies, or peptides) is constructed and expressed in a host capable of displaying the ligand (e.g. phage, or yeast). The key

principal underlying all combinatorial library screens is that each host within the library harbors the genetic material (typically in plasmid form) that directs the biosynthesis and display of a monoclonal antibody or peptide creating the all-important genotype to phenotype linkage needed for efficient enrichment and recovery of clones with desired properties. Antibody libraries are usually constructed via cloning of the variable heavy (VH) and variable light (VL) domains of immunoglobulin G (IgG) repertoires from animal or human donors and formatting them as single-chain variable fragments (scFv) by fusing VH to VL using a flexible linker [65, 66]. Single domain antibodies (sdAb) comprising the VH domains of camelid or shark immunoglobulins have also been used [67]. The small size and single-chain format of scFv and sdAbs enables display on the phage surface and also simplifies library construction and cloning. Recent advances in yeast display and molecular cloning technology have enabled the construction and screening of full-length IgG libraries [68, 69] and synthetic diversity repertoires [70, 71] but these platforms have not yet been employed for BBB-targeting antibody discovery. Antibody libraries can be derived from hosts not exposed to the target antigens (non-immune) or hosts that have been specifically immunized (immune). The advantage of immune libraries is that immunization drives clonal expansion of antigen-specific lymphocytes [72] and promotes *in vivo* affinity maturation via somatic hypermutation [73, 74] which pre-biases the library towards high-affinity antigen-specific antibodies. Peptide libraries have also been used to identify BBB-targeting ligands. Typically these consist of randomized or rationally designed 10-20mer repertoires [75].

Once a suitable ligand library is constructed, the next key parameter is the choice of display platform. Phage display is the most widely used platform with the filamentous

bacteriophages such as M13, f1, and fd being the hosts of choice given their simple propagation in *E. coli* hosts [76, 77]. To achieve ligand display, antibodies or peptides are fused to endogenous viral coat proteins resulting in the display of 1-5 copies of the ligand on the phage surface depending on the particular format used [78]. One critical property enabling screening for RMT phenotype is that phages, given their small size, are amenable to packaging in vesicles [66, 79] and therefore phage displayed libraries can be directly screened on model BBB cell lines or *in vivo* for endocytosing or transcytosing clones.

Another virus-based platform applied in BBB-targeting work takes advantage of the established selective homing and gene-transfer properties of adeno-associated viruses (AAV) [80]. Various AAV serotypes have been used for gene therapy applications as they are known to selectively transduce certain cell-types; this property is termed tropism. For example, AAV9 known, for CNS tropism, has been shown to cross the BBB and deliver gene-replacement therapies to neuronal cells after intravenous (IV) injection with promising therapeutic results achieved in models of pediatric disease [81, 82]. Peptide libraries can be displayed on the virus surface via fusion to viral coat proteins [83], but unlike phage and yeast AAV is not amenable to antibody display and therefore has been used less frequently in BBB-targeting screens.

Yeast surface display (YSD) is a eukaryotic platform that was originally developed in the late 1990's for quantitative measurement and engineering of antibody properties such as affinity and stability [84–87]. Peptides, antibodies, and a host of other proteins have been displayed on the yeast *Saccharomyces cerevisiae* surface via fusion to the Aga2p yeast mating protein [88, 89].

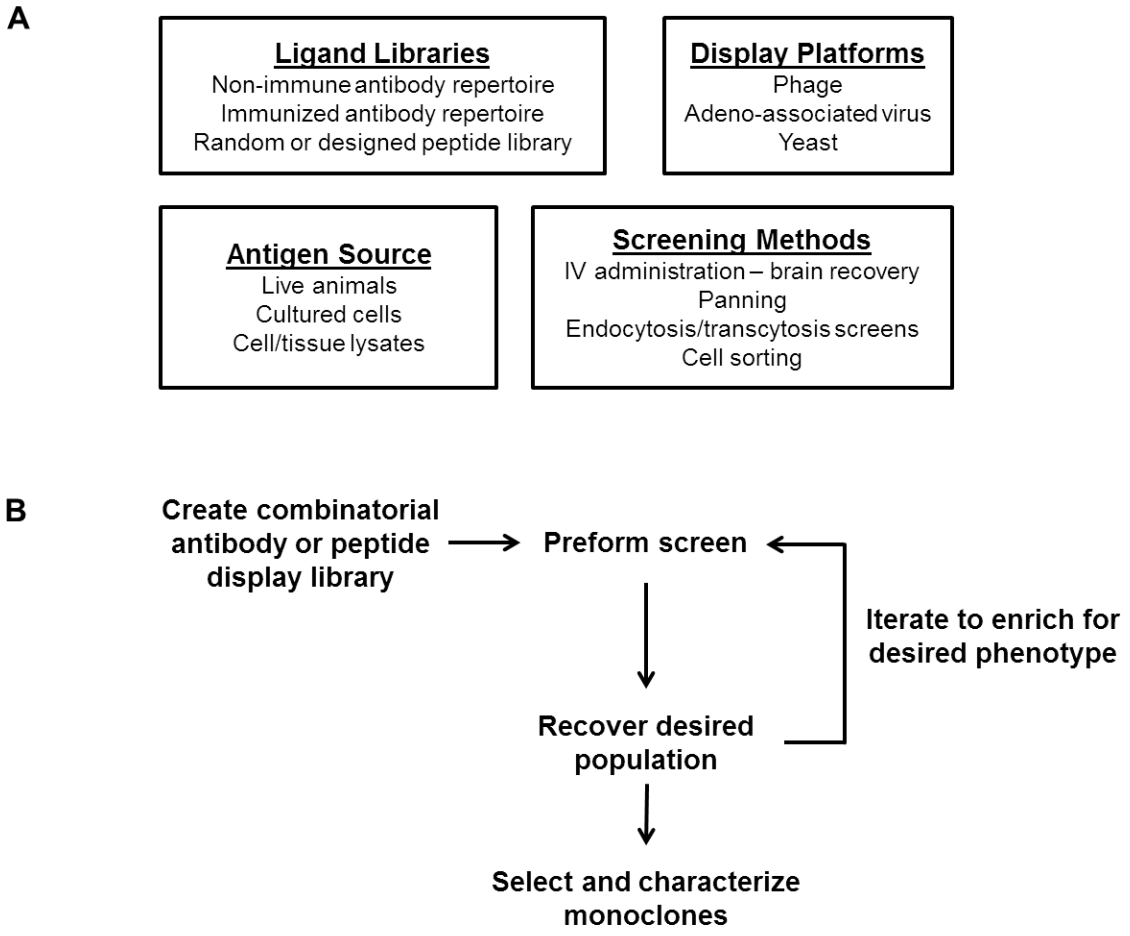

Figure 1-3. Overview of combinatorial library screening approaches. (A) The important design parameters for a BBB screening campaign are summarized. Ligand libraries can be comprised of antibodies or peptides and can be displayed in the phage, AAV, or yeast platforms. These libraries are screened against various *in vivo* or *in vitro* antigen sources using a screening method chosen to meet the goals of the campaign. (B) Flowchart demonstrating the generall workflow in the typical screening campaign

The ligand of choice is fused to Aga2p at the N- or C-terminus and expressed in a flocculin-deficient yeast strain in which the cell-wall anchored Aga1p protein is overexpressed, EBY100 [84]. During translation and folding in the endoplasmic reticulum Aga2p and Aga1p are covalently linked via disulfide bonds, are subsequently shuttled to the yeast surface, and anchored to the cell wall thereby displaying between

30,000 and 100,000 copies of the ligand on the cell surface [90]. Other yeast strains and display anchors have been described [91] but have not been employed in BBB-targeting screens. As discussed in section 1.4.2, our lab has recently pioneered two novel YSD screening platforms for discovery and engineering of antibodies targeting BBB membrane proteins [92–94].

Figure 1-3 B shows the generic workflow that is followed in most combinatorial library screening campaigns. Once the library is created and expressed in the desired display platform the screening campaign is carried out. Iterative rounds of screening are employed to enrich the library for clones with the desired binding/trafficking phenotype in the context of a chosen antigen source. After sufficient rounds of screening have been performed individual clones are selected and characterized. The antigen presentation and screening methods used in the screening rounds can be broken down into *in vivo* and *in vitro* categories. *In vivo* methods employ live animals or *ex vivo* tissue fractions as the source of antigens. A common *in vivo* screening approach is to inject phage or AAV libraries intravenously in rats or mice and recover clones that target the brain by simply collecting the brain after sufficient time for the particles to circulate, bind, and traffic. Brain-resident clones can then be recovered from brain homogenates and propagated for additional rounds of screening. Isolation of different brain fractions (e.g. parenchyma versus capillaries) enables separation and recovery of clones that preferentially cross the BBB versus those that remain trapped in the vasculature [95, 96]. Alternatively, antigen mixtures can be prepared from *ex vivo* brain capillaries and used as substrates for screening providing an *in vivo*-relevant source of antigens. *In vitro* methods utilize cultured cells or lysates thereof as the source of antigens.

Traditional *in vitro* models of the BBB include immortalized brain endothelial lines from rat (RBE4 [97]), mouse (bEnd.3 [98]), and human (hCMEC/D3 [99]), or primary cultured endothelial cells from freshly isolated brain capillaries. Recently, our lab has developed a fully human stem cell-derived model of the BBB [100, 101] and begun using it for combinatorial library screens [95]. A common *in vitro* setup to screen for BBB-targeting and RMT phenotype is to culture BBB cells in the top chamber of a two chamber Transwell system. Phage libraries are initially applied to the upper chamber which contains a tight monolayer of BBB cells grown on a filter between the two chambers. The premise of this setup is that the barrier established by the cultured cells is sufficiently tight to restrict non-specific paracellular diffusion of phages and that any phage reaching the bottom chamber would need to transcytose the cells to get there. After allowing sufficient time for binding, endocytosis, and trafficking the culture medium from the bottom chamber is collected and phages propagated. Alternatively, the cells in the upper chamber can be acid washed to remove surface-bound particles and lysed to isolate internalized phages.

Both *in vivo* and *in vitro* approaches come with pros and cons, and these must be understood and balanced when designing screening campaigns. The major advantage of using *in vivo* antigen sources over *in vitro* sources is that libraries are screened against the endogenous protein expression landscape. It is well established that BBB cells cultured in the petri dish tend to have altered protein expression profiles [102, 103] and therefore screening on *in vitro* lines alone can result in enrichment of culture artifacts [93]. This problem is avoided by performing screens *in vivo* or using antigens derived from *ex vivo* brain capillaries. On the other hand, *in vivo* screening setups are

inherently more expensive, time consuming, and complex. Additionally, with *in vivo* virus-based screens uptake in peripheral tissues and high non-specific background binding are significant concerns that in some cases limit recovery of specific clones [104]. Ultimately, each screening campaign is unique and it is up to the researcher to decide which approaches best meet the goals of the screen.

The key advantage of using the phenotypic combinatorial library screening approaches discussed above is that no *a priori* knowledge about the target antigens is required. In a nutshell, the ligand library is presented with a library of antigens with which to interact under various screening constraints and, assuming a highly diverse library, the opportunity exists to sample the entire antigen landscape. This is especially important in the context of the under-characterized nature of the BBB membrane proteome discussed above as the discovery of new BBB targeting reagents that bind and traffic with as yet unknown or under-characterized RMT proteins is possible and has been reported [67]. One caveat that must be considered with this approach is that once targeting ligands are selected their cognate antigens must be determined through downstream work such as immunoprecipitation coupled with mass spectrometry [105] or expression cloning [106].

1.4.2 BBB-targeting screens in AAV, phage, and yeast display platforms

This section will discuss several relevant examples of combinatorial library screens aimed at discovery of BBB-targeting ligands in the context of the three different display platforms discussed above to highlight recent advances in the field and motivate the need for innovative screening approaches. As mentioned above the AAV platform is

amenable to display of combinatorial peptide libraries on the virus surface, albeit in a limited capacity compared with phage and yeast. As such, it has been used only sparingly in BBB-targeting screens. One example was a screening campaign designed to isolate AAV with chimeric coat proteins having the ability to cross the seizure compromised BBB [96]. The coat proteins of several AAV serotypes (1-6, 8, and 9) were shuffled to create a chimeric AAV coat protein library and this library was administered to rats 1 day after induction of limbic seizures. Brains were subsequently harvested, neurons from seizure-sensitive brain regions isolated, and viral DNA extracted. This screening procedure was iterated for 3 rounds and two chimeric AAV were isolated which showed the ability to cross the seizure-compromised BBB and deliver genes to affected neurons [96]. Interestingly, these clones were highly-specific for seizure compromised brain regions and did not cross the healthy BBB. This study highlights the fact that the protein expression profile of the BBB can be altered in disease and screens can be designed to specifically target the diseased regions. This general approach has met with success in similar screens carried out using phage display for targeting stroke [107], glioma [108], and lysosomal storage disorders [109].

Unlike AAV, phages can be engineered to display both peptides and antibody fragments on their surface and are easily recovered and propagated in bacterial hosts. These two properties along with the ability to perform RMT-based screens have made phage the display platform of choice for BBB ligand discovery. Additionally, phage screening workflows are highly amenable to campaigns where subtractive steps aimed at removing undesirable clones from the library are incorporated into the screen design. This approach has been taken in recent attempts to isolate BBB-targeting ligands with

little or no corssreactivity in peripheral vasculature [67, 110]. Discovery of ligands which recognize a BBB-specific protein are highly desirable as this targeting strategy would potential limit uptake in peripheral organs, mitigate off-target effects, and result in a larger percentage of the administered does reaching the brain. In a landmark screening campaign carried out by Muruganandam and colleagues, subtractive panning of a phage display library of non-immune llama sdAbs was coupled with endocytosis screening to isolate internalizing sdAbs with BBB-selective binding and trafficking. Briefly, the phage displayed sdAb library was first incubated with cultured human lung microvasculature endothelial cells (HLMEC) and non-binding phages recovered from this subtractive step were subsequently incubated with primary human cerebromicrovascular endothelial cells (HCEC) at 37ºC to promote internalization. Phages capable of internalization into HCEC were recovered from cell lysates after surface bound phages were removed by acid washing. This procedure was iterated for four rounds and resulted in the isolation of two sdAbs, FC5 and FC44, which bound selectively to HCEC and were capable of transcytosis across an *in vitro* BBB model. Importantly, when injected IV in rats FC5 and FC44 were capable of homing to the brain with negligible uptake in the lungs; this validated the success of the subtractive panning approach. In follow-up work, FC5 was shown to bind to a cell surface glycoprotein and internalize into endothelial cells via clathrin-mediated endocytosis [111]. Given its *in vivo* brain selectivity, proven endocytosis mechanism, and ability to transcytose across an *in vitro* BBB model FC5 has been further studied as a ligand for brain drug delivery. When constructed as an sdAb-Fc fusion and tethered to the analgesic peptide dalargin or produced in an FC5-Fc/anti-mGluR1 bispecific format, FC5 mediated BBB crossing,

target engagement with neurons, and analgesia in both cases [112, 113]. In comparison, none of these properties were observed in animals administered dalargin or anti-mGluR1 alone or when using the same fusion protein formats with a non-specific sdAb in place of FC5. Given its success in pre-clinical models FC5 is a shining example of the power of the combinatorial screening approach especially when one considers its putative antigen. Although its discoverers remain tight-lipped about this, it has been suggested in a patent application that FC5 binds TMEM30a [114] a member of a membrane flippase complex known to be involved in phospholipid translocation at the plasma membrane [115] but not annotated to be involved in RMT at the time of FC5's discovery. TMEM30a is a double-pass transmembrane protein with two short N- and C-terminal cytoplasmic regions and a long interceding extracellular domain [116]. This membrane topology is at odds with typical RMT proteins which are often single-pass transmembrane proteins. Thus, it is unlikely that TMEM30a would have been rationally chosen for RMT target development. This observation provides strong support for the merit of the combinatorial screening approach and motivates continued efforts to isolate additional novel BBB-targeting ligands. To this end, subtractive panning of a non-immune human scFv phage display library on cultured rat heart and lung endothelial cells was coupled with a positive panning step on primary rat brain endothelial cells and two clones displaying selective binding to both *in vitro* and *in vivo* brain endothelial cells were isolated [110]. Currently, experiments are underway to characterize the ability of these scFv to target the *in vivo* BBB. Alternative approaches to target the *in vivo* BBB via IV administration of phage libraries to rodents have also been carried out and a handful of brain targeting ligands identified [117, 118]. However, investigation of their

biodistribution and trafficking across the BBB has not been attempted and thus their potential as brain drug delivery reagents remains unclear.

A common issue faced in phage screens is that expression and amplification biases limit the diversity of the enriched pools, especially in campaigns requiring many rounds of screening to attain measurable enrichment. This bias arises from the inefficiency of the bacterial protein processing machinery in properly expressing and folding eukaryotic proteins and imposes limits on the antibody repertoires that can be sampled during screening [119]. Therefore, yeast display has arisen as an attractive alternative to phage display. With its eukaryotic protein expression and processing machinery, yeast should be able to sample a greater repertoire of antibodies that cannot be properly expressed in phage. This was directly examined in recent work by Bowley and colleagues [119]. An scFv library derived from an HIV-1 positive human donor was constructed and cloned into the phage and yeast display formats. Due to differences in transformation efficiency, the resultant phage library contained ~10^9 members while the yeast display library harbored only ~10^7 transformants. Despite this two orders of magnitude difference in library size, when the two libraries were screened in parallel against the same HIV antigen, gp120, the yeast library identified all 6 scFv discovered through phage screening in addition to 12 unique scFv not identified in the phage screen. Therefore, YSD is an attractive platform for BBB-targeting screening with the potential to discover novel antibodies not accessible with phage.

Traditionally, YSD screening is carried out by incubating yeast libraries with soluble antigens (e.g. purified recombinant proteins), applying appropriate labeling reagents, and using fluorescence activated cell sorting (FACS) for quantitative

detection and enrichment of antibodies with desired binding characteristics [84]. Our lab has recently developed two novel YSD screening methods that buck tradition and enable screening against the BBB membrane proteome without the need for recombinant protein production and purification. The first example of this was performed by Dr. Xin Xiang Wang in which a method for biopanning of yeast libraries on cultured cells was developed [92]. YSD biopanning as pioneered by Dr. Wang is conceptually analogous to other biopanning methods in that yeast displayed libraries are incubated on monolayers of cultured cells in order to recover clones that specifically interact with cell surface epitopes. One advantage of YSD biopanning is that the high avidity of ligands displayed on the yeast surface enables the recovery of low affinity lead molecules that might be missed with other platforms [120, 121]. In addition, yeast are large enough to be visualized by simple light microscopy and as a result the progress of binding and washing steps can be directly observed. Therefore, unlike in phage screens, the effectiveness of a washing step can be monitored during the screen and stringency adjustments made as necessary. The promise of this approach for BBB-targeting screening was demonstrated via panning of a non-immune human scFv library [65] on an immortalized rat brain endothelial cell line, RBE4. After 4 rounds of biopanning 34 unique RBE4-binding clones were identified [93]. One drawback of the YSD platform is that given their large size, ~5 μm, yeast cannot be used to directly screen for RMT phenotype. Rather, downstream characterization experiments, such as internalization assays with soluble scFv, are carried out to identify the subset of clones capable of internalization and trafficking. In the case of the RBE4 biopanning study several of the lead scFv identified were capable of internalization into RBE4 cells (4 out

of 16 tested). One clone, scFvA has been subsequently shown to target the BBB after IV administration [122]. These studies demonstrate the ability of the yeast display platform to deliver a novel targeting reagent capable of homing to the BBB *in vivo*. While trafficking of scFvA has been proven *in vitro*, studies are ongoing to assess this capability *in vivo* and further characterize scFvA for BBB drug delivery.

As an alternative approach, screening of yeast display libraries for binding to detergent solubilized membrane proteins directly in cell lysates was pioneered by Dr. Yong Ku Cho. The so-called yeast display immunoprecipitation (YDIP) method is diagrammed in Figure 1-4. Membrane protein antigens from cell lines (e.g. RBE4) or *ex vivo* tissue fractions (e.g. brain capillaries) are selectively tagged via the use of a membrane impermeable biotinylation reagent that appends biotin to primary amines. Subsequently, membrane proteins are liberated from the plasma membrane and solubilized via addition of non-ionic detergents such as TritonX-100. These membrane protein lysates are incubated with the YSD library of choice and can subsequently be enriched for desired binding phenotype via labeling and FACS as with traditional YSD screens. Dr. Cho showed that this approach could be used to enrich a non-immune scFv library for clones binding RBE4 membrane proteins over three rounds of YDIP screening resulting in 11 unique scFv [94]. These scFv differed from those found in the biopanning screen discussed above yet used the same starting library and cell line. This result suggests that YDIP, by virtue of eliminating steric hindrance constraints inherent in YSD biopanning, can likely access a complimentary and potentially larger membrane protein antigen repertoire. Another advantage of the YDIP method is the ability to capture, elute, and interrogate target antigens using traditional proteomics approaches

such as SDS-PAGE, western blotting, and mass spectrometry. This was demonstrated via immunoprecipitation and mass spectrometry identification of neural cell adhesion molecule as the antigen for one of the scFvs discovered in the biopanning screen [105].

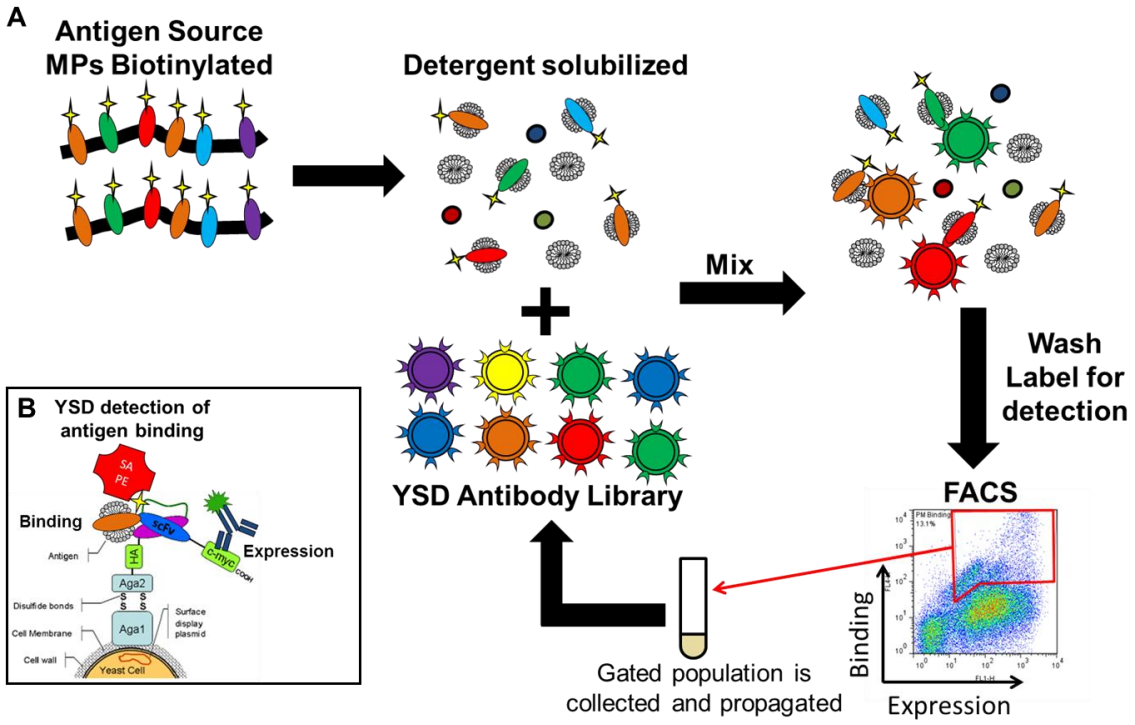

Figure 1-4. Yeast display immunoprecipitation. (A) Schematic of the YDIP method. Membrane proteins (MPs) specifically tagged with biotin (yellow star) are solubilized with detergents and incubated with the YSD library of choice. After washing to remove non-specifically captured proteins, yeast are labeled to detect the desired phenotypes (see inset B), then analyzed and sorted via FACS. The population recovered from the sort is then propagated and the entire process iterated as needed. (B) Example of the labeling schemes used in YDIP. Here, full length expression of scFv on the yeast surface is measured with fluorescently labeled antibodies directed against the cmyc epitope tag and scFv binding to a biotinylated MP is measured with fluorescently labeled streptavidin.

While the YDIP screening campaign described above was successful at identifying novel antibodies against BBB membrane proteins, the 11 lead hits were not further characterized for their applicability as BBB-targeting reagents. Results from *in*

vitro-in vivo crossreactivity experiments carried out with the lead scFvs identified in the YSD biopanning study suggest a low correlation between binding the RBE4 cell line and recognizing antigens in rat brain capillaries (only 1 out of 34 clones bound to *in vivo* antigens) demonstrating the high likelihood of enriching scFv against culture artifacts when cell lines alone are used as the screening substrate [93]. Despite this drawback, the initial demonstrated by the founding YSD biopanning and YDIP studies motivates further development, modification, and optimization of these approaches. Therefore, the overarching goal of the body of work presented in this dissertation was to develop and apply innovative screening strategies, building on YDIP and YSD biopanning, to identify novel antibodies targeting the RMT machinery at the BBB. In Chapter 3 we extend the YDIP method to the use of antigen preparations from *ex vivo* sources and to specifically target membrane protein complexes involved in RMT via detection of endocytosis marker proteins. The work described in Chapter 4 leverages the unique antigen recognition molecules from lamprey, variable lymphocyte receptors, and couples the YDIP and YSD biopanning methods to efficiently enrich an immunized library for VLR that target cell-surface epitopes of BBB membrane proteins expressed *in vivo*. The following section introduces variable lymphocyte receptors and their recent applications to provide additional context for the work in Chapter 4.

1.5 Variable lymphocyte receptors

To date, most of the antibody libraries used in screens for BBB-targeting have been constructed from non-immune mammalian repertoires. Compared to immune libraries of comparable size, non-immune libraries tend to yield lower affinity lead

molecules [70, 123]. This arises from the fact that immunization and cloning of the immune antibody repertoire results in a library biased towards high affinity antigen-specific clones. Traditionally, mammalian antigens are used to immunize mammalian hosts. However, screening of immunized mammalian antibody libraries against mammalian antigens is inherently problematic given that self-tolerance to highly conserved protein and carbohydrate epitopes limits the diversity of accessible targets [124]. Thus, employing alternative antibody platforms with the ability to access a greater diversity of the mammalian antigen landscape would represent a significant advancement over previous BBB-targeting screens and provide the potential to identify novel BBB membrane protein antigens. Lamprey variable lymphocyte receptors are a class of recently discovered antigen recognition molecules that fit this bill.

The presence of an adaptive immune system in jawless vertebrates (lamprey and hagfish) was suggested by experiments carried out in the 1960's and 70's demonstrating the production of specific agglutinins after challenge with particulate antigens [125, 126]. Despite their best efforts, for decades immunologist could not find immunoglobulin-like genes in lamprey or hagfish. Finally in 2004 Zeev Pancer and colleagues identified the elusive antigen receptors of lamprey via suppression subtractive hybridization transcriptome profiling. Transcripts from immunostimulated lymphocytes were subtracted against transcripts from myeloid cells and erythrocytes and the lymphocyte-specific transcripts were interrogated [127]. This analysis resulted in the discovery of highly diverse antigen recognition molecules that were termed variable lymphocyte receptors (VLR).

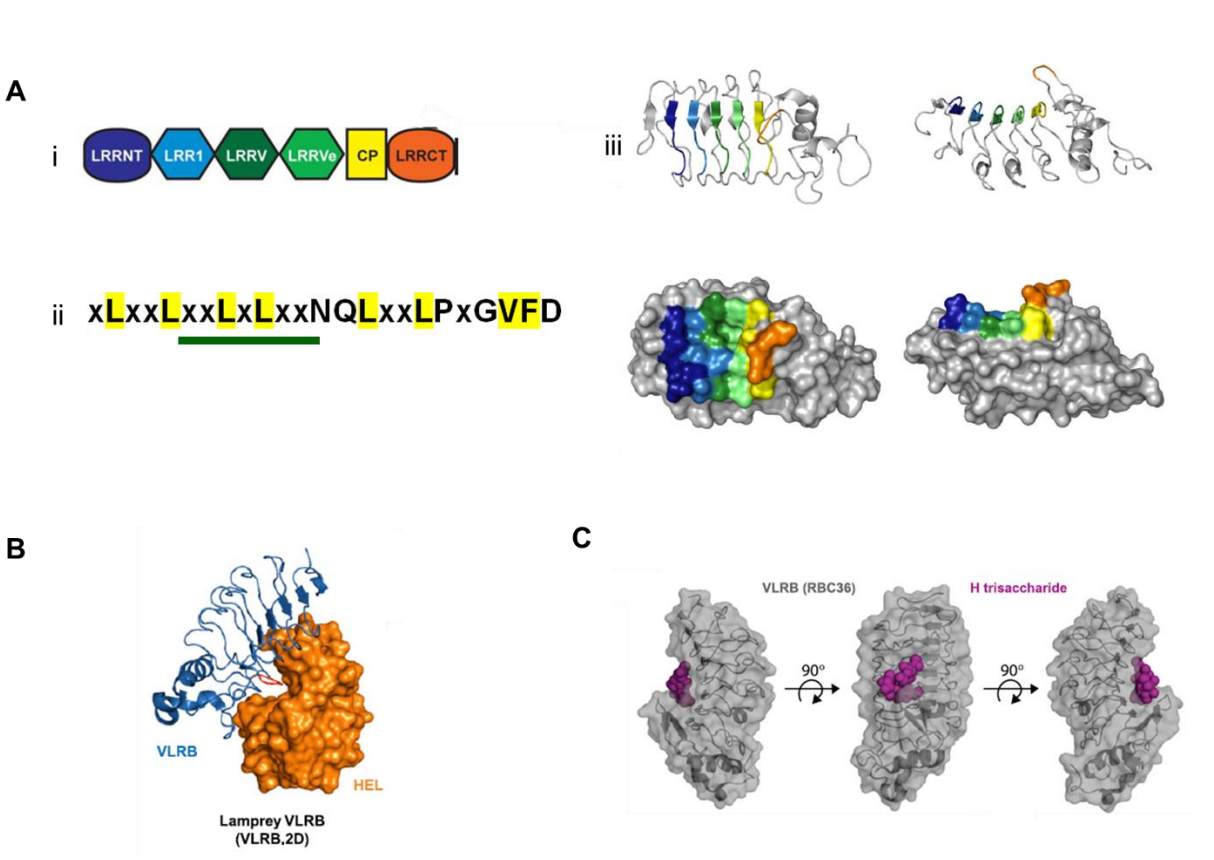

Figure 1-5. Variable lymphocyte receptor structure and antigen recognition. (A) VLRs are comprised of a single chain of (i) leucine rich repeat modules. (ii) The consensus sequence of a typical LRR is shown with conserved hydrophobic residues forming the hydrophobic core of the protein highlighted in yellow. Residues contributing to the parallel beta sheets that comprise the concave surface of the VLR are underlined in green. (iii) The crystal structure of a typical VLR is shown in ribbon and space-filling representations demonstrating the crescent-shaped solenoid fold characteristic of VLRs. Adapted from [127]. (B) Shows the crystal structure of a VLR bound to hen egg lysozyme, and (C) shows the crystal structure of a VLR bound to a carbohydrate antigen. Both (B) and (C) adapted from [128].

An overview of VLR structure and antigen recognition is presented in Figure 1-5. VLRs are single-chain proteins composed of a variable number of leucine-rich repeat (LRR) modules that assemble into a horseshoe-shaped solenoid fold (Figure1-5 A; [128]). Each VLR is comprised of an N-terminal LRR (LRRNT), followed by LRR1, a variable number of LRRV modules (typically 1-9) the last of which is termed LRRVe, a connecting peptide (CP), and the C-terminal LRR (LRRCT). Highly variable residues

(indicated with an x in the consensus LRR sequence) residing in the parallel beta sheets which make up the concave surface of the VLR (denoted by a green underline in the consensus LRR sequence) as well as a variable loop in the LRRCT make up the antigen binding surface [129, 130]. Examination of crystal structures solved with VLR-antigen complexes has revealed some unique features of VLR binding. The crystal structure in Figure 1-5 B shows a VLR binding to hen egg lysozyme (HEL). Residues on the concave surface beta sheets interact with a ridge just above the HEL active site and the LRRCT loop extends inward to interact with active site residues [131]. Thus, the more C-terminal LRRs and the LRRCT loop form a binding pocket that interacts with HEL. This binding pocket-type paratope is also apparent in crystal structures of VLRs binding to carbohydrates (e.g. Figure 1-5 C) and may be one of the reasons that VLRs have been found to bind various mammalian carbohydrate epitopes with high affinity and specificity [132–134].

Lampreys last shared a common ancestor with mammals >500 million years ago; this tremendous phylogenetic distance combined with the unique crescent-shaped geometry of the antigen-binding site described above may enable VLRs to recognize novel antigenic targets, including highly conserved proteins and carbohydrates that are not recognized by mammalian antibodies. Therefore, over the past decade VLRs have been explored as alternatives to immunoglobulins in various applications. The major focus of this work has been on identifying VLR that can be used in cancer biomarker detection. In one study, a VLR that recognized the CDRH3 of a chronic lymphocytic leukemia (CLL) B-cell receptor was isolated after immunization of lamprey with B-cells from a CLL patient and could be used to monitor the reoccurrence of cancer after

immunotherapy-induced remission [135]. In another study, a VLR that recognized the Thomsen-Friedenreich pancarcinoma carbohydrate antigen, TFα, was isolated [134]. This VLR was used to detect the presence of TFα in non-small cell lung cancer and positive binding of the VLR was correlated with poor prognosis. In yet another study, a VLR that recognized a novel plasma cell-restricted epitope on human CD38 that had not been previously found using Ig-based antibodies was isolated [136]. Taken together these studies demonstrate that VLR can be used to detect both protein and glycan cancer biomarkers and have the potential to recognize novel mammalian epitopes that cannot be accessed by immunoglobulins. This motivates the continued exploration of VLRs in the cancer biomarker field and beyond.

To this end, VLR have recently been shown amenable to YSD library screening for discovery and engineering of VLR against protein and glycan antigens [134, 137]. Tasumi and colleagues screened both non-immune and immunized libraries of VLR displayed on the yeast surface for binders to β-galactosidase (β-gal), HEL, and human blood-group trisaccharides. Using soluble purified antigens during binding screens VLR with equilibrium binding affinities ranging from the low nanomolar to the low micromolar range were isolated against all antigens tested [137]. One of the anti-HEL VLR, VLRB.HEL.1, had an affinity of ~155 nM. To demonstrate the ability to engineer VLR with improved affinity Tasumi created a library of VLRB.HEL.1 variants by swapping of the LRRCT loop with LRRCT amplicons from a large pool of lamprey cDNA. After several rounds of YSD screening of this mutant library a clone with an affinity of 119 pM was isolated [137]. This astounding 1,300-fold improvement in affinity from one round of mutagenesis is all the more impressive when one considers that 4 rounds of

mutagenesis and screening were required to achieve an 1,800-fold improvement in affinity for the strongest reported fluorescein binding scFv [87]. This study demonstrates the ability to rapidly screen through large combinatorial libraries using YSD methods to discover and engineer VLR with desired binding characteristics.

In summary, VLRs are a recently discovered class of antigen recognition molecules possessing a unique structure and mode of antigen recognition compared with immunoglobulins. VLR have been employed for cancer biomarker applications, have proven ability to bind to new mammalian epitopes, are amenable to traditional YSD screening methods, and through the above detailed work have been shown to possess comparable affinity and stability to traditional immunoglobulins. The field of VLRs is still in its early days and it is likely that as more work is done the utility of these novel, antigen-binding molecules will continue to grow.

Chapter 2 Targeting receptor-mediated transport for the delivery of biologics across the blood-brain barrier

This chapter was adapted from: Lajoie, J.M., Shusta, E.V., “Targeting receptor-mediated transport for the delivery of biologics across the blood-brain barrier”, Annual Reviews in Pharmacology and Toxicology, 2015. 55:613-31. Here we review the current state-of-the-art targeting ligands for RMT-based brain drug delivery.

2.1 Introduction

Biologics including monoclonal antibodies (mAbs), recombinant enzymes, and gene therapies have been developed to treat disorders of the central nervous system (CNS). However, the full promise of these therapies has yet to be realized due to the inability of biologics to cross the blood-brain barrier (BBB) and enter brain to a substantial extent after intravenous (IV) administration [5]. The BBB comprises specialized endothelial cells (ECs) possessing properties such as continuous tight junctions (TJs), lack of fenestrae, low levels of pinocytotic uptake, and efflux transporter expression [9–11, 138]. The combination of these distinctive barrier properties renders the BBB impenetrable to the majority of both small and large molecule drugs. As a result, identifying routes for non-invasive brain drug delivery and developing targeting strategies to ferry biologics into the brain has been a research arena of growing importance. There are approximately 100 billion capillaries in the human brain, with an inter-vessel distance of around 40 μm, and a total drug transport surface area of ~20m^2 [7, 8]. Because of the high vascular density, brain cells are readily accessible to

circulating drugs provided that they can cross the BBB. Below, we describe the general non-invasive transendothelial routes available for crossing the BBB and motivate the potential delivery utility of RMT systems.

2.2 Receptor-mediated transport at the BBB

The development of effective strategies to transport biologics to the brain can be informed by an understanding of the endogenous transport systems employed at the BBB to shuttle nutrients, metabolites, and proteins between the blood and the brain. The major molecular transport routes at the BBB are illustrated in Figure 1-2. Paracellular diffusion is effectively eliminated by TJs and therefore is not an appropriate target for biologic delivery in the absence of TJ disruption (Figure 1-2 A i). Carrier-mediated transport (CMT) is used to shuttle hydrophilic small molecule nutrients such as glucose and amino acids [139] (Figure 1-2 A ii). CMT tends to be size and stereo-selective and has been used to shuttle small molecule drugs to the brain via linkage of the drug to the natural CMT ligand [20], but has not been successfully used for transport of large molecule biologics. Lipophilic small molecules less than 600 kDa can readily diffuse across the endothelial plasma membrane (PM). However, efflux pumps such as p-glycoprotein (P-gp), breast cancer resistance protein (BCRP), and multidrug resistance protein-1 (MRP-1) located at the apical (blood-facing) PM of ECs recognize many lipophilic compounds and efflux them back into the blood [140] (Figure 1-2 A iii). While efflux pumps such as P-gp are implicated in the transport of small peptide fragments like amyloid-β (Aβ) [141], the polarization in the brain-to-blood direction is not helpful for biologic delivery. Adsorptive-mediated transport (AMT) occurs when cationic

serum proteins interact with negatively charged domains on the apical PM triggering endocytosis into the EC, subsequent vesicular transport within the cell, and eventual release into the brain [142] (Figure 1-2 A iv). While this method has been used to ferry a range of cationized proteins into the brain [143–145], it is inherently non-specific and therefore may not be an ideal drug delivery target. Finally, receptor-mediated transport (RMT) uses the vesicular trafficking machinery of brain ECs to deliver a range of proteins including transferrin, insulin, leptin, and lipoproteins to the brain [28, 31, 146, 147] (Figure 1-2 A v). The RMT process involves four key steps (Figure 1-2 B). First, a circulating ligand binds to a cognate transmembrane receptor expressed on the apical plasma membrane (e.g. transferrin binds the transferrin receptor) (Figure 1-2 B i). Next, endocytosis takes place via membrane invagination and eventual formation of an intracellular vesicle containing receptor-ligand complexes [148] (Figure 1-2 B ii). Once inside the cell vesicular trafficking occurs whereby the vesicle can be routed to various final destinations [149, 150] (Figure 1-2 B iii-v). In the case of transcytosis, the vesicle is shuttled to the basolateral (brain side) PM and exocytosis occurs releasing the vesicle's contents into the brain parenchyma [151] (Figure 1-2 B v). RMT is an attractive route for delivery of biologics to the brain since this vesicle-based mechanism allows for transport of a wide range of endogenous proteins; from uniform proteins like transferrin (~80 kDa) to large heterogeneous molecules such as lipoproteins (up to 80 nm in diameter) [28–31].

2.3 Targeting biologics to the brain via RMT

The general strategy employed to deliver biologics into the brain via RMT was developed in the early 1990's and involves the conjugation of a receptor targeting moiety with the therapeutic of interest [33, 152, 153]. The targeting moiety could be the endogenous RMT ligand, a peptide ligand mimic, or an anti-receptor antibody. Upon iv administration, at least a portion of the RMT-targeted therapeutic enters the brain by RMT (Figure 1-2 B). The RMT approach has been adapted to the delivery of many different biologics including monoclonal antibodies, recombinant proteins, RNA, DNA, and nanomedicines. The method of coupling the biologic to the RMT targeting moiety is a key aspect of this strategy (reviewed extensively in ref. [34]) and merits brief mention here. Broadly, there are two options for the formulation of RMT-targeting biologics. In the first approach, the RMT targeting moiety and biologic can be directly tethered together by chemical linkage, e.g. streptavidin/biotin linkage, or construction of a fusion protein [34, 154]. The second approach involves the formulation of liposomes or polymeric nanoparticles decorated with RMT targeting ligands, and loaded with the biologic of interest [34].

While first introduced over 20 years ago, RMT-based drug delivery has recently gained increased visibility in academic and pharmaceutical company settings as a viable method to treat CNS disorders. This review will first discuss the most well-studied BBB RMT targets with a focus on the latest studies as earlier work with these systems has been reviewed elsewhere [7, 34, 155]. Next, novel alternative RMT targeting vectors will be introduced. Finally, significant attention will be paid to recent studies

demonstrating the ability to engineer binding properties of RMT targeting vectors in order to attain improved intracellular trafficking and transcytosis across the BBB.

2.4 Targets for RMT-based brain drug delivery

2.4.1 Transferrin receptor

Transferrin receptor (TfR) was one of the first RMT systems studied for BBB drug delivery applications [33]. TfR is expressed at a high level at the BBB [59, 156] and mediates iron delivery to the brain via binding and intracellular trafficking of the iron binding protein transferrin (Tf) [157]. Numerous studies have shown that using TfR targeting to deliver drug payloads to the brain can achieve therapeutic outcomes in animal models.

Several recent studies have explored brain delivery through Tf linkage. For example, PEGylated liposomes decorated with Tf and a cell penetrating poly-L-arginine peptide were constructed for the brain delivery of imaging agents and DNA [158]. Upon iv administration in rat, 4% injected dose (ID) reached the brain after 24 hours. When nanoparticles were loaded with an expression plasmid for β-galactosidase (β-gal), β-gal activity in brain lysates was 2-fold higher in rats treated with liposomes compared with those treated with naked DNA. Another recent approach employed a cyclic iron mimicking peptide, CRTIGPSVC, as the RMT targeting ligand [159]. CRTIGPSVC binds to apo-Tf causing it to adopt its iron-bound holo-Tf conformation, and can thereby gain access to the brain through Tf-TfR interaction. This peptide exhibited promise for use in treatment of brain tumors through delivery of the herpes simplex virus thymidine kinase gene to a mouse model of human glioma. The delivery was accomplished via iv

administration of a CRTIGPSVC-targeted adeno-associated virus and phage (AAVP) hybrid vector [160, 161] resulting in significant tumor shrinkage [159].

Despite its use as a TfR targeting vector, Tf is not an ideal RMT targeting ligand as endogenous Tf is present at high concentrations in the bloodstream requiring the injected RMT vector to compete with enodgenous Tf for TfR binding [162]. As an alternative, antibodies targeting the TfR have been developed for RMT-based delivery [33, 152, 153]. These mAbs bind to epitopes on the extracellular domain of TfR distal to the Tf binding site, and thus do not compete with Tf for TfR binding. There is a significant body of literature demonstrating the efficacy of anti-TfR antibodies for brain delivery of a broad range of biologics with resultant therapeutic effects [34]. A few of the most recent highlights are discussed below.

A fusion of the cTfRMAb, a chimeric mAb that binds to the mouse TfR [163], and tumor necrosis factor α decoy receptor (cTfRMAb-TNFR) was created for treatment of a Parkinson's Disease (PD) model in mice [164]. One hour after iv injection, cTfRMAb-TNFR uptake into mouse brain was 1.4%ID [165]. Subsequently, mice having the 6-hydroxydopamine-induced model of PD were treated every other day for 3 weeks with 1 mg/kg cTfRMAb-TNFR fusion protein, TNFR alone, or saline [166]. In cTfRMAb-TNFR treated mice, there was a 130% increase in striatal tyrosine hydroxylase (TH) enzyme activity, and behavioral testing indicated significant neuroprotection in mice treated with fusion protein compared with controls. This approach was also used to deliver erythropoietin and glial derived neurotrophic factor (GDNF) to the PD model mouse brain with 306% [167] and 272% [168] increases in TH activity, respectively. In another recent example, a GDNF expression plasmid was encapsulated in anti-TfR (OX26 mAb;

[33]) decorated, PEGylated liposomes and administered to a rat model of PD. In order to diminish off-target effects, the GDNF gene was placed under the control of the tyrosine hydroxylase promoter to drive gene expression in target cells (dopaminergic striatal cells) [169]. After 3 weeks of once weekly liposome injection, behavioral testing indicated significant neuroprotection compared with controls and a corresponding 77% increase in striatal tyrosine hydroxylase activity [169].

In addition to PD, treatment of a wide array of neurological disorders has been demonstrated using anti-TfR antibodies. For example, the cTfRMab was fused with a single chain fragment variable (scFv) antibody against amyloid-β (Aβ) (cTfRMAb-scFv) [170] yielding 40-60% reductions in brain Aβ fibrils when administered iv to a mouse model of Alzheimer's Disease (AD) [171, 172]. As will be discussed in detail later in this review, researchers at Genentech and Roche have also shown reduction in brain amyloid levels via anti-TfR-mediated delivery of anti-Aβ [43] and anti-BACE [39, 41, 42] antibodies to mouse models of AD. Also, anti-TfR targeted systems have been employed for treatment of lysosomal storage disorders such as those represented by the mouse model of mucopolysaccharidosis type VII (MPS-VII). Anti-TfR mAb (8D3; [173]) decorated, PEGylated liposomes loaded with plasmid encoding β-glucuronidase (GUSB) were administered iv in a single dose, and at 48 hours post-injection GUSB activity in the brain was 10-fold higher in treated MPS-VII mice compared with saline controls [174]. Finally, treatment of a murine stroke model was achieved by delivery of a caspase-3 inhibitor peptide loaded into anti-TfR mAb (R17-217; [173]) decorated, PEGylated chitosan nanoparticles. When nanoparticles were administered iv after middle cerebral artery occlusion and reperfusion, a significant reduction of infarct

volume and neurological deficit was observed in mice treated with targeted nanoparticles compared with non-targeted controls [175].

While use of anti-TfR mAbs for brain drug delivery is expanding, delivery efficiency using TfR as an RMT target may be limited. First, although TfR is enriched at the BBB, it is also expressed in vascular beds and parenchyma of other organs leading to undesirable, widespread distribution of TfR-targeted therapeutics. Second, full transcytosis of TfR to the brain side may actually be limited. For instance, iron uptake in the rat brain exceeds that of Tf [176] while horseradish peroxidase (HRP) labeled Tf accumulates in brain capillaries without appreciable penetration into the brain parenchyma, suggesting limited TfR transcytosis [177]. To address these issues, engineering of TfR targeting antibodies has recently been used to modulate intracellular trafficking of TfR and its conjugated drug payloads, and these approaches will be discussed in the Improved Brain Penetration section below. Despite these putative limitations, the growing body of literature indicates that anti-TfR antibodies tethered to biologics can reach the brain and mediate pharmacologic effects.

2.4.2 Insulin Receptor

The insulin receptor (IR) is expressed at the BBB [59] and is responsible for the import of blood-borne insulin into the brain via RMT [146, 178]. Use of insulin as an RMT targeting vector has not been pursued, given both a short serum half-life of around 10 minutes and the potential for exogenously administered insulin to cause hypoglycemia [179]. Thus, much as the case was for the TfR, mAbs against the IR have been employed for brain delivery of biologics. Initially, a mouse mAb against the human

IR (83-14) was used [180]; but more recently, a fully humanized version of 83-14 was created by grafting the complimentary determining regions (CDRs) from 83-14 onto human antibody framework regions [181]. This so-called HIRMAb antibody and HIRMAb fusion proteins are currently under development by ArmaGen Technologies, and have been widely tested in monkeys, with some forms slated for human clinical evaluation as described below.

Of particular translational interest, the HIRMab has been studied for the brain delivery of enzyme replacement therapies for treatment of genetic lysosomal storage disorders [154, 182–184]. For example, the HIRMAb was fused to α-L-iduronidase (IDUA), the enzyme missing in mucopolysaccharidosis Type I (MPS-I, Hurler's Syndrome) [182]. When administered to cultured MPS-I human fibroblasts, the HIRMAb-IDUA fusion mediated a 70% reduction in glycosaminoglycans (GAGs) [182], compounds which accumulate with deleterious effects in tissues of MPS-I patients [185]. Furthermore, approximately 2%ID reached the rhesus monkey brain 2 hours after iv injection. Given its in vitro potency and in vivo pharmacokinetic profile, this fusion protein is under development by ArmaGen Technologies for treatment of Hurler's Syndrome in humans and has been designated AGT-181 [186]. The long term safety of AGT-181 treatment was assessed in a pair of studies in rhesus monkeys. In the first study, monkeys were dosed twice weekly with between 0 and 20 mg/kg AGT-181 for four weeks [186]. Over the study period no changes in glycemic control, cerebrospinal fluid (CSF) glucose levels, or CSF/plasma glucose ratio were observed. The production of anti-drug antibodies (ADA) was also measured to gauge the immune response to the chronic dosing regimen and only one out of eight monkeys demonstrated a low level of

ADA reactivity in serum with all others under the limit of detection [186]. In the second study, dosing was increased to between 0 and 30 mg/kg and twice weekly injections were performed for 6 months [187]. The results of this study were similar to the first with no significant changes in plasma glucose levels, or CSF/plasma glucose ratios over the 6 month dosing regimen. Hypoglycemia was observed peaking at 180 minutes after each injection in the 30mg/kg group. However, this effect was mitigated by adding glucose to the injection medium. Glucose tolerance at the end of the study was identical for all treated groups. With the exception of the hypoglycemia observed for the 30 mg/kg group, the results of these studies indicated that dosing with the HIRMab-IDUA does not negatively affect glucose homeostasis. In addition, limited ADA is observed indicating little or no immunogenic effect of long term administration of the fusion protein. Taken as a whole, AGT-181 may ultimately be a safe and efficacious treatment for Hurler's syndrome and is slated to enter the clinic in 2014 [37]. As such, AGT-181 represents the first effort to bring RMT-targeted antibodies to the clinic for treatment of brain disease. Therefore, the clinical trial could also serve as an important enabling study for other antibody targeting systems currently under investigation and optimization.

In addition to AGT-181, the HIRMAb has been fused to numerous other therapeutic proteins. For example, an anti-Aβ scFv HIRMAb fusion was created for treatment of AD [188]. The HIRMAb-scFv was shown to cross the intact BBB as approximately 1%ID reached the rhesus monkey brain 2 hours after iv injection [189]. Other HIRMAb-protein fusions include GDNF [190, 191], TNFR [192, 193],

erythropoietin [194], and paraoxonase-1 [195, 196] all having similar pharmacokinetic parameters as the AGT-181 and HIRMab-scFv when administered to rhesus monkeys.

2.4.3 Low density lipoprotein receptors

The low density lipoprotein receptor (LDLR) and low density lipoprotein receptor-related proteins 1 (LRP1) and 2 (LRP2) are expressed in brain capillary endothelial cells [55, 59, 156]. The LDLR family (LDLRf) receptors mediate the transport of lipoproteins and a diverse array of other ligands across the BBB via RMT [29, 197, 198]. Brain entry via an LDLRf-mediated route has been posited to have significant potential since the rate of brain uptake of iv administered melanotransferrin (P97) and receptor associated protein (RAP), two ligands for LRP1, greatly exceed that of transferrin indicating a potentially higher capacity RMT system [197, 199]. While anti-receptor antibodies have not been reported for biologics delivery via the LDLRf, numerous studies have explored the use of LDLR and LRP ligands and peptide ligand mimics as vectors for brain delivery.

ApoB, and ApoE are major protein constituents of lipoprotein particles, mediate particle interactions with lipoprotein receptors including LDLR, LRP1, and LRP2 [200–202], and nanoparticles decorated with ApoE have been shown to cross the BBB in vivo [203, 204]. As one particularly interesting application employing LDLRf for biologic delivery, enzyme replacement therapies have been delivered to brain [185, 205]. These studies built on previous work in which a lentiviral vector driving the expression of a fusion protein of the ApoB receptor binding domain and an Aβ degrading enzyme, neprilysin, was used to transduce liver. Transduction of liver cells with this construct led

to in vivo production of the fusion protein, subsequent delivery to the brain, and reduction of brain amyloid levels in mice [206]. Analogously, Wang and colleagues created an expression plasmid for a fusion of IDUA with a peptide derived from amino acids 148-173 of ApoE for the treatment of MPS-I mice [185]. Hydrodynamically-driven tail vein injection of naked plasmid DNA [207] was used to transduce liver cells in MPS-I mice. Two days after injection of DNA, elevated IDUA levels were detected in brain parenchyma and immunofluorescence microscopy showed localization of protein in perivascular cells, neurons, and astrocytes. Therapeutic relevance was shown when 5 months of prolonged gene expression by maturing red blood cells in MPS-I mice resulted in normalization of brain levels of glycosaminoglycans and β-hexosaminidase, compounds which are elevated in tissues of MPS-I patients [185]. In parallel, Sorrentino and colleagues created an expression plasmid for a fusion of sulphamidase with the receptor binding domain of ApoB for treatment of MPS-IIIA mice [205]. An AAV2/8 vector was used to deliver plasmid DNA via iv injection resulting in sustained production of the fusion protein by the liver. At 3, 5, and 7 months after administration of the viral vector, sulphamidase activity in the brains of MPS-IIIA mice reached 10-15% of enzyme activity seen in healthy controls, while changes in brain enzyme activity in mice treated with a non-targeted sulphamidase were not significant [205]. Immunofluorescence microscopy revealed sulphamidase protein co-localized with neurons and astrocytes. In addition, improved behavioral phenotypes were observed in mice treated with the ApoB-targeted construct, whereas similar improvements were not observed in mice treated with non-targeted control [205]. These studies provide strong

evidence that the LDLRf mediated delivery of fusion proteins results in entry of protein to the brain with resultant therapeutic effects.

Angiopep-2, a peptide discovered through screening of a rationally designed peptide library based on the Kunitz protease inhibitor (KPI) domain [208, 209], has shown promise as a delivery vector in the treatment of glioma [35, 210, 211]. The KPI is a conserved LDLRf binding domain shared by a number of LDLRf ligands. Angiopep-2 was selected as an RMT vector because it displayed an elevated rate of transcytosis on an in vitro BBB model, and a larger uptake in the mouse brain after in situ perfusion compared with similar peptides [208], and was subsequently shown to enter the brain via LRP1 [212]. An Angiopep-2-paclitaxel conjugate called ANG1005 was developed to treat glioma as paclitaxel is a P-gp substrate and has restricted brain penetration as an unfused compound [211]. ANG1005 is being developed by Angiochem for treatment of glioma with a number of Phase1 clinical trials completed [35, 36] and Phase 2 trials underway [213]. Angiopep-2 has also been investigated for its ability to deliver genes [214] and peptides [215] to the brain.

2.5 New RMT targets

TfR, IR, and LDLRf mediated brain biologic delivery is becoming increasingly well-established with a substantial literature indicating the capability to deliver therapeutics that elicit beneficial effects. One significant drawback of the aforementioned RMT systems is their fairly ubiquitous expression leading to peripheral organ uptake. When combined with the fairly modest trans-BBB RMT transport capacity, relatively low levels of brain uptake result (around 1%ID in the examples

discussed above). Thus, there has been substantial effort focused on identifying new BBB RMT targets that may have better BBB specificity. Many of these targets were identified through screening of combinatorial peptide and protein libraries. The strategies used in their identification and discussion of their trans-BBB delivery properties has been reviewed elsewhere [216]. Below we discuss two particularly interesting targets, the FC5 antibody and the viral coat peptide RVG29, that have demonstrated the ability to cross the BBB in vivo.

2.5.1 FC5

FC5 is a single domain llama antibody (sdAb) consisting of a single variable heavy domain that was isolated in a phage display screen for antibodies that bind and endocytose into human cerebrovascular endothelial cells [67]. When injected iv, FC5 accumulated in mouse brain [67]. A follow-up study sought to determine the mechanism of FC5 internalization into endothelial cells. The authors showed that FC5 internalization was likely a receptor-mediated process and that FC5 interacted with a cell surface α(2,3)-sialoglycoprotein, later identified as TMEM-30A [111, 114]. Recently, Haqqani and colleagues employed a novel mass spectrometry based quantification method to measure the serum and CSF pharmacokinetics of FC5 in the rat [217]. Rats were dosed with 7 mg/kg FC5 or control sdAbs in 3 consecutive injections 1 hour apart to account for the short serum half-life of these constructs. The plasma pharmacokinetics of FC5 and control sdAb were essentially the same, but CSF level of FC5 was approximately 25-fold higher than control sdAb at 15 minutes after the last injection indicating specific accumulation into the CSF, likely via a trans-BBB route [217]. These studies indicate the

potential for FC5 to cross the intact BBB in vivo, and work is underway to test FC5-drug conjugates.

2.5.2 Rabies virus glycoprotein

Kumar and colleagues approached the brain delivery problem by observing that neurotropic viruses like rabies virus must cross the BBB in order to enter the brain and infect brain cells [218]. Thus, they developed a peptidyl targeting vector based on the portion of the rabies virus glycoprotein (RVG) that had been previously shown to bind to the neuronal nicotinic acetylcholine receptor (AchR) [219]. The resultant 29-mer peptide (RVG29) was shown to allow selective brain uptake, leading to a 3-fold increase in RVG29 accumulation in brain compared with mock peptide after iv administration in mice. Comparatively limited uptake of RVG29 in the liver and spleen was observed [218]. Subsequently, RVG29 linked to GFP silencing RNA (GFPsiRNA) was administered to transgenic GFP-expressing mice and reduction of GFP transgene expression was selective to the brain. The therapeutic potential of RVG29 mediated siRNA delivery was subsequently demonstrated by treating immune deficient mice injected with Japanese encephalitis virus with RVG29-linked to an antiviral siRNA. Treated mice had an 80% survival rate at 30 days post infection whereas control mice all died by 10 days post infection [218]. Another study used RVG29 to decorate dendrigraft poly-L-lysine (DGL) nanoparticles loaded with caspase-3 shRNA-coding plasmid (RVG29-DGL-shRNA) for treatment of a rat PD model [220]. Rats suffering from rotenone-induced PD were treated once weekly for 4 weeks with iv injections of the RVG29-DGL-shRNA. At the end of the treatment regimen, activated caspase-3

levels were reduced as much as 3-fold in rats treated with the RVG29-DGL-shRNA compared with non-targeted controls and treatment with RVG29-DGL-shRNA limited dopaminergic neuronal loss [220].

In another study, RVG29-targeted exosomes were used for brain delivery of siRNA. Exosomes are extracellular vesicles shed by numerous cell types, can be found in the majority of body fluids, and play a key role in cell-cell communication through activation of cell surface receptors on target cells, and through transfer of material between cells [221–223]. The brain delivery of BACE-1 siRNA using RVG29 targeted exosomes was investigated for treatment of Alzheimer's disease [223]. Immature mouse dendritic cells were transfected with a plasmid coding for a known exosome-resident protein, Lamp2b, with RVG29 fused to the extra-exosomal terminus. After 4 days of culture, RVG29 decorated exosomes were purified from culture supernatant and loaded with anti-BACE-1 siRNA via electroporation. When administered iv in mice, the RVG29 exosome treatment resulted in a 60% knockdown of BACE-1 gene expression in the brain leading to a significant reduction in $A\beta^{1-42}$ levels [223]. In addition to the significant therapeutic effects observed in brain, the exosome treatment did not produce any toxic or immunogenic effects in mice even after repeat dosing and exosomes did not accumulate in liver, a common problem when using liposomes for delivery. While this study indicates that exosomes may be a viable route for biologics delivery across the BBB, the production complexity and questions of formulation heterogeneity likely need to be addressed for clinical applications. Despite the fact that the mechanism by which RVG29 traverses the BBB has not been definitively shown, the initial therapeutic

results described in the aforementioned studies illustrate that RVG29 may be a very interesting targeting vector moving forward.

2.6 Engineering RMT targeting vectors for improved brain penetration

While RMT vectors having improved tissue specificity could certainly improve the efficiency of brain drug delivery, the intrinsic limits on transcellular transport for a given RMT system could also restrict the overall success of RMT-based delivery. For example, several studies investigating the details of transport of anti-TfR mAbs at the BBB have shown that despite substantial binding and endocytosis into BBB ECs, there was limited transcytosis into the brain parenchyma [224–228]. After either iv injection or in situ brain perfusion of radiolabeled anti-TfR antibody in rats, immunofluorescence and capillary depletion experiments indicated antibody was predominantly localized to brain capillaries with limited amounts entering the parenchyma [224, 225]. Similar results were observed after iv injection or brain perfusion of anti-TfR antibodies in mice [226–228]. Collectively, these studies suggest that the mAbs become “trapped” in the brain endothelial cells upon endocytosis. One hypothesis for antibody accumulation within the BBB ECs is that lack of antibody dissociation from the receptor upon endocytosis or transcytosis limits release from ECs into the brain [41]. Another possibility is that the intracellular trafficking of the receptor is affected by the binding interaction with the antibody [42, 43]. Thus, gaining a greater understanding of RMT targeting vector properties that govern intracellular trafficking fate may enable the development of more effective BBB drug delivery vectors through antibody engineering. Indeed, in a recent series of studies, it has been demonstrated that engineering of RMT targeting vector

binding properties (affinity, avidity) can be used to improve intracellular trafficking and transcytosis of BBB-targeted antibodies in vitro and in vivo.

To explore the effects of binding affinity on RMT efficiency, a high affinity parental anti-TfR antibody, anti-TfR^{A} (K_d=1nM), was engineered to have reduced affinity (K_d=6.9-111 nM, anti-TfR^{B}-anti-TfR^{D}) by alanine mutagenesis [41] (Figure 2-1). Interestingly, the lowest affinity variant (anti-TfR^{D}) exhibited a roughly 3-fold increased brain uptake compared with parental anti-TfR^{A} antibody when administered iv in mice at high doses of 20-50 mg/kg and measured 24 hours post-injection. In addition, immunofluorescence microscopy of brain sections taken from anti-TfR treated mice revealed that while the high affinity antibody was predominantly localized to the brain capillaries at 24 hours post-injection as described in previous studies, the lower affinity variants were increasingly localized to the brain parenchyma. Subsequently, a bispecific antibody containing anti-TfR^{A} and anti-BACE arms, anti-TfR^{A}/BACE, was produced (Figure 2-1). This bi-specific antibody by virtue of its now monovalent anti-TfR binding capability had reduced affinity for TfR (K_d~20nM) [229]. When administered to mice iv at a dose of 25 mg/kg, the bispecific antibody caused an approximately 36% reduction in brain Aβ$^{1-40}$ levels compared with control IgG [41]. Furthermore, the efficacy of the anti-TfR^{A}/BACE (K_d~20nM) was compared with lower affinity anti-TfR^{D}/BACE (K_d~600 nM) bispecific antibody via pharmacokinetic and pharmacodynamic analysis [39]. A single iv dose of 50 mg/kg yielded peak antibody concentrations of ~45 nM in brain homogenates at 1 day post-injection for either anti-TfR^{A}/BACE or anti-TFR^{D}/BACE [39]. Administration of either antibody led to a significant reduction in plasma and brain Aβ$^{1-40}$ levels (~30% reduction in plasma and ~40% reduction in brain). Over a 10 day

evaluation window, anti-TFR^{D}/BACE outperformed anti-TfR^{A}/BACE as the plasma clearance of anti-TfR^{A}/BACE was significantly faster than that for Anti-TFR^{D}/BACE leading to prolonged brain exposure of the lower affinity variant. As a result, the reduction in Aβ$^{1-40}$ levels achieved after single-dose iv administration lasted 4 days longer in mice treated with anti-TfR^{D}/BACE. Thus, while both antibodies achieved therapeutic results, the lower affinity anti-TfR^{D}/BACE had more desirable pharmacokinetic and pharmacodynamics properties.

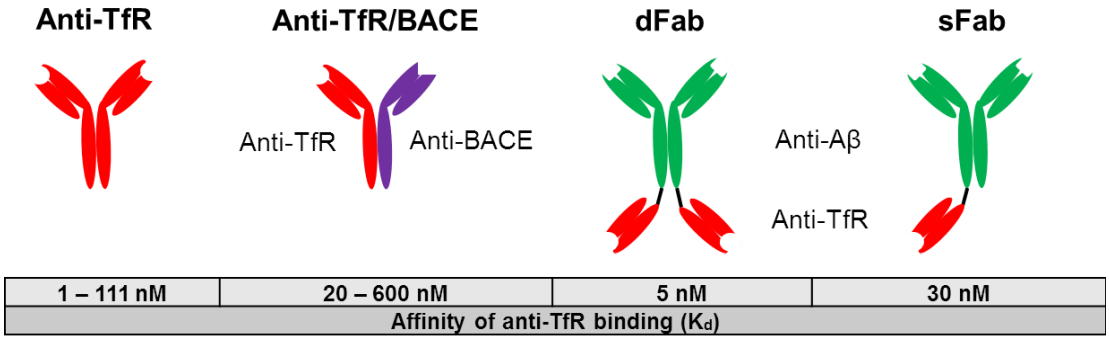

Figure 2-1. Anti-TfR constructs enabling increased brain penetration. Cartoon depictions of the various anti-TfR constructs engineered for improved brain penetration are shown above their measured equilibrium binding affinities.

The mechanism by which lower affinity, monovalent interactions with endothelial cell surface TfR led to increased brain penetration of anti-TfR bispecific antibodies was next investigated [42]. Bi-specific antibodies with one anti-TfR arm and one control IgG arm (anti-TfR/Ctr) were employed to ensure any effects were the result of the anti-TfR interactions. First, a significant dose dependent decrease in cortical TfR was observed 4 days after mice were injected iv with 5-50 mg/kg of Anti-TfR^{A}/Ctr while no significant decrease was observed for anti-TfR^{D}/Ctr, indicating TfR^{A}/Ctr promoted TfR degradation

(Figure 1-2 B iii). Subsequent in vitro and in vivo analyses revealed that upon antibody internalization, a greater percentage of anti-TfR^{A}/Ctr was trafficked to the lysosome (Figure 1-2 B iii) compared with anti-TfR^{D}/Ctr. Thus, high affinity anti-TfR interactions with endothelial cell surface TfR appear to alter the trafficking of TfR-antibody complexes once internalized from a recycling/transcytosis route (Figure 1-2 B iv, v) to a degradation route (Figure 1-2 B iii).

In direct analogy to the comparisons described above between the high affinity bivalent anti-TfR^{A} antibody and the moderate affinity, monovalent anti-TfR^{A}/BACE bispecific antibody, another study examined the effects of monovalent versus divalent anti-TfR antibody constructs on intracellular trafficking and trans-BBB delivery [43]. Anti-TfR Fab fragments were fused to an anti-Aβ antibody (mAb31 [230]) to create either bivalent (dFab, TfR K_d~ 5nM) or monovalent (sFab, TfR K_d~30 nM) anti-TfR constructs (Figure 2-1). When mice were administered sFab weekly for 3 months at both low- (0.4 mg/kg) and midrange doses (2.7 mg/kg), an increased reduction in brain amyloid plaque load was observed compared with parental, untargeted Ab31 administration. Similar to findings with the low versus high affinity variants examined with bispecific antibodies, sFab is internalized and transcytosed across BBB ECs (Figure 1-2 B ii, v), while the divalent dFab instead accumulates within BBB ECs, particularly in the lysosomes (Figure 1-2 B iii). Taken together with the bispecific study, it appears that lowered affinity and reduced valency can both help direct productive transcytosis by avoiding lysosomal sequestration. Previous studies support these findings and have indicated that the valency of the RMT targeting moiety interaction with TfR plays a key role in endocytosis and intracellular trafficking [153, 231]. For example, to address the role of

RMT vector avidity, differing amounts of Tf (between 3 and 100 Tf molecules) were conjugated to gold nanoparticles (~85 nm in diameter) and their ability to cross the BBB in vivo was assessed [231]. The authors showed that the highest avidity particles were sequestered in brain blood vessels but did not enter the brain, while particles with mid-range avidity were transcytosed into the brain parenchyma. Those particles with lowest avidity did not bind to brain capillaries, likely due to competition with endogenous Tf. Although the lowering of affinity either by monovalent antibody interactions or by engineered lowered affinity antibodies has proven effective for increasing trans-BBB transport, brain uptake remains limited (0.3%ID for Anti-TfR^{D} [41]). In addition, one of the prevailing issues with low affinity RMT targeting vectors is the high necessary dose (~25 mg/kg) that would translate to a large amount of antibody (~2 g/75 kg human) for each treatment dose in humans. For chronic administration, this could potentially be cost prohibitive.

Finally, it is important to note here that not all RMT systems will have the same mechanisms of internalization and intracellular trafficking; and therefore, when engineering RMT vector binding properties for increased brain penetration, the trafficking properties of the target RMT system must be taken into account. For example, TfR is constitutively endocytosed and trafficked within the cell via a clathrin-mediated route [232, 233]. By contrast, a receptor like ICAM-1 undergoes cell adhesion molecule (CAM) mediated endocytosis only upon interaction with multivalent ligands or immune cells [234]. Given these differing mechanisms, binding, internalization, and intracellular trafficking of the receptors may respond differently to engineered targeting ligands. To demonstrate this point, a recent study compared the in vitro binding and in

vivo biodistribution of TfR and ICAM-1 targeting vectors [235]. On the one hand, free anti-TfR (8D3) and anti-ICAM-1 (YN1;[236]) mAbs administered to cultured cells in vitro bound to the EC cell surface at comparable levels, but a greater percentage of anti-TfR mAbs internalized into the ECs. In addition, when administered iv the anti-TfR antibodies accumulated in mouse brain to a greater extent than anti-ICAM antibodies. On the other hand, ~250 nm polystyrene nanoparticles (NPs) decorated with ~300 anti-ICAM antibodies showed increased cell surface binding and internalization compared with comparable anti-TfR NPs in vitro. In vivo studies indicated that anti-ICAM NPs showed increased uptake in the brain (~2.2-fold over anti-TfR NPs and ~1.9-fold over anti-TfR antibody) with increased brain selectivity (i.e. decreased accumulation in liver) [235]. These results indicate that the efficiency and specificity of brain delivery of different RMT targeting ligands are dependent on the trafficking dynamics of the targeted receptor. Thus, when considering similar approaches for the other RMT targets discussed in this review it will be necessary to approach the problem by taking into account the unique properties of the RMT system of interest.

2.7 Conclusion

While the BBB continues to present a formidable obstacle for the treatment of CNS diseases, the work described in this review demonstrates that there are a growing number of strategies to target RMT systems at the BBB for delivery of biologics. Targeting of the well-studied RMT systems at the BBB (e.g. TfR, IR, LDLRf) has demonstrated that receptor-targeting antibodies or ligand mimics can be used as RMT targeting vectors to deliver biologics to the brain, with impressive therapeutic outcomes

in a number of animal models. The promise of these strategies will likely be bolstered by the ongoing clinical development of RMT targeting biologics at companies such as ArmaGen Technologies and Angiochem. Until recently, the mechanistic details of RMT binding and intracellular trafficking that ultimately lead to transcytosis were largely unexplored. The work dealing with anti-TfR antibody engineering illustrates that it is possible to alter binding interactions of targeting vectors with their cognate RMT receptor to improve binding, intracellular trafficking, and transcytosis at the BBB. It is likely that such studies will be extended to other known RMT-targeting vectors to develop even more effective brain delivery constructs. Identification of alternative RMT targets such as FC5 and RVG29 along with a sustained search for new RMT targets will further enhance the use of the RMT approach for brain delivery of biologics.

Chapter 3 A yeast display immunoprecipitation screen for discovery of antibodies targeting endocytic complexes at the blood-brain barrier

In this chapter we develop and apply an innovative yeast display immunoprecipitation-based screen for detection and enrichment of antibodies against BBB membrane protein complexes involved in endocytosis.

3.1 Introduction

Yeast surface display (YSD) is a powerful tool for combinatorial library screening and has been used over the past 20 years to discover and engineer antibodies against a wide range of targets [65, 84, 237]. Classically, YSD screening is carried out using soluble antigens (e.g. purified recombinant proteins) with fluorescence activated cell sorting (FACS) enabling quantitative detection and enrichment of antibodies with desired binding characteristics. Our lab has recently developed the yeast display immunoprecipitation (YDIP) method [105]; YDIP is a modification on traditional YSD techniques whereby antibodies can be screened for binding to detergent-solubilized membrane proteins directly in cell and tissue lysates [238]. This has facilitated the discovery and engineering of antibodies against membrane protein targets [46, 94, 239, 240] without the need for laborious and expensive purified antigen preparation techniques. An open question was whether YDIP could be extended to enable targeted discovery of antibodies against membrane protein complexes involved in a cellular function of interest. Protein-protein interactions (PPIs) control many key cellular processes involving membrane proteins including cell-cell interactions, cell motility,

signal transduction, and vesicular trafficking. Discovery and investigation of membrane protein complexes is therefore essential to further our understanding of the function and regulation of these diverse and essential processes in health and disease. To this end, antibodies targeting PPIs are needed for basic research as well as therapeutic intervention. While numerous high throughput methods exist to discover and characterize PPIs (reviewed in [241, 242]) none of the current methods incorporate antibody discovery in-line with PPI screening. The YDIP method is uniquely positioned to fill this void as membrane protein complexes bound to the yeast surface via displayed antibody interaction with one complex member can be probed with secondary reagents to detect other members of the complex, providing information on the functional nature of the complex. Thus, we envisioned a functional YDIP (fYDIP) screen that combines detection of bound membrane proteins with detection of a relevant PPI partner to isolate antibodies that bind membrane protein complexes involved in a target function of interest. In this manner, the fYDIP method can be thought of as similar to a traditional co-immunoprecipitation experiment where elution and western blotting are replaced by direct detection of interacting proteins captured on the yeast surface.

We chose to focus the initial proof-of-concept screen on the endocytosis trafficking machinery at the blood-brain barrier (BBB). Given its uniquely restrictive phenotype and role in maintaining brain homeostasis the BBB endothelium has been the subject of intensive study to better understand its function and regulation in development, health, and disease [10, 138]. One area of particular interest is the application of antibodies targeting cell surface receptors that undergo receptor-mediated endocytosis (RME) for the non-invasive delivery of therapeutics across the BBB [243,

244]. Discovery of novel antibody reagents that target these types of receptors or the host of accessory proteins involved in functional endocytic complexes will augment this work by facilitating both further advances in brain drug delivery and basic research into the PPIs that regulate endocytosis and vesicular trafficking at the BBB. Because it is well studied and numerous BBB drug delivery targets are internalized via clathrin mediated endocytosis (e.g. Transferrin Receptor (TfR), Insulin Receptor (IR), and Lipoprotein receptors), this process was chosen as the target for the initial fYDIP screen. During clathrin mediated endocytosis the adaptin 2 (AP-2) protein directly binds to the cytosolic tail of transmembrane receptors such as TfR and serves as a functional hub for endocytosis via recruitment of clathrin and other accessory factors to the site of membrane invagination [245, 246]. AP-2 is the ideal candidate for this initial study as its only known function is in endocytosis at the plasma membrane and it is involved in simultaneous PPIs with both membrane and cytosolic partners. Therefore, measurement of the association of AP-2 with membrane protein complexes bound on the yeast surface during screening can serve as a definitive functional marker for antibodies targeting endocytosis machinery.

Here we present the fYDIP screening procedure as applied to discovery of antibodies targeting endocytosis trafficking machinery at the BBB. Detergent solubilized plasma membrane fractions recovered from isolated bovine and rat brain capillaries were used during screening and initial clone characterization to ensure in vivo relevance of the target antigens. A non-immune human single chain fragment variable (scFv) antibody library was screened to enrich for scFv that bind to membrane protein complexes associated with AP-2. Through this screening procedure and a non-

exhaustive sampling of the resultant enriched library we have discovered two novel scFv that target intracellular accessory proteins known to be involved in endocytosis and membrane trafficking, validating the fYDIP approach as a means to isolate antibodies against desired membrane protein complexes. In the future this general approach could be applied to a wide range of applications where antibodies against PPIs of interest are sought.

3.2 Methods

3.2.1 Media, Cells, and Plasmids

Saccharomyces cerevisiae strain EBY100 was used for scFv surface display. The naïve human scFv library [65] was a gift from Dr. K. Dane Wittrup at MIT. For yeast surface display experiments, EBY100 yeast were first grown overnight at 30^0C 260 rpm in SD-CAA media (20 g/L dextrose, 6.7 g/L yeast nitrogen base, 100 mM sodium phosphate buffer pH 6.0, 5.0 g/L bacto-casamino acids without tryptophan and uracil). The next day, yeast cultures were set to an OD_{600} of ~0.4 and grown for approximately 3 hours until an OD_{600} of 1 was reached. Next, surface display was initiated via switching to SG-CAA induction media (Galactose replaces glucose in the SD-CAA recipe) and cultures grown at 20^0C, 260rpm overnight. HEK293 cells (CLR-1573) purchased from the American Type Culture Collection (ATCC) were grown in minimum essential medium (MEM, M4526, Sigma-Aldrich) supplemented with 10% fetal bovine serum (FBS, 10437, Thermo Fisher), 2 mM L-glutamine, 20 mM HEPES, and 1x antibiotic/antimycotic (15240062, Thermo Fisher) at 37^0C, 5%CO2, in a humidified incubator. RBE4 cells were a kind gift from Dr. Roux [97] and were cultured in the same

incubator as HEK293 cells. The RBE4 media consisted of a 1:1 of ratio MEM and Ham's F10 (11550043, Thermo Fisher) supplemented with 10% FBS, 100 mg/mL streptomycin, 100 units/mL penicillin G, 0.3 mg/mL geneticin, and 1 µg/L basic fibroblast growth factor (WiCell). The pIRES-rFc plasmid used for scFv-Fc expression was a kind gift from Dr. Brantley Herrin at Emory University. HEK293F cells (R79007, Thermo Fisher) used for the production of scFv-Fc proteins were maintained in Freestyle F17 Medium (A1383504, Thermo Fisher) at 37^0C, 8% CO_2, and 135 rpm in a humidified incubator.

3.2.2 Animals

Male Sprague Dawley rats (*Rattus norvegicus*) at 225 – 250 grams were purchased from Envigo and used in terminal experiments. Briefly, rats were anesthetized with isoflurane, decapitated, and brains dissected out. All rat experiments were approved by the UW-Madison Institutional Animal Care and Use Committee (IACUC).

3.2.3 Preparation of crude plasma membrane fractions from cultured HEK293 cells

HEK293 cells were scraped into PBS and washed once. Lysis was achieved by incubating cells in 10 mM Tris-HCl pH 8.0, 10 mM NaCl, 1 mM $MgCl_2$ for 30 minutes on ice followed by homogenization in a dounce homogenizer. Cell lysate was cleared via centrifugation at 2000xg for 10 minutes at 4^0C. The supernatant was recovered, added to an ultracentrifuge tube, and the tube filled with buffer containing 10 mM Tris-HCl pH 7.5, 250 mM sucrose, 50 mM NaCl. Membranes were pelleted by centrifugation at

200,000xg for 90 minutes at 4^0C. The supernatant was discarded and membrane protein complexes were resuspended and solubilized in tris-buffered saline (TBS) containing 1% TritonX-100 (TX-100; IB07100, IBI Scientific). All buffers contained 1x protease inhibitor cocktail (PIC; 11836170001, Roche) and 2mM EDTA.

3.2.4 Brain capillary isolation and plasma membrane fractionation

Capillaries were isolated from bovine or rat brains following the method of Lidinsky and Drewes [247] with modifications. Isolated capillaries were incubated with 5 mM sulfo-NHS-LC-biotin (PG82075, Thermo Fisher) for 2 hours at 4^0C to selectively tag membrane proteins with biotin. The reaction was quenched by addition of glycine to a final concentration of 100mM and incubation for 10 minutes on ice. Endothelial plasma membranes were fractionated from the capillaries using a two-step hypotonic lysis procedure as follows: incubation in (1) distilled water at 4^0C for 2 hours and (2) 10 mMTris-HCl pH 7.4 at 4^0C for 30 minutes. After each lysis step the capillaries were pelleted by centrifugation at 15,000xg. Next, the lysed capillaries were sonicated in 50mM Tris-HCl pH 7.4 to liberate the plasma membranes. Subsequent centrifugation at 25,000xg resulted in a supernatant containing dispersed plasma membrane fragments and a pellet containing the capillary basement membranes. All buffers contained 1x PIC and 2mM EDTA. The supernatant fraction is referred to as brain capillary plasma membranes (BCPM). Membrane protein complexes were solubilized via the addition of TX-100 to a final concentration of 1% v/v and free biotin was added to a final concentration of 1 mM prior to fYDIP experiments as described below.

3.2.5 fYDIP screening and individual clone assay

fYDIP screening is a modification on the previously reported YDIP method [94, 238]. The first round of screening was carried out using a magnetic activated cell sorting (MACS) protocol [248] to recover scFv binding to biotinylated BCPM antigens. $5x10^9$ yeast from the naïve human scFv library described above were incubated with 8.8 mg bovine BCPMs for two hours at 4^0C. Yeast were subsequently washed twice with ice cold TBS+1%TX-100+1%BSA (TBSTXA) and once with ice cold TBS+1%BSA (TBSA). Washed yeast were resuspended in ice cold TBSA, streptavidin microbeads (Miltenyi, 130-048-102) were added, and the mixture was incubated at 4^0C for 30 minutes. After washing and resuspension in TBSA, the suspension was then applied to an LS column (130-042-401, Miltenyi) in a Midi-MACS separator magnet (130-042-302, Miltenyi) to capture microbead bound yeast. The column was washed twice with TBSA and removed from the magnet. Yeast were eluted from the column and regrown in SD-CAA media. Subsequent rounds of screening used fluorescence activated cell sorting (FACS) to enrich desired clones. In the second round of screening, 10^8 yeast were incubated with 1 mg BCPMs as above. Full length scFv expression was detected via labeling with a rabbit-anti-cmyc epitope Ab (PA1-981, Thermo Fisher) followed by a goat-anti-Rabbit IgG-Alexa488 secondary Ab (A-11008, Thermo Fisher). scFv binding to complexes containing biotinylated BCPM antigens was detected by labeling with mouse-anti-biotin Ab (BTN.4, Labvison) followed by a goat-anti-mouse IgG-allophycocyanin secondary Ab (A-865, Thermo Fisher). Yeast were sorted on a Becton Dickson SORP FACSAriaII (University of Wisconsin Carbone Cancer Center) to recover

clones double positive for scFv expression and binding to biotinylated BCPMs. The final screening round applied the functional filter of the fYDIP method seeking to identify scFv that target protein complexes containing biotinylated membrane proteins and AP-2. 10^7 yeast were incubated with 0.5 mg BCPMs as above. Binding to complexes containing biotinylated membrane proteins was detected with streptavidin R-Phycoerythrin conjugate (SA10041, Thermo Fisher) and association with AP-2 was detected via labeling with mouse-anti-AP2α (Clone AP.6, Thermo Fisher) followed by goat-anti-mouse IgG-allophycocyanin. Yeast were sorted to recover clones double positive for binding to complexes containing both biotinylated membrane proteins and AP-2. Individual clone fYDIP assays were carried out via incubation of 10^6 monoclonal yeast with ~50 µg rat BCPM antigens for two hours at 4^0C, labeling as described above, and analysis on a BD FACSCalibur cell analyzer.

3.2.6 Immunoprecipitation and western blotting

scFv-Fc fusion proteins were subcloned into the pIRES-rFc vector, produced via transient transfection of HEK293F cells, and purified as previously in Chapter 4. Immunoprecipitation of antigens from RBE4 cell lysates was carried out using Dynabeads Protein G (1003D, Thermo Fisher) following the manufacturers protocol. RBE4 cell lysates were produced as follows: membrane proteins were biotinylated as previously described [94], scraped into TBS+1% v/v TX-100+1xPIC+2mM EDTA, and incubated at 4^0C for 15 minutes. 15 µg purified scFv-Fc were coated on 2.25 mg of Dynabeads and incubated with ~500 µg cell lysate proteins for 2 Hrs at 4ºc. After washing, captured complexes were eluted via low pH conditions and equal volumes of

eluate were separated via SDS-PAGE prior to coomassie staining and excision of bands for MS/MS analysis or transfer to nitrocellulose and western blotting. The following primary and secondary antibodies were used in the western blotting experiments described in the results section. Primary antibodies: Mouse-anti-AP2α (610502, BD Biosciences), Mouse-anti-Myh9 (MABT164, EMD Millipore), Mouse-anti-AHNAK (MA1-10050, Thermo Fisher). Secondary Reagents: IRDye680RD Streptavidin conjugate (925-68079, Li-Cor Biosciences), IRDye680RD Donkey-anti-Rabbit conjugate (926-68073, Li-Cor Biosciences), IRDye800CW Donkey-anti-Mouse conjugate (926-32212). Labeled nitrocellulose membranes were imaged on a Li-Cor Odyssey Imager.

3.2.7 Mass spectrometry

In gel tryptic digestion was carried out using Trypsin Gold, Mass Spectrometry Grade (V5280, Promega) and ProteaseMax Surfactant, Trypsin Enhancer (V2701, Promega) via the manufacturer's protocols. Tryptic peptide samples were then desalted with Omix C18 pipette tips (Agilent Technologies), dried *in vacuo*, and dissolved in 3% acetonitrile (ACN), 0.1% formic acid in water. Samples were analyzed using a Waters nanoAcquity UPLC system coupled to a Thermo Scientific Orbitrap Elite mass spectrometer. Peptides were loaded onto a 75 µm inner diameter microcapillary column fabricated with an integrated emitter tip and packed with 15 cm of Bridged Ethylene Hybrid C18 particles (1.7 µm, 130Å, Waters). Mobile phase A was composed of water, 5% DMSO, and 0.1% formic acid. Mobile phase B was composed of ACN, 5% DMSO, and 0.1% formic acid. Separation was performed using a gradient elution of 5% to 35% mobile phase B over 40 min at a flow rate of 300 nL/min. Survey scans of peptide

precursors from 400-2000 *m*/*z* were acquired at a resolving power of 120k (@ 400 *m*/*z*) with an AGC target of 1×10^6 and maximum injection time of 150 ms. The top ten precursors were then selected for data-dependent HCD MS^2 analysis with an isolation width of 2.5 Da, a normalized collision energy (NCE) of 35, a resolving power of 15k, an AGC target of 5×10^4, a maximum injection time of 250 ms, and a lower mass limit of 100 *m*/*z*. Precursors were subject to dynamic exclusion for 10 s with a 10 ppm tolerance.

3.2.8 Data Processing

Resulting data were processed using Proteome Discover 1.4 (Thermo Fisher Scientific). The Sequest HT search algorithm was used to search MS/MS spectra against the SwissProt *Rattus Norvegicus* reference database (October 2015) to identify proteins. Trypsin was specified as the enzyme with up to two miscleavages allowed. The precursor tolerance was set to 10 ppm, and fragment mass tolerance was set to 0.02 Da. Carbamidomethylation of cysteine was included as a fixed modification, and oxidation of methionine, deamidation of asparagine and glutamine, and NHS-LC-biotin modification of lysine were included as dynamic modifications. Reported peptides were filtered to a false discovery rate of 1% using percolator. Reported proteins were filtered to require at least two unique peptides for identification.

3.3 Results

3.3.1 Detection of TfR:AP-2 interactions on the yeast surface

The fYDIP concept was first tested with a model system, the TfR:AP-2 complex, since TfR is known to undergo clathrin mediated endocytosis via interaction with AP-2 [45, 249]. Thus, the ability of the fYDIP method to detect this interaction on the yeast surface was assessed via incubation of yeast displaying an anti-TfR scFv (H7 [66]) with detergent solubilized crude plasma membrane fractions from HEK293 cells. Yeast displaying an irrelevant scFv against hen egg lysozyme (HEL), D1.3, were used as a negative control. After 2 hour incubation at 4^0C where TfR-containing membrane protein complexes could be captured on the yeast surface, H7 or D1.3 binding to TfR and complex association with AP-2 were assayed via labeling with antibodies against TfR and AP-2 followed by flow cytometric analysis. It was clear that H7 captured membrane protein complexes containing TfR and AP-2 whereas D1.3 had no measurable binding to such complexes (Figure 3-1 A and B). The specific capture of TfR:AP-2 complexes was further confirmed by elution from the yeast surface and western blot (WB) analysis. The WB revealed the presence of both TfR and AP-2 in the H7 YDIP eluate compared with an absence of both proteins for negative control scFv D1.3 which matched well with the flow cytometry results (Fig 1C). Taken together these data prove that membrane protein complexes harboring relevant AP-2 PPIs can be captured and detected on the yeast surface. Therefore, the basic YDIP library screening procedure can be augmented via the use of anti-AP-2 antibodies to screen for scFv that bind membrane protein complexes associated with AP-2.

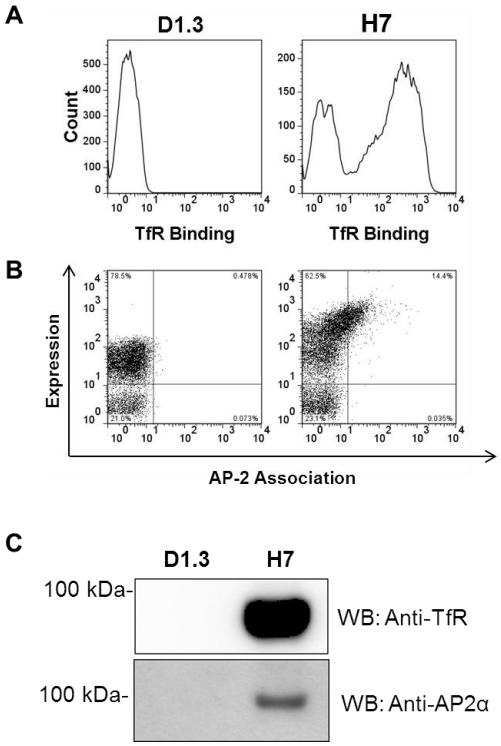

Figure 3-1. Yeast surface display capture of TfR:AP-2 complexes. Yeast displaying anti-TfR scFv, H7, or a negative control scFv, D1.3, were incubated with biotinylated detergent solubilized HEK293 plasma membrane antigens. Capture of protein complexes was assessed via antibody labeling and flow cytometry. (A) Flow cytometry histograms (TfR binding detected via anti-biotin antibody) demonstrate the capture of TfR by H7 yeast. (B) Flow cytometry dot plots (x-axis detection with anti-AP2 antibody, y-axis detection with anti-cmyc antibody) demonstrate the presence of measurable levels of TfR-associated AP-2 in the H7 captured complexes. (C) The flow cytometry readout is validated after elution of complexes from the yeast surface and western blotting for TfR (Anti-TfR) and AP-2 (Anti-AP2α).

3.3.2 fYDIP screening for scFv that target endocytic complexes

Given the ability to capture and measure known membrane protein complexes associated with AP-2 on the yeast surface, we proceeded with screening of a non-immune human scFv library [65] via fYDIP. To increase the *in vivo* relevance of the scFv isolated from this screening procedure we chose to use plasma membrane preparations derived from animal sources rather than *in vitro* cell lines. Given the size of the starting library (approximately 10^9 clones), large amounts of plasma membrane

antigens were needed to provide sufficient antigens to enable exhaustive screening. As a result, bovine brain was chosen as the antigen source for the fYDIP screen given the ability to recover large amounts of brain capillary plasma membrane (BCPM) proteins. For example, in our hands ~4.4 mg of BCPM proteins were recovered from one bovine brain compared with ~1.6 mg from 10 rat brains. Bovine brains were obtained, capillaries isolated, membrane proteins biotinylated, and BCPMs fractionated (Figure 2 i-ii) via established protocols. After recovery of the BCPMs membrane protein complexes were solubilized by addition of TritonX-100 to a final concentration of 1% v/v to enable screening.

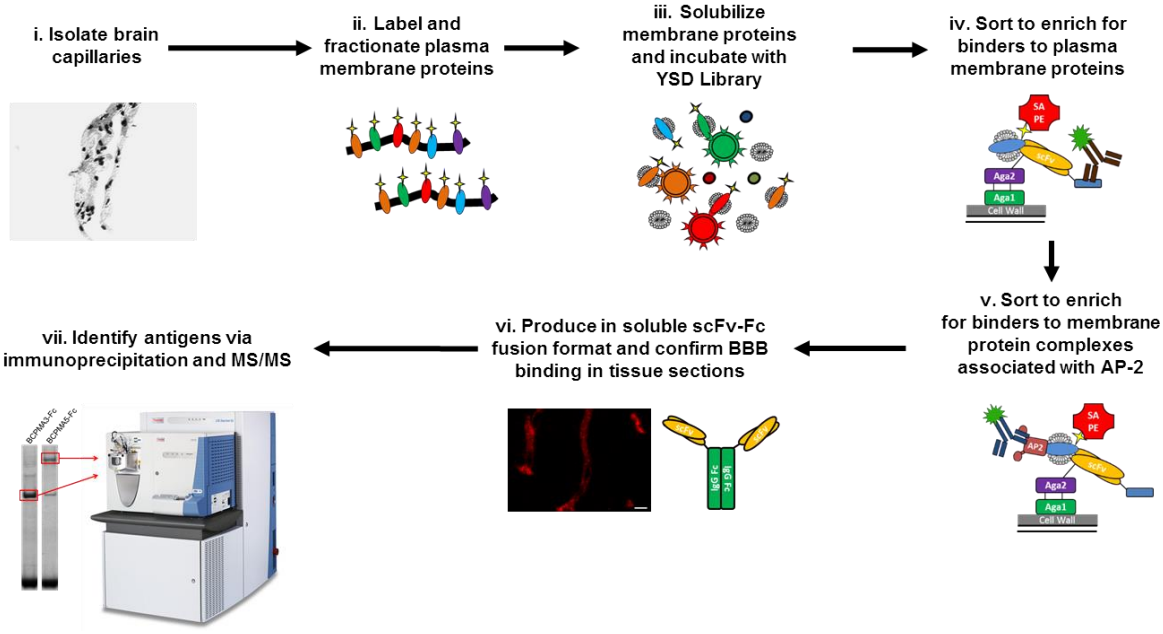

Figure 3-2. fYDIP screening workflow. (i-iii) Capillaries are isolated from cow or rat brains, membrane proteins are tagged with biotin, plasma membranes fractionated, and membrane protein complexes solubilized via addition of detergents. These preparations serve as the antigen source for subsequent screening. (iv) Initial rounds of screening enrich the library for scFv binding to complexes containing biotinylated membrane proteins. (v) The functional filter is applied to enrich scFv that bind membrane protein complexes containing both biotinylated membrane proteins and AP-2. (vi) Lead candidates are reformatted as scFv-Fc fusion proteins and binding to *in vivo*-relevant antigens is confirmed via labeling of brain tissue sections. (vii) scFv-Fc antigens are identified via immunoprecipitation and mass spectrometry.

The overall fYDIP screening and validation workflow is diagrammed in Figure 3-2. The approach taken in the fYDIP procedure was to first enrich the library for scFv binding any complex containing biotinylated membrane proteins (Figure 3-2 iv) and to subsequently focus the enrichment by applying the functional filter requiring binding to complexes containing both biotinylated membrane proteins and AP-2 (Figure 3-2 v). Since the frequency of scFv binding to complexes containing biotinylated membrane proteins was small in the starting library ~5% (Figure 3-3 A) and AP-2 containing complexes were expected to represent only a fraction of the total membrane protein complexes in the antigen solution this two-tiered screening approach was taken to avoid the loss of rare scFv clones targeting the desired functional complexes. In all rounds of screening the yeast libraries were incubated with BCPMs for 2 hours at 4^0C. In the first round $5x10^9$ yeast, a 5 times oversampling of the library size, were screened with a magnetic activated cell sorting (MACS) procedure employing streptavidin coated beads. The second round of screening used fluorescence activated cell sorting (FACS) and yeast double positive for scFv expression and biotinylated membrane protein binding were enriched. As shown in Figure 3-3 A, 5% of the scFv expressing clones in the starting library bound to BCPM antigens and this was increased to 24% and 66% via MACS and FACS respectively. Additional rounds of screening in this manner were carried out but significantly reduced the sequence diversity of the enriched pools (data not shown).

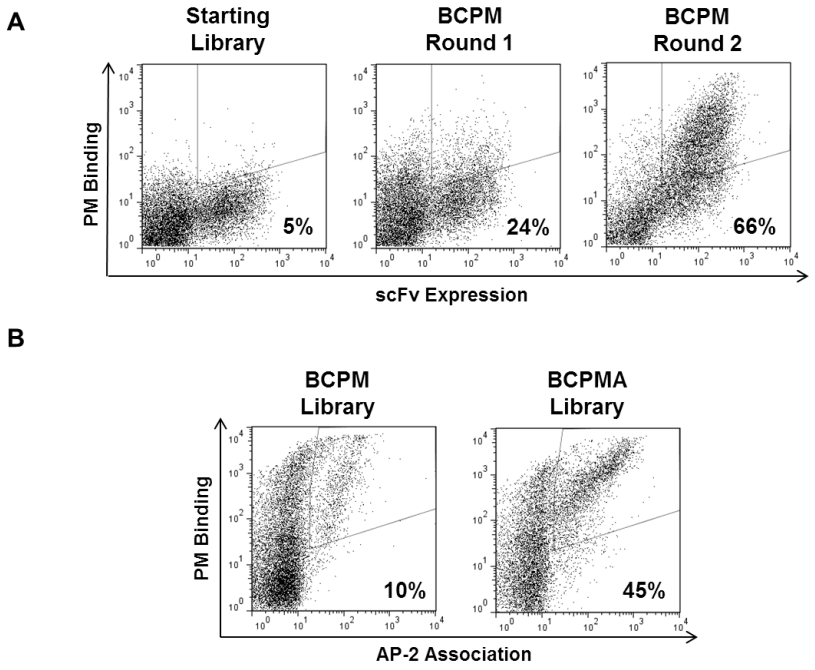

Figure 3-3. scFv library screening via fYDIP. (A) Analytical flow cytometry dot plots demonstrate enrichment of scFv binding to complexes containing biotinylated plasma membrane (PM) proteins over two rounds of screening. scFv expression is detected on the x-axis via anti-cmyc antibody and biotinylated PM binding is detected on the y-axis via anti-biotin antibody. The percentage of expressed cells falling in the gated region is displayed in the lower right of each plot. (B) Analytical flow cytometry dot plots demonstrate the enrichment of clones that bind to complexes containing both biotinylated PM proteins and AP-2 through one round of functional screening. Biotinylated PM binding is detected on the y-axis via streptavidin and AP-2 association is detected on the x-axis via anti-AP2α antibody. The percentage of PM binding clones that fall in the gated region is displayed in the lower right of each plot.

Therefore, the BCPM Library resulting from two rounds of screening was chosen as the starting point for the functional screening step. Functional screening was carried out via incubation of the library with BCPM antigen preparations and recovery of clones double positive for binding to complexes containing biotinylated membrane proteins and AP-2 as determined by simultaneous labeling with streptavidin and an antibody against the AP-2 α subunit (Figure 3-2 v). This functional enrichment procedure resulted in the BCPM-Adaptin (BCPMA) Library with 45% of the BCPM binding clones having measurable AP-2 association versus 10% in the BCPM Library (Figure 3-3 B). The

diversity in the BCPMA pool was assessed by sanger sequencing of clones from the library and 38 out of 70 clones tested harbored unique scFv sequences indicating the enrichment of a highly diverse antibody population. Subsequent work was focused on validating the results of this screening procedure via confirmation of individual clone binding to complexes containing biotinylated membrane proteins and AP-2, demonstration of binding to antigens expressed at the *in vivo* BBB, and identification of antigens to confirm targeting of complexes involved in endocytosis.

3.3.3 Analysis of individual clones from the BCPMA library

Binding of the 38 unique clones from the BCPMA library to membrane protein complexes was tested via fYDIP assay. Rat antigens were used in place of bovine antigens as there was a 95% crossreactivity of the library clones between the species (data not shown) and rats are a more relevant and tractable animal model for laboratory study. Monoclonal yeast were incubated with BCPM antigens from rat brain and analyzed via flow cytometry to measure the presence of biotinylated membrane proteins and AP-2 in the scFv-bound complexes. 33 of the 38 clones bound to complexes containing biotinylated membrane proteins. Furthermore, 19 of the 33 had measurable association to AP-2 in the complex. Figure 3-4 A-C provides results for a select panel of the BCPMA clones that can be compared with non-binding control, D1.3, and a clone from the BCPM Library, BCPM7, which is positive for biotinylated antigen binding but not AP-2 association.

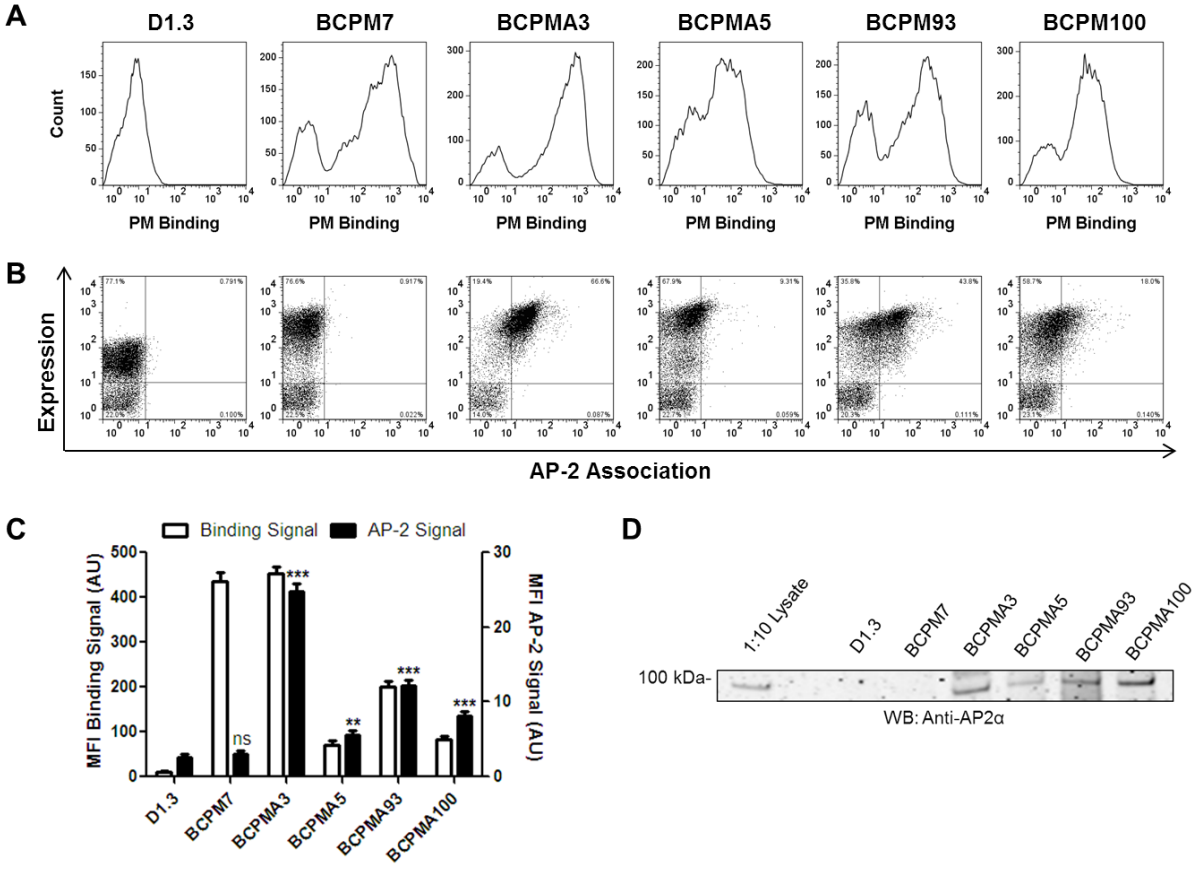

Figure 3-4. Individual clone analysis via fYDIP assay. The indicated monoclonal yeast were incubated with rat BCPMs and analyzed via flow cytometry (A-C). (A) Flow cytometry histograms demonstrate binding to complexes containing biotinylated PM proteins detected via anti-biotin antibody. (B) Flow cytometry dot plots for the assessment of AP-2 association in the bound complexes. scFv expression is detected on the y-axis and AP-2 association is detected on the x-axis as in Figure 3-3. (C) Quantification of the mean fluorescence intensity (MFI) of the PM Binding signal (white bars, left axis) and AP-2 association signal (black bars, right axis) for each monoclonal scFv in (A) and (B). Data are the mean of n=3 independent experiments and error bars represent standard deviation. Significance of AP-2 association signal above background was assessed using unpaired Student's t-tests comparing each individual clone with the negative control D1.3 background signal intensity. ns= not significant, **p<0.001, ***p<0.0001. (D) fYDIP eluates for the indicated monoclonal scFv were analyzed via anti-AP2α western blot to confirm the presence of AP-2 in the captured complexes.

To show definitively that the selected clones bind to AP-2 associated complexes the bound antigens were eluted from the yeast surface and analyzed via WB (Figure 3-4 D). The eluate from all four BCPMA clones tested contained measurable amounts of AP-2 as shown using an antibody against the alpha subunit whereas no AP-2 was found in

the D1.3 or BCPM7 eluates. Importantly, comparing the results for BCPM7 and BCPMA3, which have a similar level of binding to complexes containing biotinylated membrane protein antigens (MFI of biotinylated binding signal was >400 AU for both clones, Figure 3-4 A and C), demonstrates the specificity of this assay in identifying membrane protein complexes containing AP-2 PPIs; AP-2 association in the bound complexes as determined by flow cytometry was significantly above background for BCPMA3 whereas there was no significant difference for BCPM7 (Figure 3-4 B and C) and this result was mirrored in the western blotting analysis of eluted complexes (Figure 3-4 D). Taken together with the previous validation of the detection of known membrane protein AP-2 interactions with the TfR:AP-2 model system (Figure 3-1), these results demonstrate that fYDIP can be used to accurately discriminate between scFv that bind protein complexes containing AP-2 PPIs and those that do not. Thus, the analysis of clones from the BCPMA Library revealed that >50% of scFv tested bound membrane protein complexes with AP-2 PPIs and further analysis of this cohort was pursued.

A 10 clone subset of the 19 scFv that were identified in the non-exhaustive analysis described above were subcloned from the yeast surface display vector into a mammalian expression vector with rabbit IgG Fc fused at the C-terminus for efficient production, purification, and application of the scFv-Fc in downstream assays. 7 of the 10 clones were confirmed to bind to rat brain capillary antigens via immunofluorescence analysis. Rat brain cryosections were incubated with the scFv-Fc and subsequently anti-rabbit fluorescent secondary antibodies and fluorescently labeled lectin as a brain vasculature marker. Examples of the four BCPMA clones (BCPMA3-Fc, BCPMA5-Fc,

BCPMA93-Fc, BCPMA100-Fc) with the strongest brain capillary binding signal are shown in Figure 5 along with BCPM7-Fc as a non-AP-2 associated control.

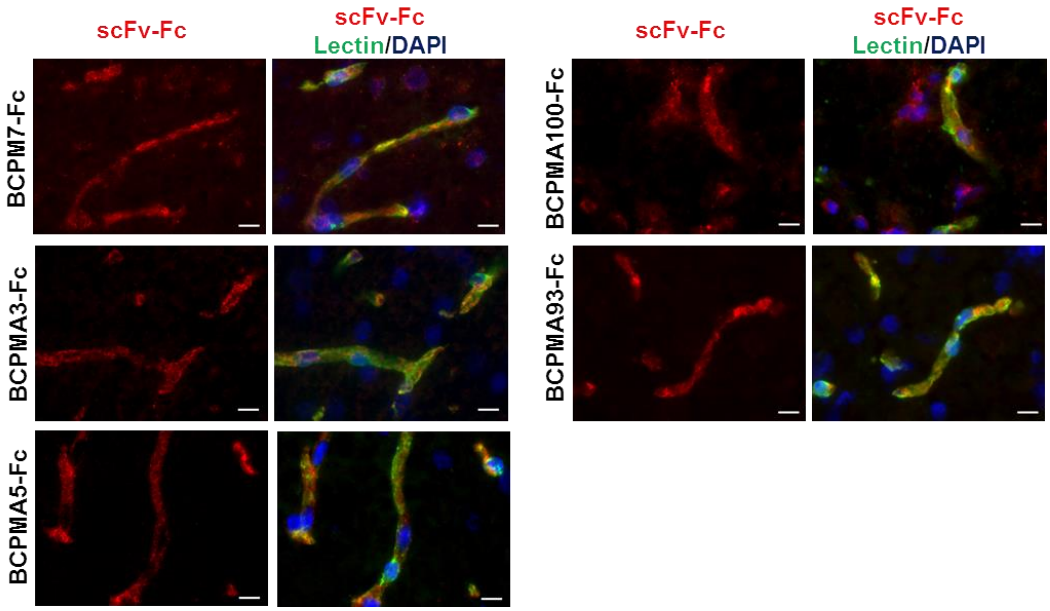

Figure 3-5. fYDIP-isolated scFv-Fc bind to antigens in rat brain capillaries. Brain cryosections were labeled with the indicated scFv-Fc proteins (red channel), counter-labeled with fluorescent lectin (green channel) as a capillary marker, and DAPI (blue channel).

There is clear co-localization of the scFv-Fc binding signal (red) with lectin labeling (green) for all clones confirming that the scFv-Fc shown target antigens expressed at the rat BBB *in vivo*. These results demonstrate that the fYDIP procedure can be successfully targeted towards a tissue subfraction of interest resulting in a high correlation between (1) binding of yeast surface displayed scFv to detergent solubilized membrane protein complexes and (2) soluble scFv binding to target antigens in their native context in tissue sections.

3.3.4 Immunoprecipitation, mass spectrometry, and validation of target antigen complexes

While the fYDIP assay with individual clones confirmed that several scFv from the BCPMA library bind to complexes containing biotinylated membrane proteins associated with AP-2, additional information was needed to definitively confirm the functional relevance of the captured complexes. Endocytosis assays on live cells were not feasible as none of the scFv-Fc tested bound to cell surface epitopes (data not shown). As an alternative to functional assays, immunoprecipitation coupled to nanospray liquid chromatography–tandem mass spectrometry (nanoLC-MS/MS) was pursued for de novo identification of antigens. With antigens identified, literature searching could be used to gain insight into their function. BCPMA3-Fc and BCPMA5-Fc were chosen for this analysis with BCPM7-Fc again serving as a control in immunoprecipitation experiments. Lysates from an immortalized rat brain endothelial cell line, RBE4, were used to provide an economical and scalable source of material for immunoprecipitations. Protein G magnetic beads were coated with scFv-Fc and incubated with RBE4 cell lysates to specifically capture antigen complexes. Eluted proteins were first analyzed via anti-AP-2α and streptavidin western blot to verify capture of AP-2 associated membrane protein complexes (Figure 3-6 A). Matching the results of the fYDIP assay, BCPMA3-Fc and BCPMA5-Fc immunoprecipitated complexes containing both biotinylated membrane proteins and AP-2. On the other hand, the BCPM7-Fc complex contained biotinylated membrane proteins but lacked AP-2. These results also confirmed the capture of distinct complexes as the pattern of eluted biotinylated proteins differ between the clones. Eluted proteins from the same

immunoprecipitation reactions were subsequently run on SDS-PAGE and gels stained with coomassie to visualize protein bands (Figure 3-6 B).

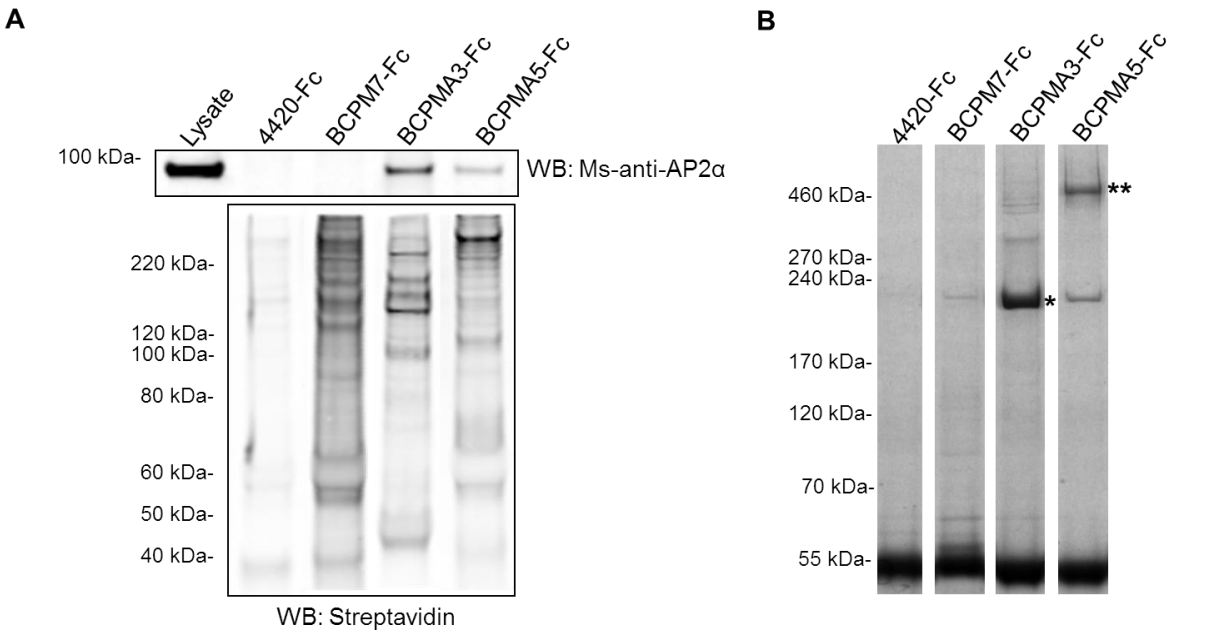

Figure 3-6. Immunoprecipitation of antigen complexes. The indicated scFv-Fc were coated on Dynabeads Protein G and incubated with RBE4 cell lysates to specifically capture antigen complexes. Anti-fluorescein scFv-Fc, 4420-Fc, was used as a negative control. Eluates were analyzed by (A) anti-AP2α or streptavidin western blot and (B) Coomassie gel staining. The starred bands were excised, digested with trypsin, and analyzed via nanoLC-MS/MS. * Specific band identified as Myh9, ** Specific band identified as AHNAK. The intense band seen around 55 kDa in all lanes is the eluted scFv-Fc.

Examination of the coomassie stained gel revealed that the major constituent of the BCPMA3-Fc complex was a protein of about 220kDa (* band in Figure 3-6 B) while a prominent band above 460 kDa (** band in Figure 3-6 B) was observed for the BCPMA5-Fc captured complex. These bands were excised from the gel, digested with trypsin, and resultant peptides were analyzed via nanoLC-MS/MS on an Orbitrap Elite system. Following data processing and Sequest HT database search, the BCPMA3-Fc band was identified as Myosin 9 (Myh9) with 146 unique peptides yielding 64% sequence coverage and a Sequest HT score of 915. The BCPMA5-Fc band was

identified as AHNAK with 250 unique peptides yielding 75% sequence coverage and a Sequest HT score of 733. Peptides used for identification of Myosin 9 and AHNAK are listed in Supplementary Table 3-1.

The protein identification results were further confirmed with follow-up western blotting experiments. Initial testing verified that BCPMA3-Fc could be used as the primary antibody for specific western blot detection of its antigen recognizing a protein of approximately 220 kDa (data not shown) corresponding to the major band seen in the coomassie stained gel. Next, RBE4 cell lysate and elutions from immunoprecipitation of the lysates with BCPMA3-Fc or a generic rabbit IgG (rabIgG) as negative control were simultaneously probed by western blotting with BCPMA3-Fc and a mouse-anti-Myh9 antibody (Figure 3-7 A). BCPMA3-Fc and the anti-Myh9 antibody recognized the same exact protein band in the cell lysate and specific elution product indicating a direct binding of BCPMA3-Fc to Myh9 thereby confirming Myh9 as its antigen. On the other hand BCPMA5-Fc did not work in western blot indicating that it likely recognizes a conformational epitope. Western blotting of RBE4 lysate and elution products from immunoprecipitations with rabIgG, BCPMA5-Fc, BCPM7-Fc, or BCPMA3-Fc was performed with an anti-AHNAK antibody (Figure 3-7 B). AHNAK was only present in the BCPMA5-Fc immunoprecipitation product confirming the specificity of interaction of BCPMA5 with a unique complex containing AHNAK that is not recognized by BCPM7 or BCPMA3. The results of these immunoprecipitation experiments confirm the MS/MS identification of Myh9 and AHNAK. Taken as a whole, the proteomics techniques used to detect members of the captured complexes confirm the following: (1) BCPMA3 binds to Myh9 that interacts with multiprotein complexes containing at least AP-2 and

biotinylated membrane proteins, (2) BCPMA5 binds to multiprotein complexes containing at least AHNAK, biotinylated membrane proteins, and AP-2. As detailed in the Discussion section both Myh9 and AHNAK are intracellular proteins that associate with the plasma membrane and actin cytoskeleton and play known roles in membrane trafficking and endocytosis. Therefore, the proof-of-concept fYDIP screening campaign presented here was successful in isolating antibodies against membrane protein complexes involved in endocytosis.

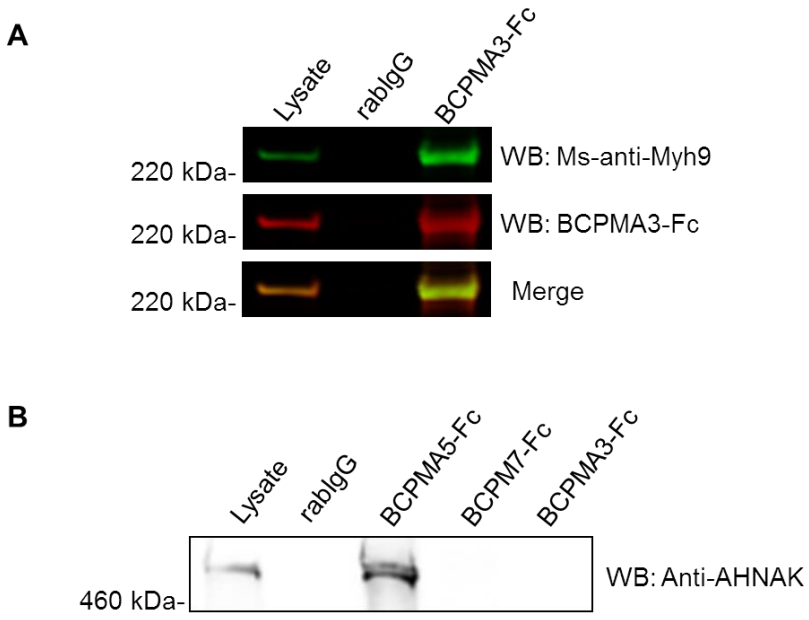

Figure 3-7. Confirmation of MS/MS identification of Myh9 and AHNAK. The indicated antibodies were used to immunoprecipitate complexes from RBE4 lysates as in Figure 3-6. Non-specific rabbit IgG (rabIgG) was used as a negative control. (A) Western blot confirms that Myh9 is the antigen of BCPMA3. Both mouse-anti-Myh9 (green channel) and BCPMA3-Fc (red channel) recognize the same band of approximately 225 kDa in the starting lysate and specific elution product. (B) Western blot confirming BCPMA5 binds specifically to a unique complex containing AHNAK. Anti-AHNAK detection reveals the presence of AHNAK only in the BCPMA5-Fc elution product.

3.4 Discussion

This work demonstrates that the fYDIP method can be used to isolate scFv against membrane protein complexes involved in a cellular function of interest via detection of relevant PPIs captured on the yeast surface. The target of this proof-of-concept study was the endocytosis machinery at the BBB and interaction with the well-studied clathrin mediated endocytosis adaptor protein AP-2 was used as the functional marker during screening. We first confirmed that membrane protein interactions with AP-2 can be captured on the yeast surface and measured using flow cytometry (Figure 3-1). Then, fYDIP screening was employed to enrich a non-immune scFv library for binders to complexes harboring AP-2 PPIs thereby targeting the enrichment of scFv that recognize proteins that function in endocytosis (Figure 3-2). Two rounds of screening for binding to any complex containing biotinylated membrane proteins followed by one round of functional screening resulted in the BCPMA Library which harbored a high frequency of clones binding to complexes containing biotinylated membrane proteins and AP-2 (Figure 3-3). In addition, >50% of scFvs sequenced from the BCPMA Library were unique demonstrating that the fYDIP procedure can yield a diverse antibody population from which to select lead candidates. Finally, two lead candidates, BCPMA3 and BCPMA5, were studied in detail and immunoprecipitation coupled with nanoLC-MS/MS was carried out, identifying Myh9 and AHNAK as prominent members of the captured complexes (Figure 3-6).

Subsequent confirmatory western blot experiments proved a direct binding interaction between BCPMA3 and Myh9 and that BCPMA5 specifically captures a

complex whose major constituent is AHNAK (Figure 3-7). Myh9 is a member of the nonmuscle myosin-2 family of actin-based molecular motors which play essential roles in numerous cellular processes [250]. Importantly, there are several reports in the literature that confirm that Myh9 functions in endocytosis. Three recent proteomics studies have identified Myh9 in complexes containing known endocytosis machinery including both intracellular accessory proteins (e.g. AP-2, AnnexinA2, Clathrin, Eps15) and transmembrane proteins (e.g. ATP13A2, TrpC5, VCAM-1) [251–253]. The circumstantial evidence for involvement in endocytosis provided by these studies has been confirmed in recent reports that used genetic and/or biochemical approaches to perturb Myh9 [254, 255]. For example, siRNA knockdown of Myh9 or inhibition with blebbistatin prevented the endocytosis of ligand activated C-X-C chemokine receptor type 4 (CXCR4) in T-lymphocytes and subsequent GST pulldown assays revealed that Myh9 interacts directly with the cytosolic tail of CXCR4 [255]. A similar body of evidence supports AHNAK's role as a scaffolding protein linking the plasma membrane to the actin cytoskeleton and implicating AHNAK in numerous membrane-related functions including cell-cell adhesion, membrane repair, and endocytosis [256]. For example, AHNAK is recruited to the plasma membrane in a calcium dependent manner via binding to the Annexin A2/S100A10 heterotetramer [257, 258] and this complex is required for phagocytic uptake of *Salmonella typhimurium* by epithelial cells [259]. AHNAK recently gained prominence as a marker of enlargeosomes, helping to regulate the exocytosis of non-secretory vesicles upon membrane disruption in muscle cells [256]. Providing further support for a role in endocytosis, separate proteomic studies have identified AHNAK in complexes containing Myh9 [251], and EGFR [260, 261]. The

literature evidence presented above shows that the fYDIP procedure was successful in isolating scFv that target protein complexes involved in endocytosis validating the original hypothesis that detection of AP-2 PPIs on the yeast surface could be used as a reliable functional readout. Therefore, this work establishes fYDIP as a high throughput screening method capable of isolation of antibodies against PPIs of interest. Given this general approach it may be possible to apply fYDIP to other discovery campaigns where antibodies against PPIs are sought.

Several aspects of the fYDIP platform provide distinct advantages over alternative methods for PPI screening and anti-PPI antibody discovery. First, this platform integrates the discovery of antibodies in-line with PPI screening which is not the case with other high throughput methods such as two hybrid-based assays [262], protein microarrays [242], or proteomic phage display [263]. Furthermore, most high throughput PPI studies require application of tags to individual bait and prey proteins or protein libraries and subsequent exogenous expression in host cell lines. These artificial manipulations can alter the nature of PPIs and also limit the application of these methods in animal models. On the other hand, fYDIP requires no such genetic manipulations and is capable of high throughput PPI screening and antibody discovery using target antigens from animal sources. In the arena of discovery of antibodies and peptides against protein functions of interest, particularly endocytosis, phage display has been the predominant method of choice [264]. Whereas fYDIP yields a diverse pool of lead candidates, *in vitro* phage screens for internalizing antibodies or peptides often result in libraries dominated by a small handful of clones [67, 79]. In addition, we have shown here and in previous work [240] that YDIP is compatible with antigen

preparations derived from animal sources yielding a high percentage of antibodies that target *in vivo* relevant antigens. While in vivo phage screens such as the IV injection of a library and recovery of target organs have been carried out [117, 265], high levels of non-specific phage binding has limited their success. iPhage has recently been introduced for the receptor-independent uptake of phage displayed peptide libraries in cells and subsequent selective enrichment of peptides targeting subcellular compartments of interest via fractionation techniques [266]. While iPhage has garnered much attention given the ability to isolate peptides against subcellular compartments of interest, this platform cannot enrich for peptides that target specific functional complexes because the enrichment is solely based on subfractionation of organelles from lysed cells. On the other hand, the current work shows that fYDIP can target a subcellular proteome of interest (e.g. the plasma membrane) and further identify a subfraction of that proteome based on functional markers. In the future, it may be possible to extend fYDIP to target various organellar interactomes using proximity-based tagging methods [267, 268].

Finally, it is notable from the BBB biology standpoint that both Myh9 and AHNAK expression are specifically upregulated at the BBB compared with other CNS cell-types [54, 269, 270] and both proteins have been identified in a previous BBB membrane proteome study [61]. The brain section immunofluorescence data presented here are in agreement with these studies as we observed specific staining of the brain vasculature by both BCPMA3-Fc and BCPMA5-Fc with limited reactivity to parenchymal antigens (Figure 5). This highlights the ability of fYDIP to reliably enrich scFv against relevant proteins from the target proteome of interest. Identification of antigens isolated via

fYDIP could also motivate further study into their overall role in the target tissue. For example, in addition to their roles in endocytosis, both AHNAK and Myh9 are implicated in the establishment and maintenance of barrier properties [270–273]. In the case of AHNAK, Gentil and co-workers showed that AHNAK is selectively expressed in barrier forming endothelial cells at the BBB and co-localizes with the tight junction protein ZO-1 [270]. To date, Myh9's role in barrier integrity at the BBB has not been studied but several reports in the literature have suggested it plays an important role in the establishment and maintenance of apical junction complexes in intestinal epithelium [271, 272, 274]. In the future, further study of both AHNAK's and Myh9's function in the brain endothelium should be pursued to better understand their role in barrier integrity and membrane trafficking at the BBB.

Supplemental Table 3-1: Peptides used for identification of Myosin 9

Sequence	Sequence	Sequence
NAEQFKDQADKASTR	RQAQQERDELADEIANSSGK	LTEmETmQSQLmAEK
SmmQDREDQSILcTGESGAGKTENTK	NKHEAMITDLEER	NTDQASMPDNTAAQK
SmmQDREDQSILcTGESGAGK	QAQQERDELADEIAnSSGK	HLAAENR
TLEDEAKTHEAQIQEMR	VEEEAAQKNmALK	VVQEQGTHPK
IAQLEEQLDNETKER	EmEAELEDERKQR	nAEQFKDQADK
KmEDGVGcLETAEEAKR	ELEDATETADAmNR	HEAMITDLEER
RQLEEAEEEAQR	QIATLHAQVTDmK	VKVNKDDIQK
KANLQIDQINTDLNLER	EMEAELEDERKQR	ALEQQVEEmK
EQLEEEEEAKRNLEK	DFSALESQLQDTQELLQEENR	LQEmESAVK
DLQGRDEQSEEK	TDLLLEPYNKYR	QVREmEAELEDER
AKQTLENERGELANEVK	DLEAHIDTANKNR	DDVGKSVHELEK
DLEAHIDTANKNREEAIK	KLVWVPSTK	ELETQISELQEDLESER
RGDMPFVVTR	KDQGELER	cQYLQAEKK
SmEAEmIQLQEELAAAER	THEAQIQEmR	LQEMESAVK
VEEEEERcQYLQAEKK	TEmEDLmSSKDDVGK	DVLLQVEDER
KLEEDQIIMEDQNcK	ALLQGKGDSEHK	LEVNLQAMK
KGTGDcSDEEVDGKADGADAK	EmEAELEDERK	EEAIKQLR
ELEDATETADAMNR	ERNTDQASmPDNTAAQK	DVLLQVEDERR
KEEELQAALAR	NTDQASmPDNTAAQK	RGDmPFVVTRR
QLEEAEEEAQRANASRR	EmEAELEDER	TDLLLEPYNK
ALEEAMEQKAELER	NLPIYSEEIVDMYK	EQEVSILKK
ASREEILAQAKENEK	HEAmITDLEER	TLEDEAKTHEAQIQEmR
KVEAQLQELQVK	cQYLQAEK	IMGIPEDEQMGLLR
KLEEDQIImEDQNcK	NmDPLNDNIATLLHQSSDK	LKDVLLQVEDERR
ERnTDQASmPDNTAAQK	ImGIPEDEQMGLLR	SMMQDREDQSILcTGESGAGK
QLEEAEEEAQRANASR	LKQMEDEKNSFR	FLSNGHVTIPGQQDKDmFQETmEAmR
ERNTDQASMPDNTAAQK	VAEFTTNLMEEEEKSK	AKQTLENER
DLEGLSQRLEEK	IIGLDQVAGmSETALPGAFK	TEmEDLMSSK
VRTELADKVSK	LTEMETmQSQLmAEK	IIGLDQVAGMSETALPGAFK
VEEEEERcQYLQAEK	TEMEDLMSSKDDVGK	DcmRELDDTR
KmEDGVGcLETAEEAK	HSQAVEELAEQLEQTKR	GALALEEK
QTLENERGELANEVK	QLEEAEEEAQR	RGDmPFVVTR
ATDKSFVEK	EMEAELEDERK	VEEEAAQK
mEDGVGcLETAEEAKR	AKLQEMESAVK	TEMEDLMSSK
QAQQERDELADEIANSSGK	TEmEDLmSSK	NLPIYSEEIVDmYK
mQQNIQELEEQLEEEESAR	DVDRIIGLDQVAGmSETALPGAFK	ALLQGKGDSEHKR
TEmEDLMSSKDDVGK	YKASIAALEAK	QLEEAEEEAQRAnASR
EEILAQAKENEK	KMEDGVGcLETAEEAK	ANLQIDQINTDLNLER
VAEFTTNLmEEEEKSK	ASREEILAQAK	VKPLLNSIR
LQVELDSVTGLLNQSDSK	TELADKVSK	EQLEEEEEAK
TVGQLYKEQLAK	QIATLHAQVTDMKK	GELANEVK
ITDVIIGFQAccR	EMEAELEDER	VNKDDIQK
SMEAEmIQLQEELAAAER	DELADEIANSSGK	ALEQQVEEMK
REQEVSILKK	QFRTEmEDLmSSKDDVGK	FLSnGHVTIPGQQDKDmFQETmEAmR
LKQmEDEKNSFR	ALELDSNLYR	LKSmEAEmIQLQEELAAAER
QIATLHAQVTDmKK	EEELQAALAR	ALEEAmEQK
THEAQIQEMR	qLEEAEEEAQR	LQRELEDATETADAMNR
ALEEAmEQKAELER	QMEDEKNSFR	LEEDQIImEDQNcK
NTDqASmPDNTAAQK	QmEDEKNSFR	LKQMEDEK
KQELEEIcHDLEAR	KLEMDLK	YEILTPNSIPK
LQKDLEGLSQR	mEDGVGcLETAEEAK	IAQLEEELEEEQGNTELINDR
HEmPPHIYAITDTAYR	ASIAALEAK	LVWVPSTK
EQLEEEEEAKR	VAAYDKLEK	ImGIPEDEQmGLLR
NAEQFKDqADKASTR	MEDGVGcLETAEEAKR	NFINNPLAQADWAAK
LKKLEEDQIImEDQNcK	VEEEAAQKNmALKK	TEmEDLmSSKDDVGKSVHELEK
NKHEAmITDLEER	QIATLHAQVTDMK	IAQLEEELEEEQGNTELINDRLK
LQRELEDATETADAmNR	EEILAQAKENEKK	VISGVLQLGNIVFK
QLLQANPILEAFGNAK	KKMEDGVGcLETAEEAK	VVFQEFR
NAEQFKDQADK	LEVNLQAmK	LTEmETMQSQLMAEK
SMmQDREDQSILcTGESGAGK	KKLEmDLK	VISGVLQLGNIVFKK
VSHLLGINVTDFTR	MEDGVGcLETAEEAK	AKLQEmESAVK
HEDELLAK	KMEDGVGcLETAEEAKR	IAQLEEQLDnETKER
KKVEAQLQELQVK	EQADFAIEALAK	AQTKEQADFAIEALAK
DLEAHIDTANK	LEEDQIIMEDQNcK	SKKDQGELER
RQQQLTAMK	VAEFTTNLmEEEEK	QIATLHAQVTDmKKK
KKmEDGVGcLETAEEAK	VEAQLQELQVK	

Supplemental Table 3-2: Peptides used for identification of AHNAK

Sequence	Sequence	Sequence	Sequence
VKGEYDVTMPK	VKGDVDmSLPK	FKmPDmHFK	ISmPDFDLNLKGPK
VKGDMDVSLPK	ISMPDFDLNLK	LGGGEVDLR	GSSLQGDLAVSGDIK
ISMPDFDLNLKGPK	MDIDTPDIDIHGPEGK	VQTPEVDVK	AEGPEVDVSLSK
VSVGTPEVSVEALEGGVK	VEGDLKGPEIDIEcPEGK	VDVKGPELDISASK	ISMPNIDLNLKGPK
SAKVDIDVPNVDAQGPELHmK	FKmPFLSISSPK	GEGPELDVSmPK	FSIPGVKGEGADVNVPLAK
AEGPEVDVSLSKADLDVSGPK	GHYEVTGSDDEAGKLQGSGVSLASK	ISmPDVDLHmKGPK	MDIDVPDVNIEGPEGK
VDIDVPDVDVQGPDWHLK	GDVDVSLPK	GEYDVTVPR	VDIDVPDVNIEGPDAK
VDIDVPNVDAQGPELHmK	GPEVDVKGPK	LKSGVDVSLPK	TPNVGISGPK
FSmPGFKAEGPEVDVNLQK	VKGDmDVTVPK	VPGVEAAGPK	ISmPDFDLNLKGSK
VKGEYDVTmPK	VKIPTmKmPK	ISmPDFDLNLK	GHYEVTGSDDEAGKLQGSGVSLASKK
FKmPEINIK	VKGDmDISVPK	VDVKVPDVNTEGLEGK	KPDVDVTAPK
ISMPDIDLNLKGPK	LHAPGLDmK	APAVDLKGPK	GEGADVNVPLAK
ISMPnIDLNLKGPK	GPQITGPSLK	TPQISmSDIDLNmKGPK	GPSLKGDVAASSPSmK
ISMPDVGLNLKGPK	VKGDVDISGPK	VKGPEVDVKGPK	GKGGIDVTLPK
mPDMHFK	FQVTVPGTK	SGVDVSLPK	mDIDVPDVNIEGPEGK
mPDVHFK	VKGDVDISLPK	VSSGQISGPEIKGDLK	VDINAPEVEVQGK
VDIDVPDVNVDGPDmK	LEGELKGPK	GNVDMSAPK	GPSVDVEVPDVDLEcPEAK
GGIQVPGVDVSSSLGGGSVEGQGPSLQSGDIGK	FGmPGFK	AESPEVEMNLPK	ISmPDIDLNLKGSK
LKMPDmHVNmPK	FTFSKPK	LEGDLKGPK	GGVDVSGGVSVPDINLGEGHmNVK
ADLDVSGQKVDIDVPDVNIEGPDAK	MPEMNIK	IEGnLKGPK	VTAYTVDVTGR
LKFGTFGGLGSK	VGGEIKAPAVDLKGPK	VKGDmDVAVPEIEGEmK	VSSGQISGPEIK
LKMPEmNIK	GPNVDmSGPDVEIEGPEGK	FKmPEmHFK	VDIEVPDVNIEGPEGK
MPDLHLK	MPSLEVPVPK	LKGPQITGPSLK	IKTPSFSVSAPQVSIPDVNVK
FTmPSLKGEGPELDVSMPK	TPQISMSDIDLNmKGPK	LKGPDINLPEGSVK	GEGVGIDVALPTGK
mPEmNIKPQK	MPDMHFK	ADIDVSGPK	RVTAYTVDVTGR
FSMPGFK	FKmPEmNIKAPK	AnIDVSGPK	ISMPDLHLKGPK
FKmPEmNIR	VKIPTmK	GFGVDTETPNLEGTLTGPK	VGSLDVNVK
GDVPSVGLEGPDVDLQGPEGK	GDVAASSPSmK	mPSLEVPVPK	VEGEIKVPEVDIK
ISMPDLHLK	MKGNVDMSAPK	ISMPDVDLELKGPK	AEGPEVDVSLPK
MEGPGVDIDSPDVNIEGPEGK	GGIDVTLPK	ANIDVSGPK	GPEIDmKGPGLDFEGPDAK
FKmPEmNIK	ISMPDLNLNLK	AEGPDVAVDLPK	ISmPDIDLHLKGPK
LKmPEmNIK	GFGGEWKGPQVSSSVNLDTTK	LEGDLKGTK	LKKPDVDVTAPK
VDIDVPDVNVDGPDMK	VSGPDLDLNLKGPSLK	GDVAASSPSMK	VEGDLKGPEVDIKGPK
GPQISAPGMDFNLEGPK	VSGPDLDLNLK	VKTPEMIVQKPK	VKGELDATVPNLEGDFKSPK
GDVDMSLPK	LEGELKGPELDVK	VPEVDIKGPK	VPDVNTEGLEGK
GPDINLPEGSVK	GDmDVTVPK	GSLGATGELK	ISmPDVDLNLKGPK
ISmPDIDLHLKSPK	VDVDAPDVDVQGPDWHLK	AGAISASGPELEGASHSK	VQANLDTPDINIQGPEAK
mPEINIK	VKGDVDASLPK	ISmPDIDLHLK	VKGELDATVPNLEGDFK
VDVDVPDVDVQGPDWHLK	LVGNLHFSGPK	ISMPNIDLNLK	LDANIPEVAVEGPEGK
GPSVDVDVPDVDLEcPEAK	LHAPGLDMK	ISmPDLNLNLKGPNVK	ISmPDIDLNLKGPK
ISMPDVDLHLK	FTmPSLKGEGPELDVSmPK	FSmPGFKAEGPEVDVSLSK	ISmPnIDLNLKGPK
mPFLSISSPK	FGmPGFKAESPEVEmNLPK	GDLGLKGTK	mEGPGVDIDSPDVNIEGPEGK
ISmPDFDLHLK	ISmPNIDLNLK	GGVTGSPEASVSGSKGDLK	DDGVFVQEVMQNSPAAR
ISmPDLHLK	TPEmIVQKPK	VDIDVPDVNIEGPEGK	ISmPDVDLELKGPK
GAFDGSVPK	ISmPDVDLNLK	FKAEAALPSPK	LDVNAPDIDIHGPEGK
ADIDVSGPKVDVK	IEGNLKGPK	FKmPSmSIQTHK	LQGNIGmDDAcASK
MPEMHFK	VKGAFDGSVPK	VDIDISGTK	ISmPDVDLHLKGPK
ISMPDIDLNLKGSK	VEVSAPDVSIEGPEGK	mSLPDVDLDLKGPK	VSGTDATAALSVGAPDVTLK
GDVDASLPK	VQIGADGVK	AEGPEVDVNLQK	VTLPGVSGDVNLPEIATGGLEGK
AKGLDLGGK	FKMPEMNIK	ASLGSLEGEAEAETSSPK	SNSFSDEREFSAPSTPTGTLEFAGGEGK
mKGNVDmSAPK	APDVQLNAPDVDVHGQEWNLK	GPELDISASK	ANIDVSGPKmDIDVPDVNIEGPEGK
VGGEIKAPAVDLK	GPSFNmASPESDFGVSLK	ISmPDVGLNLK	ISmPDVGLNLKGPK
AEYDVSVPK	VKGPEVDVK	FGTFGGLGSK	ISmPNIDLNLKGPK
GPSLKGDVAASSPSMK	VPEVDIK	GGVKGPQVAVK	ISmPDFDLHLKGPK
FKMPEmNIK	LEGDIKTPK	AESPEVEmNLPK	LQGNIGMDDAcASK
mPEmHFK	FSVSGVKAEGPDVAVDLPK	VDVSAPDVDVHGPDWNMK	VEGEIKVPEVDIKGPK
ISMQDVDLSLGScK	VKGEYDVTTPK	ISmPnIDLNLK	ISmPDVDLnLKGPK
VEGDLKGPEVDIK	SKGHYEVTGSDDEAGKLQGSGVSLASK	ISmPDLnLNLK	ISmPDVSLNLKGPK
FKmPDmHFKAPK	IKGDVDVSLPK	ISmPDIDLNLK	AEGEIKVPDVELK
LKGEIDASVPEmEADLRGPQIDVK	FSmPGFK	FSASGSKGEGVGIDVALPTGK	ISmPDLHLKGPK
VKGDmDVSLPK	GDISLSGPK	LDISAPDLNLEGPEGK	GPQVSSSVNLDTTK
GDVDISLPK	VKGDVDMSLPK	GPQISAPGmDFNLEGPK	ISMPDVDLNLKGPK
FSMPGFKAEGPEVDVSLPK	ADLDVSGPKVDIDVPDVNIEGPDAK	ISmADVDLNVAAPK	VEGDLEGPHVDIKGPK
mPEmNIR	LGGGEVDLRGPK	ISmPDVDLHLK	VSmPDVELNLKGPK
MPEmNIR	MSLPDVDLDLKGPK	GKGGIDVTLPKVEGK	VNVEAPDVNVEGLGGK
ISmPDVDLHMK	VDINAPDVDVQGPDWHLK	mKGNVDMSAPK	GGVTGSPEASVSGSK
MPFLSISSPK	ADLDVSGPKVDIDVPDVNIEGPEGK	GPGLDFEGPDAK	SSEVVLSGDDEDYQR
VDVSAPDVDVHGPDWNmK	VEAPDVEVHGPDWHLK	VDTDIPQVDVHGPNLK	GGQIGLQGPGLSVSGPQGHLESGSGK
VPDVDIKGPK	VKGDVDVSLPK	GPNVKGEYDVTVPR	SEDGVEGDLGETQSR
mPEmNIK	GSGIGLHGAVPDLSVK	AEGPEVDVNLPK	TDISAPGVEVHGPEWNLK
ADVDISVPK	FSmPGFKAEGPEVDVSLPK	DDGVFVQEVmQNSPAAR	GKGGVTGSPEASVSGSK
TPEMIVQKPK	EGVKDIDISSPEFmIK	ISmPDVDFNLKGPK	LPSGSGAASPTTGSAVDIR
mPDmHFKAPK	VSmPDVELNLK	mDIDTPDIDIHGPEGK	LRSEDGVEGDLGETQSR
MPDVHFK	GPGVDLPSVDLSLPK	ADLDVSGQK	TVIRLPSGSGAASPTTGSAVDIR
GDVDmSLPK	GDLKGSGIGLHGAVPDLSVK	GKGGVTGSPEASVSGSKGDLK	HEVTEISNTDVETQPGK
GHYEVTGSDDEAGK	GPSFNmASPESDFGVSLKGPK	ISGPDANVHLK	ISmPDVSLNLK
GKFSLFK	ISmQDVDLSLGScK	FKVPGVEAAGPK	ISmPDVDFNLK

Chapter 4 Creation and screening of a blood-brain barrier immunized library yields variable lymphocyte receptors that target the brain vasculature *in vivo*

In this chapter we describe the creation of a blood-brain barrier immunized lamprey variable lymphocyte receptor library and subsequent development and application of an innovative two-step yeast display-based screening platform to efficiently enrich the library for binders to extracellular membrane protein epitopes expressed at the *in vivo* blood-brain barrier.

4.1 Introduction

The brain vasculature, also known as the blood-brain barrier (BBB), is substantially more impermeable to blood-borne constituents than peripheral vasculature. Continuous paracellular tight junctions between ECs combine with a low level of pinocytosis to largely exclude the nonspecific brain uptake of molecules, proteins and cells, while a host of drug efflux transporters serve to actively pump undesired molecules that do enter the BBB ECs, back into the bloodstream [10]. While these barrier functions are essential in health, they present a significant challenge when attempting to treat neurological disorders because the majority of small molecule therapeutics and essentially all gene and protein-based drugs do not appreciably cross the BBB [5]. Therefore, effective non-invasive drug delivery strategies that can overcome this barrier are essential for the successful development of central nervous system (CNS) therapeutics.

As a result of the prominent barrier function, the BBB endothelia express numerous transport systems to facilitate brain uptake of key nutrients such as glucose and amino acids as well as proteins such as transferrin and insulin [138]. Importantly, it is possible to coopt certain endogenous receptor-mediated transport systems, such as the transferrin receptor (TfR), and insulin receptor (IR), for the delivery of drug payloads across the BBB using receptor-targeting antibodies or ligand mimics [243]. Although pharmacologic amounts of drug can be successfully delivered to the brain by targeting these receptors, several factors combine to limit their efficiency. Ubiquitous expression of TfR and IR throughout the body results in misstargeting to peripheral organs, limiting brain uptake and increasing the potential of off-target effects [34, 38]. Furthermore, affinity- and avidity-based interactions can result in lysosomal degradation of antibodies within the BBB ECs, further limiting access to the brain [42, 224]. While efforts to engineer the binding properties of TfR targeting antibodies has shown some success [41, 43, 275], typically less than 1% of the injected dose of therapeutic antibody reaches the brain parenchyma despite high concentration dosing (up to 50 mg/kg). Thus, there remains a significant need for discovery and development of novel BBB receptor targeting antibodies capable of overcoming the challenges listed above.

Genomic and proteomic profiling of BBB ECs is one approach that has been implemented to identify new BBB transport systems as described in a recent study where basigin and CD98 heavy chain were identified as potential drug carriers [64]. However, it is often difficult to determine what BBB receptors are actually capable of transport simply from sequence data as non-canonical transporters have been identified [64, 67, 111] motivating others to use phenotypic screening of large combinatorial

antibody or peptide repertoires both *in vitro* and *in vivo* to identify BBB targeting molecules [216]. However, despite considerable screening efforts, few new targeting reagents have been generated [216]. For example, there has been limited success using *in vivo* screening approaches, such as the IV injection of phage libraries [265], likely due to high phage background binding and phage uptake by peripheral organs. Furthermore, promising clones identified from *in vitro* screening platforms, such as phage and yeast display biopanning on cultured cells, often do not cross-react with *in vivo* antigens [93] as a result of altered expression profiles of BBB ECs in the petri dish [102, 103]. To date, the antibody libraries employed have been limited to nonimmune mammalian antibody fragments and nonimmune libraries tend to yield lower affinity lead molecules compared to libraries of comparable size derived from immunized animals [70, 123]. Furthermore, screening of immunized mammalian antibody libraries against mammalian antigens is inherently problematic given that self-tolerance to highly conserved protein and carbohydrate epitopes limits the diversity of accessible targets [124]. Therefore, the search for new BBB targets would benefit from the development and application of innovative screening platforms with the ability to more broadly and efficiently sample the *in vivo*-relevant BBB antigen landscape.

In this work, we developed a new screening platform to address many of the aforementioned challenges. First, we deployed a recently discovered family of highly diverse antibody-like proteins composed of leucine-rich repeats termed Variable Lymphocyte Receptors (VLRs) that function as antigen receptors in the adaptive immune system of lamprey [130]. VLRs possess diversity, specificity, affinity, and stability comparable to traditional Ig-based antibodies [128, 129]. Importantly, lampreys

last shared a common ancestor with mammals >500 million years ago, and this tremendous phylogenetic distance combined with the unique crescent-shaped geometry of the antigen-binding site may enable VLRs to recognize new antigenic targets, including highly conserved proteins and carbohydrates that are not recognized by mammalian antibodies. Next, to create a library of VLRs against *in vivo*-relevant BBB antigens, we immunized lamprey with endothelial plasma membranes fractionated from mouse brain capillaries, and the immune VLR repertoire was subsequently imported into the yeast surface display platform and subjected to further filtering. The immune VLR library was first screened against detergent-solubilized versions of the same brain EC membrane preparations used for immunization to ensure enrichment of clones against *in vivo*-relevant antigens. Subsequently, biopanning of this enriched pool on a cultured mouse brain EC line was used to enrich VLRs targeting extracellular epitopes. The resultant pool contained a reasonably diverse cohort of *in vivo*-relevant BBB cell surface-binding VLR clones including a subset that target, endocytose, and traffic into brain endothelial cells *in vivo*.

4.2 Materials and Methods

4.2.1 Cells, media, and plasmids

Saccharomyces cerevisiae strain EBY100 was used for VLR surface display. The plasmid used for VLR library cloning and display was pCT-ESO. For all yeast surface display experiments, EBY100 yeast were first grown overnight at 30ºC 260 rpm in SD-CAA media (20 g/L dextrose, 6.7 g/L yeast nitrogen base, 100 mM sodium phosphate buffer pH 6.0, 5.0 g/L bacto-casamino acids without tryptophan and uracil). The day

before an experiment all yeast cultures were re-set to an OD_{600} of ~0.4 and grown for 3-4 hours until reaching an OD_{600} of 1. Then, surface display was induced via switching to SG-CAA induction media (same recipe as SD-CAA except galactose is used instead of glucose) and cultures were grown at 20ºC, 260rpm for 16-18 hours. HEK293F cells were purchased from ATCC (CRL-1573) and maintained in Freestyle F17 Medium (Thermo Fisher) at 37ºC, 8% CO_2, and 135 rpm in a humidified incubator. The pIRES-rFc vector was a kind gift from Dr. Brantley Herrin at Emory University. bEnd.3 cells at passage 22 were purchased from ATCC (CRL-2299) and maintained in complete growth media (DMEM supplemented with 4 mM L-glutamine, 4500 mg/L glucose, 1 mM sodium pyruvate, 1500 mg/L sodium bicarbonate, and10% fetal bovine serum) at 37ºC, and 5%CO_2 in a humidified incubator up to passage 30.

4.2.2 Animals

Male C57BL/6 mice (*Mus musculus*) at 6 to 7 weeks of age were purchased from Envigo and used in terminal experiments. All mouse experiments were approved by the UW-Madison Institutional Animal Care and Use Committee (IACUC). Sea lamprey larvae (*Petromyzon marinus*) captured from the wild by commercial fishermen (Lamprey Services, Ludington, MI) were maintain in sand-lined, aerated aquariums at 16-20ºC and fed brewer's yeast. All lamprey experiments were approved by the Emory IACUC.

4.2.3 Capillary isolation, plasma membrane fractionation, and quality analysis

Brains were removed from 6-7 week old male C57BL/6 mice (~20g) and stored in DMEM on ice. Microvessels were isolated and endothelial plasma membranes

fractionated essentially as previously described [247]. Briefly, the cerebellum and white matter were dissected away and brains were rolled on Whatman 3MM chromatography blotting paper to remove the meninges. Up to 15 brains were homogenized in 20 mL DMEM+0.2%BSA in a dounce homogenizer, and the homogenate was passed over a 150 μm nylon mesh to remove large debris. The homogenate was mixed with an equal volume of 40% dextran solution and centrifuged at 5,000xg for 15 minutes at 4ºC. The supernatant was discarded, and the crude microvessel pellet was resuspended in DMEM+0.2% BSA. Microvessels were then recovered on 41 μm nylon mesh filters and washed twice with PBS. To prepare biotinylated plasma membrane proteins for yeast display library screening, microvessel membrane proteins were biotinylated prior to plasma membrane fractionation via incubation with 5 mM sulfo-NHS-LC-biotin (Thermo Fisher), which is membrane impermeable, for up to 2 hours at 4ºC. Unreacted biotinylation reagent was quenched by addition of glycine to a final concentration of 100mM and 10 minutes incubation on ice. Biotinylated microvessels were washed twice with PBS+100mM glycine to ensure complete quenching and removal of unreacted groups. Plasma membranes prepared for lamprey immunization were not biotinylated. Endothelial plasma membranes were fractionated from the purified microvessels via a two-step hypotonic lysis: (1) distilled water at 4ºC for 2 hours and (2) 10 mMTris-HCl pH 7.4 at 4ºC for 30 minutes. This was followed by sonication in 50mM Tris-HCl pH 7.4 and centrifugation at 25,000xg. This resulted in a supernatant containing dispersed plasma membrane fragments and a pellet containing the capillary basement membranes. The supernatant fraction is referred to as brain capillary plasma membranes (BCPM) and

used for lamprey immunization and yeast display screening. All buffers contained protease inhibitor cocktail (PIC; 11836170001, Roche) and 2 mM EDTA. Total protein concentration in all fractions was quantified using a BCA assay kit (Thermo Fisher) following the manufacturer's instructions. This isolation procedure yielded 255±35µg of brain BCPM proteins from 15 mice. For quality analysis of the plasma membrane fractionation via western blotting, 10µg of total protein from each fraction was separated via SDS-PAGE and transferred to nitrocellulose. Western blotting for brain capillary endothelial membrane marker Glut1 was carried out using a 1:1000 diluted rabbit anti-Glut1 pAb (PA1-46152, Thermo Fisher). Western blotting for astrocyte endfoot marker GFAP (astrocyte endfeet are tightly associated with the basement membrane) was achieved with a 1:1000 dilution of mouse-anti-GFAP mAb (556329, BD Biosciences). Further quality analysis was achieved via γ-glutamyl-transpeptidase (GGT) activity assay as previously described [276].

4.2.4 Lamprey immunizations

Sea lamprey larvae were sedated with 0.1 g/L tricainemethanesulfonate (Tricaine-S; Western Chemical, Inc.), then injected into the coelomic cavity with 50 µg of BCPMs in 30 µl of PBS. Three lampreys were immunized a total of three times at two week intervals and blood was collected two weeks after the final immunization from lampreys euthanized with 1 g/L Tricaine-S. Approximately 200 µl of blood was collected in 200 µl of PBS containing 30 mM EDTA as an anticoagulant. Blood plasma and leukocytes were separated from erythrocytes by layering the blood on top of 55% Percoll and centrifugation at 400xg for 5 minutes. Erythrocytes pelleted to the bottom

of the tube, while leukocytes collected at the 55% Percoll interface and plasma remained above the interface. Buffer was added to the plasma samples to a final concentration of 20mM MOPS/0.025% sodium azide pH 7.5 and stored at 4ºC. Leukocytes were stored in RNAlater at -80ºC until needed for VLRB cDNA library cloning.

4.2.5 VLR library cloning

RNA isolated from total leukocytes using the Qiagen RNeasy kit was reverse transcribed into cDNA using SuperScript III reverse transcriptase (Invitrogen) and oligo-dT priming. VLRB transcripts were amplified from the leukocyte cDNA by nested PCR using KOD high-fidelity DNA polymerase (Novagen). The first round of PCR utilized primers to the 5' and 3' untranslated region, (CTCCGCTACTCGGCCTGCA) and (CCGCCATCCCCGACCTTTG), respectively. The second round of PCR used primers that amplified only the VLRB antigen-binding domain from the LRRNT (GCATGTCCCTCGCAGTG) to the LRRCT (CGTGGTCGTAGCAACGTAG), and 50bp of sequence homology to the yeast surface display vector was added to each primer for cloning by in vivo homologous recombination in transfected yeast cells. PCR products were excised from 1% agarose gels, purified using the Promega Wizard gel extraction kit and eluted in water. The pCT-ESO-BDNF yeast surface expression plasmid was digested with NheI, BamHI and NcoI to linearize the vector and remove the BDNF insert. Prior to transformation with the VLR library, yeast were grown to log-phase in SD-CAA media 30ºC until the culture density reached ~1 OD_{600}. The yeast cells were harvested by centrifugation at 1,000xg, washed in Milli-Q water, and then incubated in

10 mMTris/10 mM DTT/100 mM LiOAC, pH 7.6 at 225 rpm 30ºC for 20 min. After the incubation, the yeast cells were washed in Milli-Q water and re-suspended in 1 M sorbitol at $1x10^9$ cells/ml. 200 µl of yeast cells were mixed with 1 µg of digested vector and 2 µg of the purified VLRB PCR product and added to a 0.2 cm electroporation cuvette on ice. The yeast were electroporated at 2.5 kV (12.5 kV/cm) using a Biorad Micropulser. After electroporation, the yeast cells were incubated in a 1:1 mixture of 1 M sorbitol and YPD media (Fisher Scientific) at 30ºC for 1 hr, then transferred to SD-CAA media. A small aliquot of the electroporated yeast cells was serially diluted in SD-CAA media and plated on SD-CAA agar plates to calculate the total number of transformants. Three electroporated samples were combined resulting in a library of $7.5x10^6$ VLR clones. Aliquots of the yeast library were stored at -80ºC in 15% glycerol.

4.2.6 YSD library screening with detergent solubilized BCPM proteins

VLR display libraries and negative control yeast displaying VLR-RBC36 [277] were grown and induced as described above for each round of YSD screening. Two rounds of screening via the YDIP method were carried out as previously described [238] with modifications. In each round, ~250 µg freshly isolated biotinylated BCPM proteins were solubilized in a final volume of 1 mL PBS containing PIC, 2 mM EDTA, 1mM Biotin, 1% w/v BSA, and 1% v/v TritonX-100. To ensure complete solubilization of membrane proteins the mixture was incubated for 15 minutes at 4^0C and insoluble debris was removed via centrifugation. The first round of screening was carried out using a magnetic activated cell sorting (MACS) protocol [248] to recover VLR binding to biotinylated BCPM antigens. Briefly, $2.1x10^8$ yeast, 30-fold excess of starting library

size, were incubated with 1 mL detergent solubilized BCPMs for two hours at 4^0C with rotation. Yeast were then washed twice with 1mL ice cold PBS+1% TX-100+1%BSA (PBSTXA) and once with ice cold PBS+1% BSA (PBSA). Washed yeast were resuspended in 0.5mL ice cold PBSA, then 50 µL streptavidin microbeads (Miltenyi, 130-048-102) were added, and the mixture was incubated at 4^0C with rotation for 30 minutes. Microbead-bound yeast were washed once with 1 mL PBSA and resuspended in 0.5 mL PBSA. The 0.5 mL microbead-yeast suspension was applied to an LS column (Miltenyi, 130-042-401) placed within a Midi-MACS separator magnet (Miltenyi, 130-042-302). The column was washed twice with 3 mL ice cold PBSA, removed from the magnet, and yeast were eluted via plunging with 3mL SD-CAA media. Dilutions of the eluate were plated to count the number of yeast recovered and the remaining yeast regrown for subsequent screening. In the second round of screening fluorescent activated cell sorting (FACS) was employed to further enrich for BCPM binders. $5x10^7$ yeast were incubated with 0.5mL detergent solubilized BCPMs for two hours at 4^0C with rotation. Full length VLR expression was detected via labeling with a rabbit-anti-cmyc epitope Ab (PA1-981, Thermo Fisher) followed by a goat-anti-Rabbit IgG-Alexa488 secondary Ab (A-11008, Thermo Fisher). Binding to biotinylated BCPM antigens was detected by labeling with a mouse-anti-biotin Ab (BTN.4, Labvison) followed by a goat-anti-mouse IgG-allophycocyanin Ab (A-865, Thermo Fisher).$3x10^7$ labeled yeast were sorted on a Becton Dickson SORP FACSAriaII (University of Wisconsin Carbone Cancer Center) to recover yeast double positive for VLR expression and BCPM antigen binding, and the sorted yeast were expanded in SD-CAA.

4.2.7 YSD library biopanning

A two-step biopanning method was developed and applied to remove extracellular matrix (ECM) binding VLRs from the FACS-sorted library, while enriching for VLRs that bind to extracellular epitopes using the bEnd.3 mouse brain endothelial cell (MBEC) line. For each round, two substrates were used for biopanning. One 6-well plate containing decellularized ECM from bEnd.3 culture was prepared by growing cells to ~90% confluence then switching the cells to media supplemented with 5% ~500kDa dextran sulfate (DxS; 433240050, Acros Organics) to promote robust ECM deposition [278]. After 4-6 days in DxS, cells were washed with PBS and plates were decellularized via a non-enzymatic protocol to leave behind intact ECM [279, 280]. This plate was used in the ECM subtraction step. A second plate containing bEnd.3 cells grown to confluence under normal culture conditions was also prepared and used for the MBEC binding step. Prior to incubation with yeast both ECM and MBEC, plates were blocked for 30 minutes with PBSA at 4ºC. ECM subtraction was initiated by addition of induced yeast libraries or negative control yeast expressing VLR RBC36 suspended in PBSA into wells of the ECM plate at a density of ~0.85×10^6 yeast/cm^2. The plate was incubated with gentle rocking for 2 hours at 4ºC. Non-binding yeast were recovered from the ECM subtracted plate after 2 washes with ice cold PBSA and immediately applied to the MBEC binding plate for 2 hours at 4ºC with gentle rocking. Non-binding yeast were removed by 3 washes with ice cold PBSA, and MBEC binding yeast were then recovered by scraping the cells into SD-CAA media. Dilutions of the MBEC binding cells were plated to count the number of yeast recovered and the

remainder were expanded for subsequent rounds of biopanning or individual clone analysis.

4.2.8 VLR-Fc subcloning, production, and purification

VLRs were subcloned from the yeast surface display vector into the pIRES-rFc vector using NheI and AgeI restriction sites via standard PCR amplification, restriction digestion, and ligation procedures. Soluble VLR-Fc fusion proteins were expressed by transient transfection of HEK293F suspension cultures. 80µg pIRES-VLR-Fc plasmid DNA was mixed with 160 µg PEI (23966, Polysciences) in 3 mL OptiPRO SFM (12309019, Thermo Fisher) for 15 minutes and then applied dropwise to 80 mL HEK293F cultures. Transfected cultures were then incubated for 5-7 days at 37ºC, 8% CO_2, 135 rpm in a humidified incubator and the supernatant containing secreted VLR-Fc was recovered via centrifugation and filtration. VLR-Fcs were purified from the cleared supernatant via gravity-driven chromatography over a packed bed of 100uL Protein A/G Plus Agarose beads (PI20423, Thermo Fisher). After washing, three 200µl fractions were eluted from the column with 100mM Citric Acid pH 3 and neutralized with 1 M Tris-base pH 9, which typically yielded ~0.5 mg purified proteins from an 80mL transfected culture. Purified proteins were stored for up to 2 months at 4^0C.

4.2.9 Immunolabeling of tissue and cells with VLR-Fc

14 µm coronal brain cryosections from male C57BL/6 mice were washed in PBS and then blocked and permeabilized with immunolabeling buffer (PBS + 10% goat serum + 1% BSA + 0.05% saponin) for 30 minutes at room temperature. Next, purified

VLR-Fcs at 5 µg/mL in immunolabeling buffer were incubated on the brain slices for 1 – 2 hours at room temperature. After washing, brain sections were incubated with Goat-anti-Rabbit IgG-Alexa555 secondary Ab to detect VLR-Fc binding and Isolectin B_4-Alexa488 (I21411, Thermo Fisher) as a brain capillary marker for 1 hour on ice. After washing, sections were post-fixed with 4% PFA, nuclei labeled with DAPI, and mounted in ProLong Gold antifade reagent (P10144, Thermo Fisher). Cell surface binding on live bEnd.3 cells was carried out by incubation with 5µg/mL purified VLR-Fc proteins in PBS+10% Goat serum+1%BSA (PBSGA) for 1 hour at 4ºC. After washing VLR-Fc binding was detected by staining with goat-anti-Rabbit IgG-Alexa555 pAb in PBSGA for 30 minutes on ice. After washing, cells were post-fixed with 4% PFA, nuclei labeled with DAPI, and mounted in ProLong Gold antifade reagent. For whole cell labeling, cells were prefixed with 2% PFA, then blocked and permeabilized in immunolabeling buffer prior to incubation with VLR-Fc and detection reagents as described for cell surface binding. In all cases images were obtained with a Zeiss Imager Z2 Microscope equipped with an AxioCam MRm using 10X or 63X objectives.

4.2.10 Cell-based assays

***Internalization assays*:** bEnd.3 cells analyzed by immunofluorescence microscopy were grown to confluence on glass coverslips. bEnd.3 cells used in quantitative internalization assays were grown to confluence in 96-well flat-bottomed plates (353948, Corning). Cells were serum starved for 1hr at 37ºC in serum-free complete growth media. Subsequently, purified VLR-Fc diluted in serum free complete growth media were applied to the cells. Conditions were varied depending on the experiment.

For temperature dependent internalization assays one group of cells was incubated with 10 µg/mL VLR-Fc at 37ºC and one group with the same concentration of VLR-Fc at 4ºC. Both groups were incubated for 30 minutes prior to subsequent labeling steps. For saturation experiments, all cells were incubated for 20 minutes at 37ºC with varying concentrations of VLR-Fc up to 4 µM. Samples for microscopy analysis were processed as follows. After the VLR-Fc incubation period, bEnd.3 cells were washed 3x with ice cold PBS and incubated with Goat-anti-Rabbit IgG-Alexa488 pAb in PBSGA for 30 minutes on ice to label cell surface bound VLR-Fc. Following washes, cells were fixed in 2% PFA for 10 minutes at room temperature and then blocked and permeabilized in immunolabeling buffer for 30 minutes on ice. To differentially label internalized VLR-Fc the fixed and permeabilized cells were incubated with Goat-anti-Rabbit IgG-Alexa555 pAb in immunolabeling buffer for 30 minutes on ice. After washing, cells were post-fixed with 4% PFA, nuclei labeled with DAPI, and mounted in ProLong Gold Antifade Reagent. Samples were analyzed via widefield and/or confocal microscopy as described below. Samples for quantitative analysis of internalized VLR-Fc were processed as follows. bEnd.3 cells were first acid washed by 5 changes of ice-cold 0.9% w/v saline, pH 2.5 for a total of 25 minutes to remove cell-surface bound VLR-Fc. This stripping procedure routinely resulted in the removal of ~90% of the cell-surface bound VLR-Fc signal. Cells were then fixed with 2% PFA and blocked and permeabilized in odyssey blocking buffer (927-40000, Li-Cor) + 0.1% TX-100 for 30 minutes at room temperature. Internalized VLR-Fc were detected by IRdye800CW Goat-anti-rabbit IgG pAb (925-32211, Li-Cor) and cell number in each well measured

with CellTag 700 (926-041090, Li-Cor) both diluted in odyssey blocking buffer and incubated with cells for 1 hour at room temperature. After extensive washes with ice cold PBS+0.1% Tween-20 and drying of the plate signal in each well was measured with a Li-Cor Odyssey Imager with a focus offset of 3 mm and resolution of 169 µm. VLR-Fc signal in each well was normalized to a per cell basis via dividing by the CellTag 700 signal.

Equilibrium Binding Measurements: bEnd.3 cells were grown to confluence in 96-well flat-bottomed plates, washed 3x in PBS, and fixed with 2% PFA for 10 minutes at room temperature. Fixed cells were blocked and permeabilized as described above. Equilibrium affinity titration measurements were achieved via incubation of the cells with purified VLR-Fc diluted to a range of concentrations from 800 pM to 4µM at room temperature for 2 hours. After extensive washing with ice cold PBS+0.1% Tween-20 cells were labeled for detection with the IRDye reagents and analyzed as described above. Fraction of cellular antigen sites bound by VLR-Fc was quantified using background subtracted per-cell binding signal and the data was fit to a bimolecular equilibrium binding model to determine the dissociation constant (K_D).

Competition assay: 2µM recombinant receptor ecto-domain proteins, rIR (7544-MR, R&D systems), rLDLR (2255-LD, R&D systems), and rTfR (50741-M07H, Sino Biologics) were incubated with 200 nM VLR-Fc proteins in serum free complete growth media for 30 minutes and then applied to serum starved bEnd.3 cells in 96-well plates to allow for VLR-Fc binding to cell surface receptors. Plates were incubated at 4ºC for 2 hours. After extensive washing with ice cold PBS cells were fixed with 2% PFA, permeabilized, labeled with IRDye reagents, and analyzed as described above.

4.2.11 *In vivo* VLR-Fc brain targeting experiments

Male C57BL/6 mice (~20g) were injected intravenously with 10 mg/kg VLR-Fc or positive control anti-TfRmAb (8D3, AbDSerotec) in PBS. After 1 hour of antibody circulation mice were deeply anesthetized with 100mg/kg ketamine, 10mg/kg Xylazine mixture via intraperitoneal injection. Depth of anesthesia was confirmed with toe and/or tail pinch. Subsequently, the thoracic cavity was opened and transcardial perfusion was initiated via insertion of a catheter into the left ventricle and clipping of the right atrium. Ice cold wash buffer containing Earle's balanced salts, 20 mM HEPES, 1 g/L glucose, 10 g/L BSA, and 5 mg/L DyLight488 conjugated tomato lectin (DL-1174, Vector Laboratories) was perfused at 5 mL/min for 5 minutes with a peristaltic pump to wash away unbound antibodies and label the vessel lumen with lectin. Then perfusion fixation with room temperature 4% PFA was carried out at the same flowrate for 10 minutes. Upon completion of perfusion the brain was dissected out and stored in ice cold PBS. For immunofluorescence analysis, brains were cryopreserved in OCT and stored at -80ºC prior to sectioning. For electron microscopic analysis tissue was immediately cut into 150 µm thick coronal sections on a vibratome and stored in fixative containing 4% PFA and 0.01% glutaraldehyde(GA) overnight at 4ºC with gentle agitation.

4.2.12 Sample preparation and immunofluorescence microscopy

30µm thick coronal brain sections were cut on a cryostat, and adhered to positively charged glass slides. Sections were washed with PBS to remove embedding compound and fixed with 2% PFA. Tissue was blocked and permeabilized in immunolabeling buffer for 30 minutes at room temperature. To visualize VLR-Fc in the

brain sections, tissue was incubated overnight with goat-anti-rabbit IgG Alexa555 pAb in immunolabeling buffer at 4ºC. In some cases, a goat-anti-collagen IV pAb (AB769, EMD Millipore) diluted in donkey immunolabeling buffer (goat serum replaced by donkey serum) was incubated on the sections for 2 hours at 4ºC. Subsequently, sections were incubated with donkey-anti-rabbit IgG-Alexa555 conjugate and donkey-anti-goat IgG-Alexa647 conjugate in donkey immunolabeling buffer overnight at 4ºC. In all cases, sections were post-fixed in 4% PFA, nuclei labeled with DAPI, and mounted in ProLong Gold antifade reagent. Low magnification widefield images were obtained on a Zeiss Imager Z2 Microscope equipped with an AxioCam MRm using the 10x objective. Confocal imaging was performed on a NikonAR1 microscope using a Plan Apo λ 60x oil objective with 1.4 numerical aperture and optical z-sections were obtained with a step size of 250nm. Images were 12-bit, 1024x1024 pixels, with a pixel size of 100, 110, or 120 nm. Maximum intensity projections of the Z-stacks were created using the Maximum Intensity Projection tool in NIS Elements (Nikon Metrology).

4.2.13 Sample Preparation and electron microscopy

Immunogold labeling of 150µm vibratome sections from mice injected with VLR-Fc was carried out with reagents purchased from Electron Microscopy Sciences (EMS) essentially following the manufacturers protocols. After aldehyde quenching with 0.1% $NaBH_4$, sections were permeabilized via incubation with 0.1% TritonX-100 in PBS for 30 minutes, and then blocked with AURION Goat Serum Blocking Solution (25596, EMS) for 1-2 hours at room temperature. Subsequently, sections were incubated with Goat-anti-rabbit IgG-Ultrasmall Gold conjugate (25100, EMS) diluted in PBS+0.2% AURION

BSA-c (25557, EMS) overnight at 4ºC with gentle agitation. Following extensive washing sections were fixed in 2% glutaraldehyde for 30 minutes. Silver enhancement was carried out using the R-Gent silver enhancement kit (25520, EMS) following the manufacturer's instructions to increase the size of the ultrasmall gold particles. Sections were post fixed in 0.5% osmium tetroxide, 1% potassium ferrocyanide in 0.1M sodium phosphate buffer for 1 hr at room temperature. After rinsing, sections were dehydrated through a graded ethanol series (35%, 50%, 70%, 80%, 90% for 5 minutes each, 95% for 10 minutes, and 100% for 30 minutes). The sections were then infiltrated via incubations with increasing concentrations of PolyBed812 in propylene oxide. After infiltration, sections were embedded in 100% PolyBed812 overnight at 60ºC in a drying oven. 100nm ultrathin sections were cut using a Leica EM UC6 ultramicrotome and captured on Pioloform carbon-coated 1x2 Cu slot grids (EMS) and contrasted with Reynolds lead citrate and uranyl acetate. The sections were examined on a Phillips CM120 transmission electron microscope and images captured with a MegaView III digital camera (Olympus-SIS).

4.3 Results

4.3.1 Lamprey immunization and BBBVLR library construction

Brain microvessels were isolated from mice cortices using standard mechanical homogenization and filtration techniques (Figure 4-1 A). Endothelial cell plasma membranes (PM) were fractionated from the basement membranes (BM) of the brain capillaries via hypotonic lysis, sonication and centrifugation as previously described [247]. Assessment of the preparations indicated that the BBB endothelial PM-resident

glucose transporter (GLUT-1) and gamma-glutamyl transpeptidase (GGT) enzyme were enriched in the PM fraction while the astrocyte marker, GFAP, was de-enriched (Figure 1B). Such a brain capillary PM (BCPM) antigen preparation has been previously used as an appropriate immunogen for multiplex expression cloning of BBB membrane proteins [62], and was also used here as a representative *in vivo*-relevant PM protein source for lamprey immunization and VLR library screening.

Three lampreys were immunized with 50 μg BCPM proteins three times over 6 weeks to elicit a VLR immune response against mouse BBB membrane protein antigens. Two weeks after the final immunization, plasma and lymphocytes were harvested from the blood of the lampreys. Mouse brain cryosections were stained with plasma from immunized lampreys (BBBVLR) or control non-immunized lampreys (Naïve VLR), and plasma VLR binding was detected with an anti-VLRB mAb (4C4) in order to determine if the lampreys responded to the immunization. Capillaries in mouse brain tissue sections were strongly labeled with polyclonal VLRB-containing plasma from all three immunized lampreys (red) and the staining co-localized with capillary marker IB_4 lectin staining (Green) as shown in Figure 4-1 C. In contrast, only background staining was detected with the naïve lamprey plasma sample. These results indicated that the immune challenge presented by BCPM injections elicited a polyclonal VLRB response directed against antigens present on BBB ECs *in vivo*. To efficiently screen for VLRs that bind to BBB ECs, a yeast surface display library, termed BBBVLR, was constructed by PCR amplification of VLR genes from total lymphocyte cDNA of the immunized lampreys and subsequent *in vivo* homologous recombination with the yeast surface display vector in EBY100 yeast, which yielded a library of $7.5x10^6$ VLR clones.

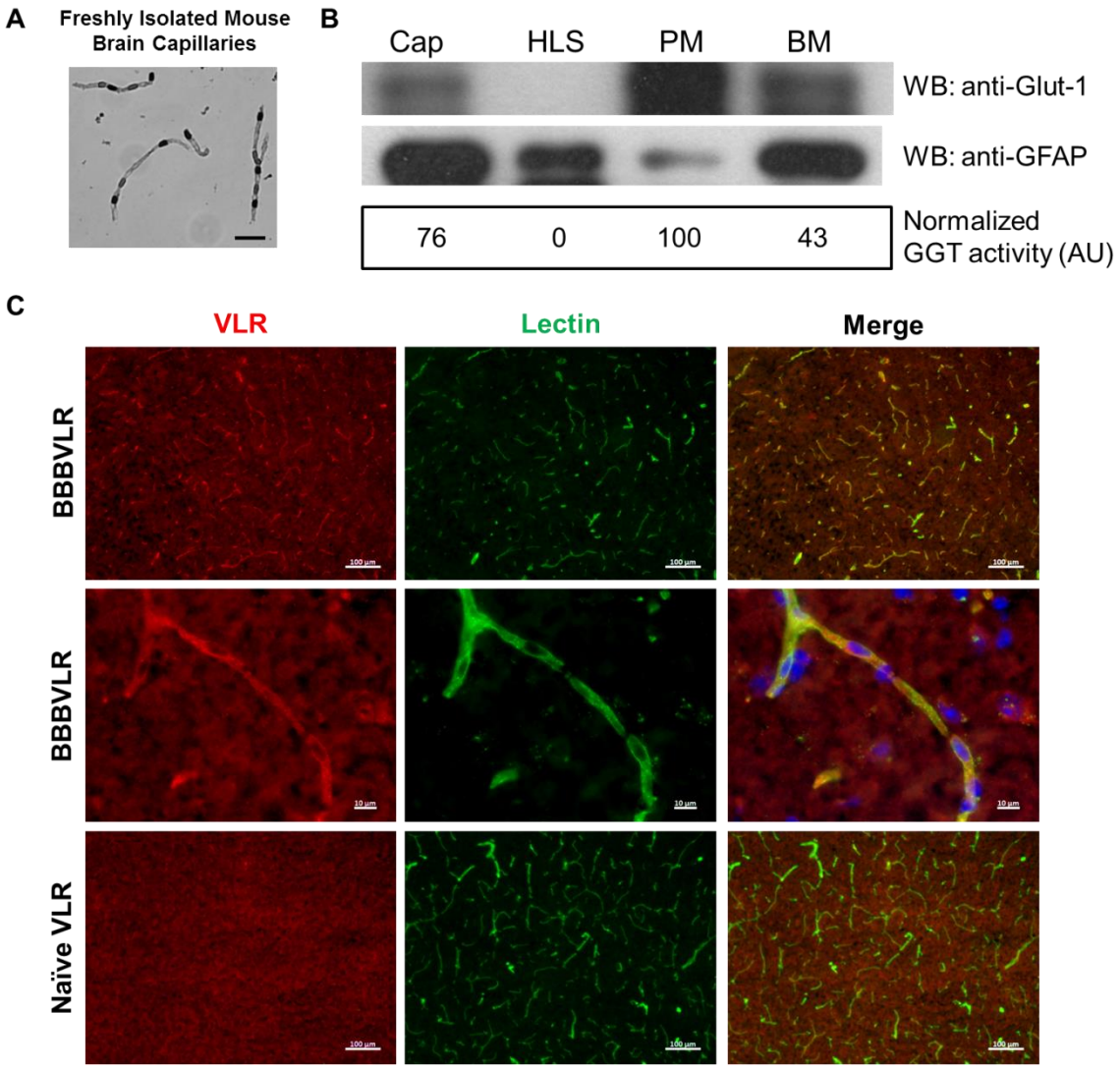

Figure 4-1. Brain capillary plasma membrane antigen characterization and lamprey immunization validation. Capillaries (A) are recovered from mouse brains via mechanical homogenization, dextran gradient centrifugation, and capture on nylon mesh filters. (B) Quality validation of PM preps fractionated from the capillaries after hypotonic lysis, sonication, and centrifugation. Cap = Capillary homogenate, HLS = hypotonic lysis supernatant, PM= Plasma membrane fraction, BM= Basement membrane fraction. Anti-Glut-1 western blot and gamma glutamyl transpepsidase (GGT) activity assay show that endothelial markers are enriched in the PM fraction. Astrocyte marker anti-GFAP western blot shows that peripheral cell-type proteins are de-enriched in the PM fraction. The PM fraction was used to immunize lamprey to generate the VLR immune plasma. (C) Plasma from immunized lamprey (BBBLVR) or naïve lamprey (Naïve VLR) was used to immunolabel mouse brain sections (red) and brains were counterstained with fluorescent lectin (Green) to highlight brain capillaries. The BBBVLR plasma showed a strong capillary-associated binding signal, whereas only background signal was observed with the Naïve VLR plasma.

4.3.2 Two-tiered library screening approach

A two-tiered screening strategy was designed and implemented in order to isolate VLRs from the BBBVLR library that bound to BBB cell-surface antigens expressed *in vivo* (Figure 4-2). The library was initially screened for *in vivo* antigen binding via a modified yeast display immunoprecipitation (YDIP) method [94, 238] using biotinylated, detergent solubilized mouse BCPM proteins as the source of antigens for library sorting (Figure 4-2 ii-iii). Subsequently, YSD biopanning [93] on an immortalized mouse brain endothelial cell (MBEC) line, bEnd.3 [98], was carried out to recover VLRs that bound to extracellular epitopes (Figure 4-2 iv).

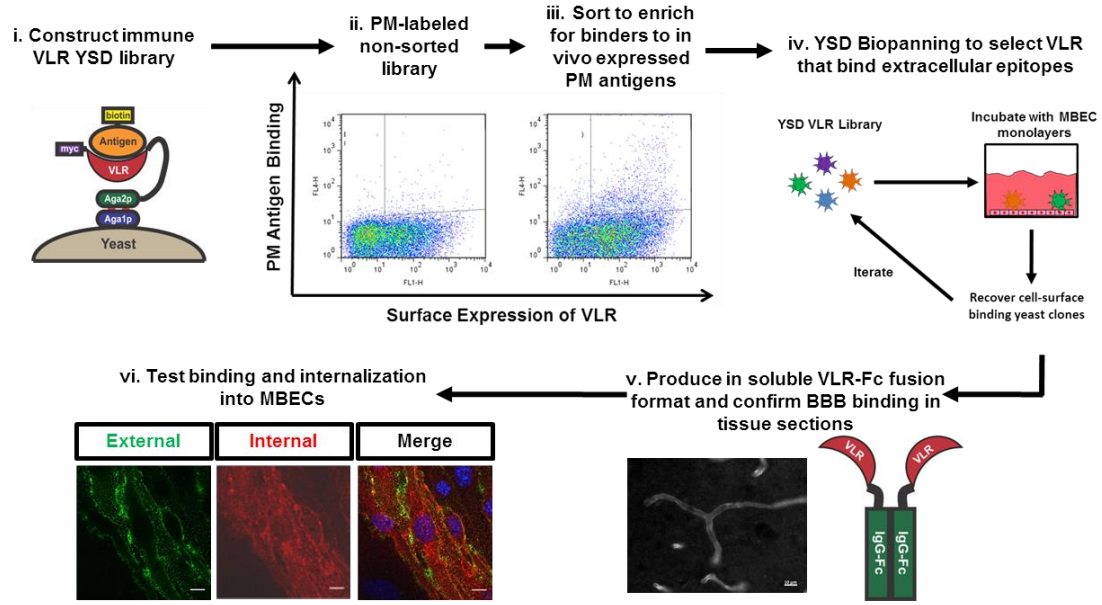

Figure 4-2. BBBVLR library screening and characterization workflow. (i) Immunized lamprey BBBVLR libraries are expressed on the yeast surface by fusion to the C-terminus of Aga2p. Each yeast cell displays thousands of copies of a single VLR clone on its surface. (ii) The immune, unsorted library is enriched for binders to BBB PM antigens expressed *in vivo* via (iii) MACS and FACS. (iv) The FACS-enriched PM-binding pool is next screened for VLRs that bind extracellular domains of membrane proteins via biopanning against an MBEC cell line. (v) Individual VLRs are reformatted as rabbit IgG-Fc fusion proteins, secreted from HEK-293 cells, and used to stain brain sections to verify binding to relevant BBB antigens in the mouse brain. (vi) Capacity for BBB transport is assessed via an internalization assay in cultured MBECs.

Two rounds of YDIP screening with freshly isolated BCPM antigen preparations were carried out, first using one round of MACS followed by one round of FACS (Table 4-1). The resultant library, BBBVLR-FACS, had an approximately 10-fold enrichment in the percentage of BCPM antigen-binding yeast over the starting library (Figure 4-3 A). Next, three rounds of YSD biopanning on MBECs yielded enrichment of cell surface binding VLRs resulting in the BBBVLR-BP3 library (Figure 4-3 B, Table 4-2). However, during initial testing of the biopanning approach, yeast cells from the BBBVLR-FACS library were observed binding to areas of the plate devoid of cells and containing MBEC-derived extracellular maxtrix (ECM) (Supplemental Figure 4-S1). Therefore, a subtractive panning step on decellularized ECM plates was developed and added to the biopanning strategy to remove ECM binders from the library.

Table 4-1. Summary of YDIP screening of the BBBVLR library

Sort Round	Starting Library	MACS	FACS
Yeast Input	$7.5x10^6$	$2.1x10^8$	$3x10^7$
Recovery Percentage	NA	11	3.1

*NA= Not applicable

Table 4-2. Summary of YSD biopanning of the BBBVLR library

	Biopanning Round	BBBVLR-BP1	BBBVLR-BP2	BBBVLR-BP3
ECM Binder Subtraction Step	Yeast Input to ECM Subtraction Plate	$1.52x10^7$	$1.52x10^7$	$1.52x10^7$
	ECM Binder Removal Percentage	2.1	4.3	0.4
MBEC Binder Enrichment Step	Yeast Input to MBECPlate	$1.49x10^7$	$1.45x10^7$	$1.51x10^7$
	MBEC Binder Recovery Percentage	0.5	3.6	8.5

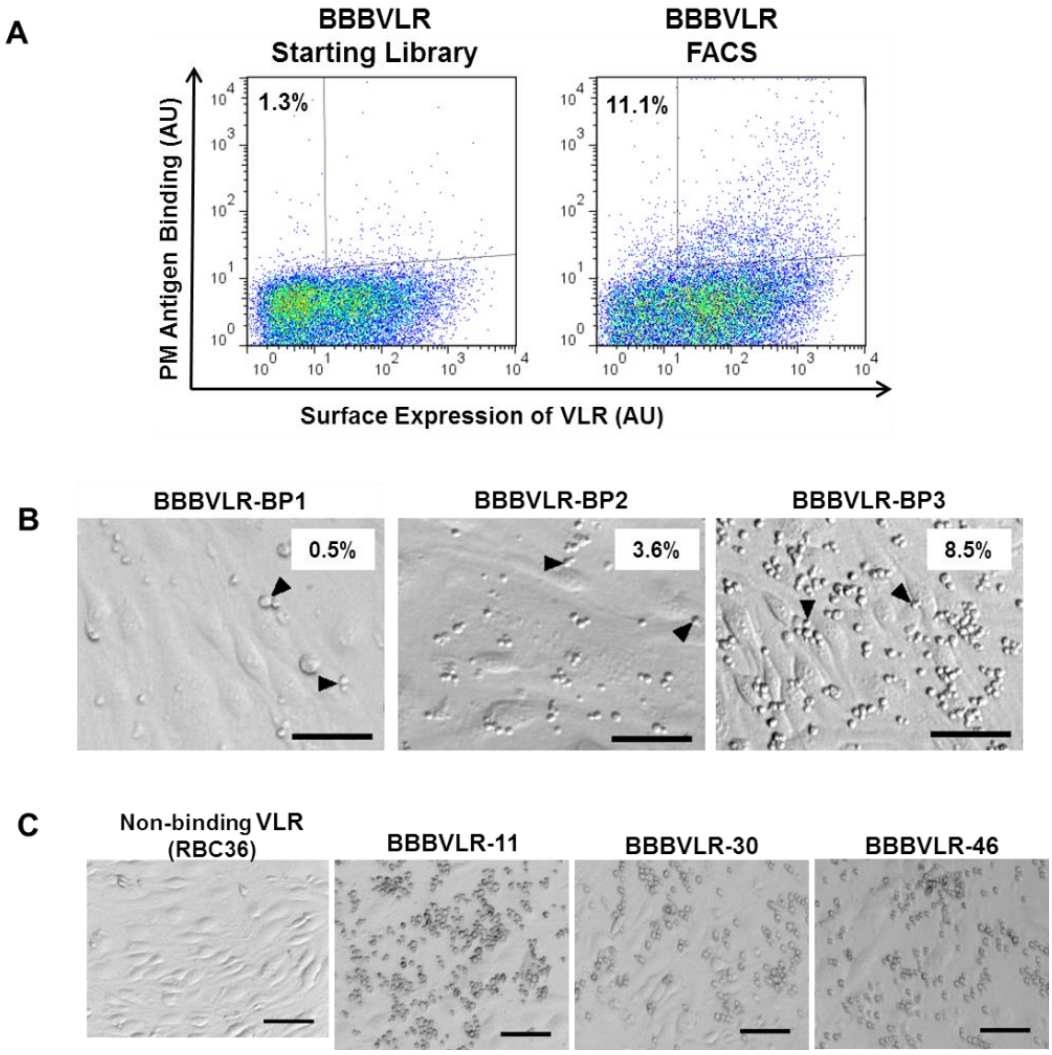

Figure 4-3. YSD screening of the BBBVLR library. (A) Analytical flow cytometry assessment of the percentage of BCPM binding clones in the library before (Starting Library) and after (FACS) one round of MACS and one round of FACS sorting of the library via YDIP. Percentage of the expressed population falling in the positive binding gate is shown in the top left corner. (B) Representative images of the enrichment of cell-surface binding clones achieved through three rounds of YSD biopanning. The percentage of MBEC binding yeast recovered in each round is displayed in the top right of each image. Clear enrichment of MBEC-binding yeast (e.g. black arrow heads, small round cells) is observed. (C) Individual clones selected from the library after the third round of biopanning are confirmed to bind MBEC cells in a biopanning assay and compared with negative control yeast displaying VLR-RBC36. Scale bar = 50 µm

In each round of biopanning, the YSD library was first incubated on plates containing decellularized ECM proteins that had been deposited by cultured MBECs. Subsequently, non-binding yeast were recovered, immediately applied to MBEC monolayers, and clones that bound the MBEC cell surface were recovered. This ECM subtractive MBEC binding (ECM-/EC+) biopanning approach enriched for cell surface binding yeast and de-enriched for ECM binders over three rounds as shown in Figure 4-3 B and detailed in Table 4-2. In the final round of biopanning a very small percentage of the library bound to the ECM plate (0.4%, Table 4-2) relative to the MBEC binding population (8.5%). Subsequently, individual clones were tested in a high-throughput biopanning assay and 204 out of 240 clones were found to specifically interact with MBEC cells as shown for a select group of clones in Figure 4-3 C. Sequencing of the VLR genes revealed that 33 of the 204 cell-binding clones were unique.

4.3.3 Initial characterization of anti-BBBVLR clones

To validate that this *in vivo-in vitro* screening strategy yielded a diverse set of MBEC extracellular targeting VLRs that also maintained binding to antigens expressed at the *in vivo* BBB, the unique clones identified above were analyzed in cell and tissue section labeling experiments. VLRs were produced as dimeric, soluble recombinant proteins by fusion to the Fc region of rabbit IgG via a flexible linker and were expressed in transiently transfected HEK293 cells (Figure 4-2 v). Of the 33 clones, 26 bound to the surface of live MBEC cells (examples shown in Figure 4-4 A). The remaining 7 clones were either produced at insufficient levels or binding was not detected. Fixed and permeabilized MBEC cells were also labeled with VLR-Fc clones to reveal subcellular

localization patterns (Figure 4-4 B) and mouse brain cryosections were stained to determine binding to *in vivo* antigens (Figure 4-4 C). Notably, the majority of the MBEC binding clones, 16 out of 26, were shown to bind antigens in mouse brain capillaries. 14 out of 16 appeared to be selective for brain vasculature whereas the other two (VLR-Fc-30 and VLR-Fc-141) bound both capillary and parenchymal antigens. In summary, a variety of surface binding, subcellular localization, and brain section labeling patterns were observed among the clones (compare clones in figure 4-4 A-C) suggesting that the screening strategy resulted in a pool of VLRs recognizing a diverse set of BBB cell-surface epitopes expressed *in vivo*.

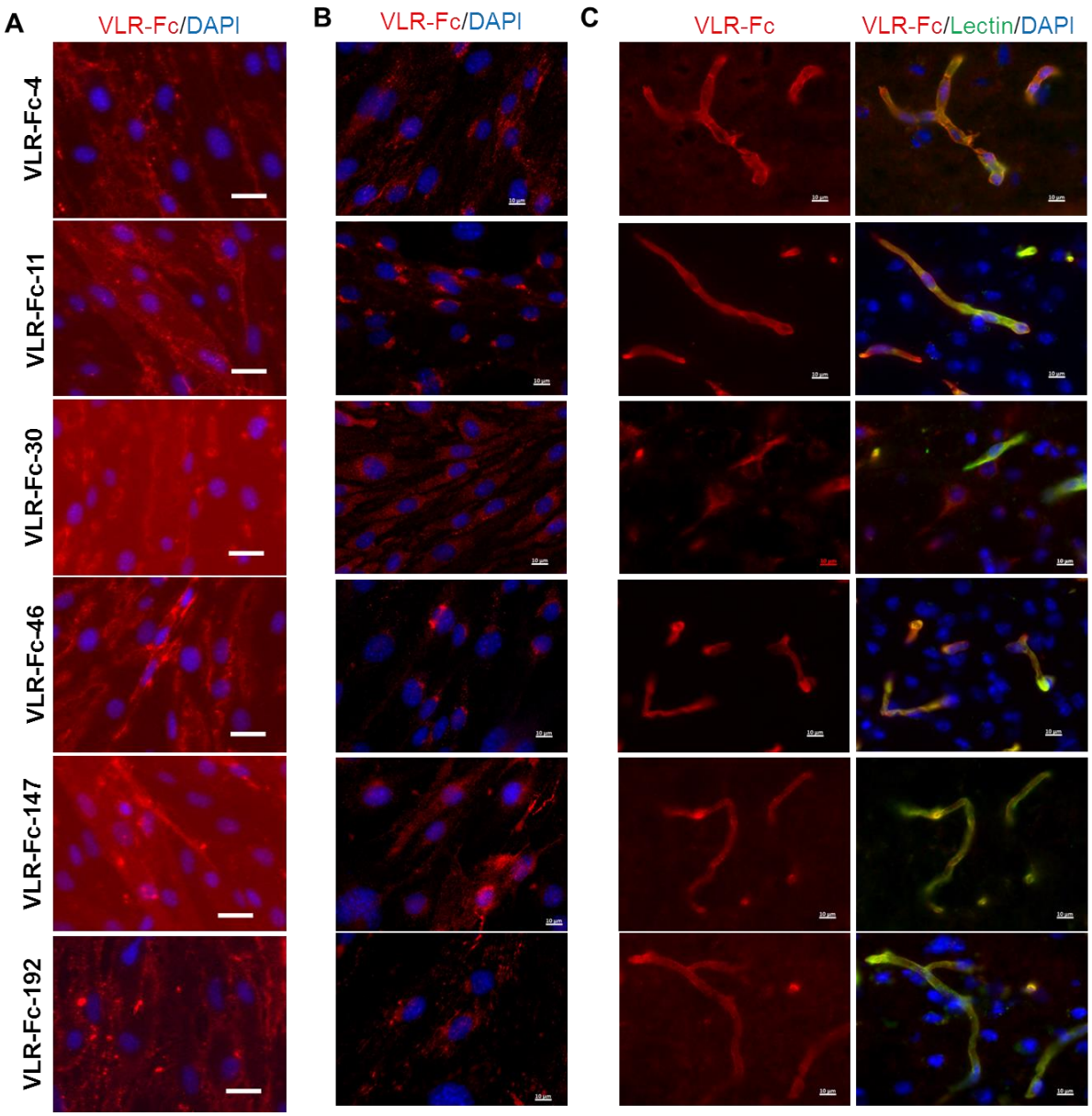

Figure 4-4. The enriched BBBVLR-BP3 library contains a diverse set of BBB binding VLR. (A) Live cell labeling, (B) labeling of fixed and permeabilized cells, and (C) staining of mouse brain tissue sections for a representative set of the 16 clones confirmed to bind mouse brain capillaries. Different binding patterns are observed suggesting that a diverse cohort of BBB cell-surface antigens are targeted by the VLR in the library. Scale bars: (A) 25 μm, (B) and (C) 10 μm.

4.3.4 Screening for VLRs that internalize into MBECs *in vitro*

Since the two tiered *in vivo-in vitro* screening procedure employed did not directly select for functional aspects of the target antigens, *in vitro* internalization assays were used to further screen the isolated VLR clones for properties compatible with brain drug delivery applications (Figure 4-2 vi). Endocytosis requires membrane fluidity and at temperatures below 10ºC this process is inhibited. Therefore, comparison of ligand internalization in cells incubated at 37ºC versus cells kept below 10ºC provides evidence for a receptor-mediated internalization mechanism. Accordingly, comparative internalization assays with VLR-Fc or a positive control anti-TfR IgG (8D3) were carried out on MBEC monolayers and 4 out of 16 VLR-Fc tested exhibited temperature-dependent internalization (Figure 4-5 A-B). MBECs were incubated with antibodies for 30 minutes at either 37ºC or 4ºC. Then, surface-bound and internalized antibodies were differentially labeled prior to confocal microscopy analysis. VLR-Fc-11, VLR-Fc-30, VLR-Fc-46, and VLR-Fc-192 were endocytosed at 37ºC evidenced by intracellular VLR-Fc signal (red channel in Figure 4-5 A) whereas VLR-Fc-147 was not (Figure 5A).Furthermore, internalization was inhibited at 4ºC for all VLR-Fc as only surface-bound antibodies were detected (green channel Figure 4-5 A). The internalized VLR-Fc signal was observed in punctate structures within the cytoplasm, indicative of endocytic vesicle trafficking and similar to punctate structures observed for the positive control 8D3.

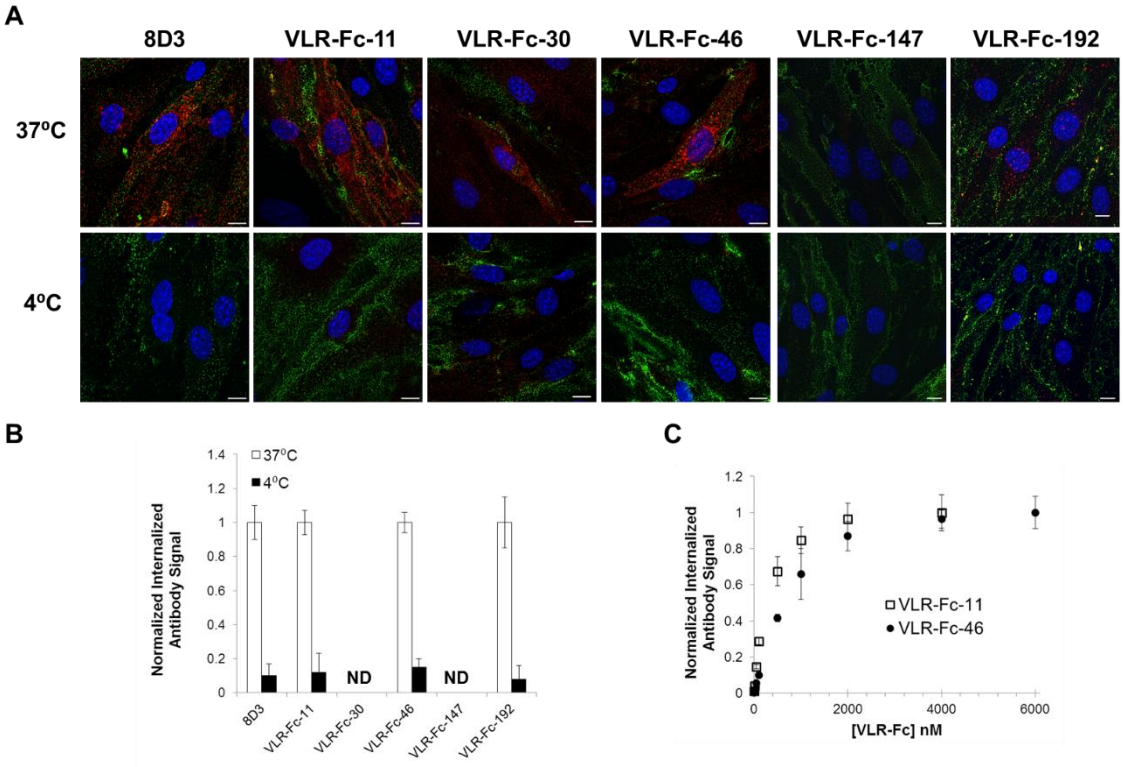

Figure 4-5. Several lead VLRs internalize into MBECs via receptor-mediated mechanisms. (A) Confocal immunofluorescence analysis reveals that certain VLR-Fc are internalized in a temperature dependent manner during 30 minute incubations on MBECs. Positive control anti-TfR IgG (8D3) can be used as a benchmark. Individual Z-slices from MBECs incubated at either 4^0C or 37^0C with the indicated antibodies are shown and are representative from n=3 experiments. Green=Cell surface bound antibody, Red=Internalized antibody, Blue=DAPI. A clear distinction can be made between internalizing (VLR-Fc-11, 30, 46, 192) and non-internalizing (VLR-Fc-147) clones. (B) 96-well assay quantification of temperature dependent internalization confirms the confocal analysis. Internalization values are normalized to internalized antibody signal per cell at 37^0C for each clone. ND=Not Detected. (C) MBEC internalization of VLR-Fc-11 and VLR-Fc-46 is saturable providing further evidence for receptor-mediated endocytosis. Data represent the mean of n=3 independent experiments and error bars show standard deviation.

Antibody internalization was also quantified via labeling and detection of intracellular antibody with IRDye secondary reagents after acid washing to remove surface bound proteins, and the results were in agreement with the confocal analysis (Figure 4-5 B). One clone, VLR-Fc-30, was found to internalize into a small subpopulation of MBEC cells when analyzed by fluorescence microscopy (Figure 4-5 A); however, due to the small size of the internalizing population (Supplemental Figure 4-S2) there was no measurable internalization signal in the quantitative assay (Figure 4-5 B). Given that VLR-Fc-30 was shown to bind both capillary and parenchymal antigens, which is a desirable property for drug delivery applications, this clone was carried on to *in vivo* experiments despite the inability to quantify internalization.

Another hallmark of receptor-mediated endocytosis is saturation of the internalization pathway. Given a finite number of receptors on the cell surface and trafficking within the cell, the amount of ligand internalized over a defined period of time will saturate with increasing ligand concentration. Indeed, saturation of the internalization pathway was observed for VLR-Fc-11 and VLR-Fc-46 at antibody concentrations around 2μM when cells were incubated for 20 minutes with varying VLR-Fc concentrations and internalization quantified as described above (Figure 4-5 C). This saturation behavior compares favorably with measurements made on the internalization of radiolabeled transferrin in reticulocytes, which saturated at between 1 and 2 μM transferring [281]. Therefore, the combined evidence for temperature-dependent and saturable internalization of VLR-Fc-11 and VLR-Fc-46 in MBECs support receptor-mediated endocytosis of these constructs.

4.3.5 VLRs target the brain vasculature and traffic *in vivo*

Given the ability of VLR-Fc-11, 30, 46, and 192 to recognize antigens in mouse brain tissue sections and to internalize into MBECs in vitro, we hypothesized that these may represent a set of novel BBB targeting ligands. As proof of this concept, we sought to determine whether VLR-Fc could localize to mouse brain capillaries after systemic administration. To this end, VLR-Fc-11, 30, 46, and 192 were administered IV to mice at a dose of 10mg/kg and allowed to circulate for 1 Hr. VLR-Fc-RBC36 was used as a negative control because it recognizes the human blood group type II H trisaccharide (Fucα1,2-Galβ1,4-GlcNAc) that is not expressed in mice. The anti-TfR IgG clone 8D3 was again used as a positive control due to its well-characterized brain capillary targeting and trafficking properties.

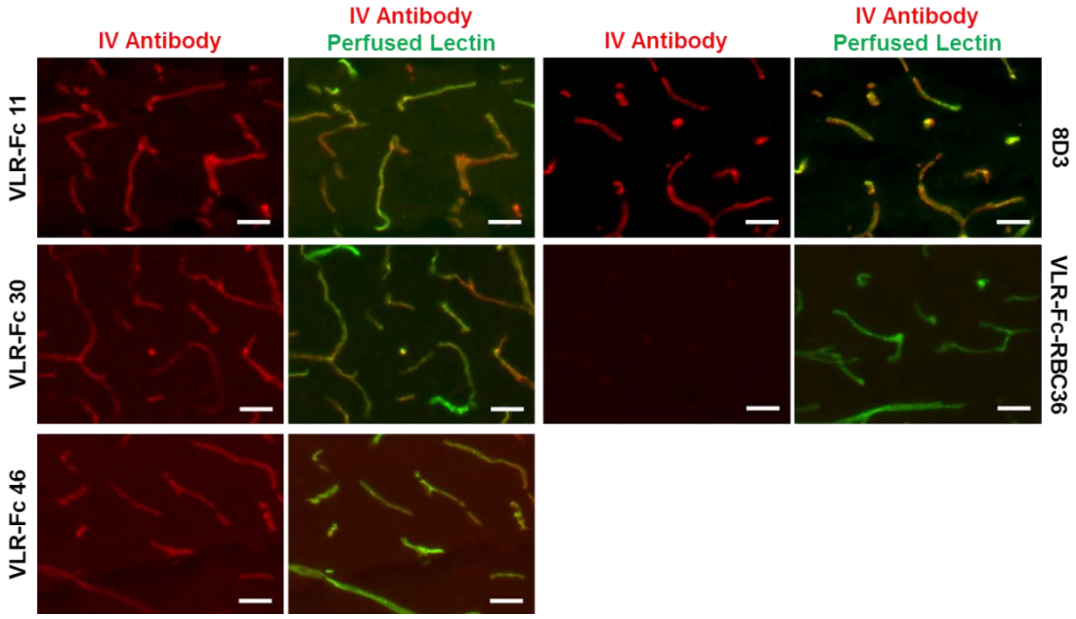

Figure 4-6. VLR-Fc target the brain vasculature after IV administration. Mice were IV administered 10 mg/kg of the indicated antibody construct (red). After 1 hr circulation mice were perfused with buffer containing fluorescently labeled lectin (green). VLR-Fc were found in capillaries throughout the brain when 30 µm cryosections were examined. Representative sections from the cortex are shown from n=3 replicates. Scale = 25 µm.

After the circulation time, the mice were perfused through the left ventricle with heparinized balanced salts buffer containing fluorescently labeled tomato lectin to clear the vasculature of unbound antibody and stain the luminal aspect of capillaries for subsequent imaging analysis. When brain cryosections from VLR-Fc injected animals were post-labeled with fluorescent anti-rabbit secondary antibody (red channel in Figure 4-6), 3 out of 4 of the clones tested (VLR-Fc-11, 30, and 46) were observed binding to their antigen in brain capillaries similar to the positive control 8D3. Residual background from VLR-Fc in the bloodstream was negligible due to efficient perfusion as indicated by lack of VLR-Fc signal in animals injected with negative control VLR-Fc-RBC36 and the strong lectin signal in the brain capillaries of all animals (green channel in Figure 4-6). Therefore, capillary localized VLR-Fc signal seen for clones VLR-Fc-11, 30, and 46 is a result of the VLR-Fc specifically engaging their target antigens on the brain capillary endothelial cells.

Subsequent observations from confocal immunofluorescence microscopy and immunogold electron microscopy analysis provided evidence for internalization and trafficking of VLR-Fc-11, 30, and 46 into brain capillary endothelial cells after IV administration. First, the VLR-Fcs were found in punctate structures within the vasculature, similar to those observed for the anti-TfR mAb control and in contrast to the continuous luminal cell-surface staining observed for perfused lectin (Figure 4-7). This distinct punctate pattern where at least a portion of the puncta for each VLR-Fc does not co-localize with the perfused lectin is indicative of internalization and trafficking within the endothelium, especially when benchmarked against the anti-TfR control which is known to endocytose and traffic at the BBB.

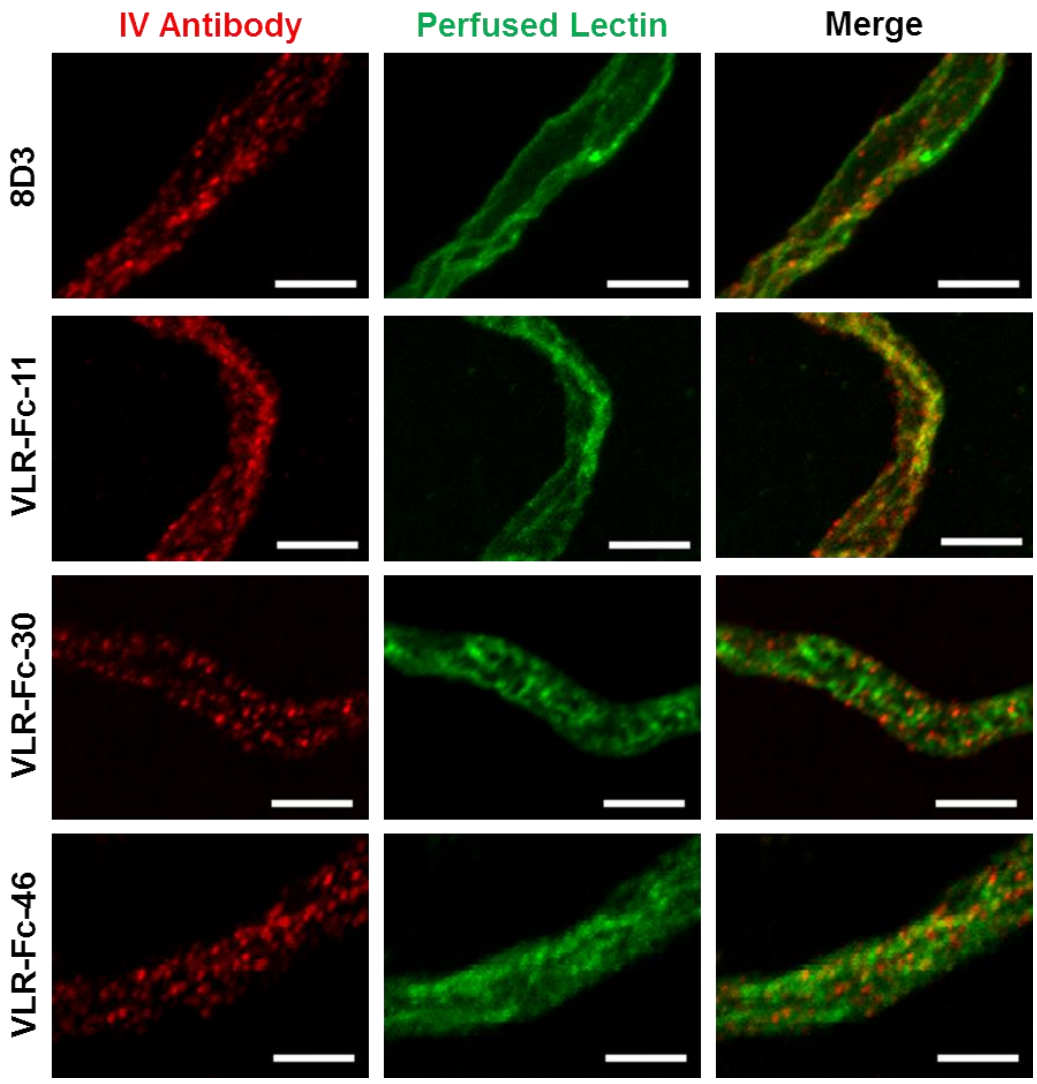

Figure 4-7. Localization and pattern of VLR-Fc signal in mouse brain capillaries provides evidence for internalization into ECs after IV administration. Max intensity projection of ~7μm Z stacks show VLR-Fc signal (red) in punctate structures within the brain capillaries distinct from the continuous cell surface labeling pattern of the perfused lectin (green). Scale = 5 μm

Furthermore, immunogold electron microscopy confirmed VLR-Fc localization at the luminal surface as well as within the brain capillary ECs. As shown in representative images in Figure 4-8, immunogold reactivity (black electron dense spheres) was observed at the luminal membrane for VLR-Fc-11, VLR-Fc-30, and VLR-Fc-46 indicating binding of the VLR-Fc to an extracellular endothelial epitope. Immunogold reactivity was also observed within coated pits at the luminal membrane providing evidence for VLR-Fc interacting with actively internalizing complexes. Significantly, immunogold reactivity was also observed within the endothelial cells near both the luminal and abluminal membrane demonstrating that upon internalization the VLR-Fc are trafficked within the ECs. In summary, the results of confocal and electron microscopy analysis provide significant evidence for VLR-Fc-11, 30, and 46 localization within the capillary endothelial cells after IV administration demonstrating that these proteins are internalized and trafficked within the endothelial cells of the BBB.

4.3.6 Additional characterization of *in vivo* BBB targeting VLR

The affinity of antigen binding, interaction with known BBB receptors, and cross-reactivity with rat and human antigens was assessed for VLR-Fc-11, 30, and 46 in order to further characterize these promising *in vivo* BBB trafficking VLR. Apparent affinity was determined by measuring the binding signal intensity to MBEC monolayers at increasing concentrations of VLR-Fc and fitting the data to a bimolecular equilibrium binding model to calculate the dissociation constants (K_D). All three clones bound their antigens with low-nanomolar affinity (Figure 4-9 A).

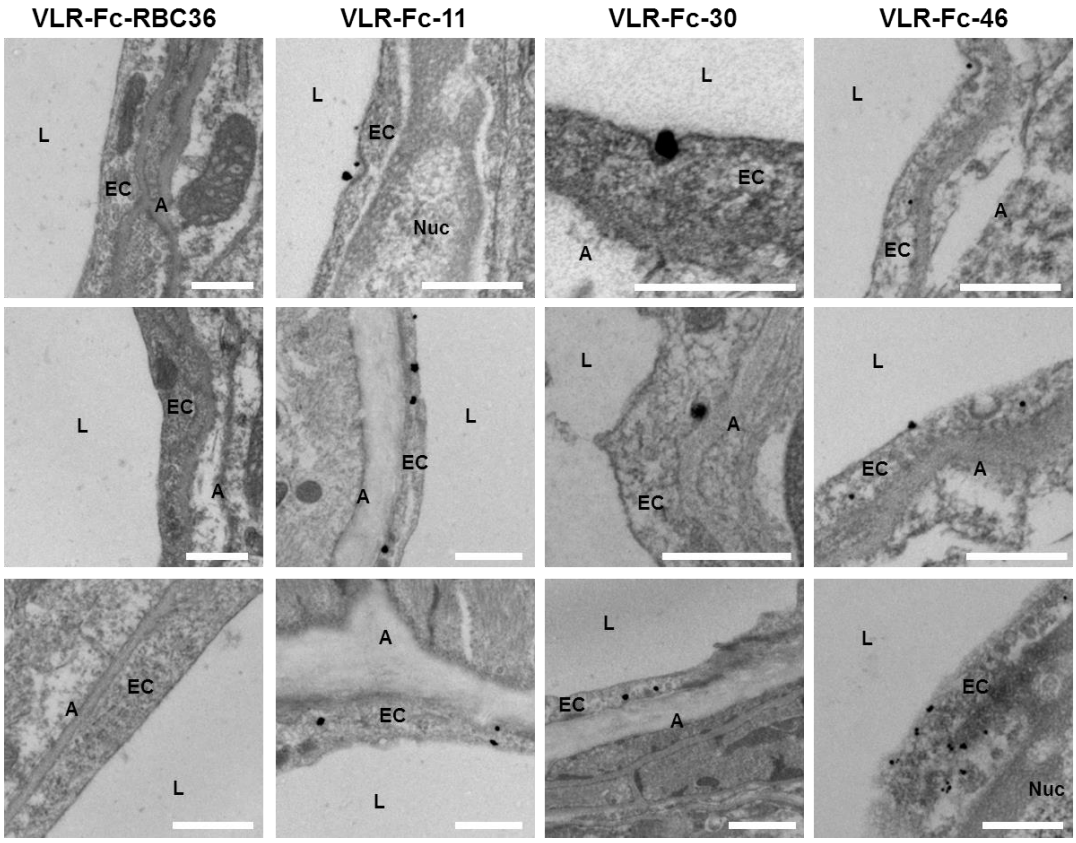

Figure 4-8. Immunogold electron microscopy confirms *in vivo* trafficking of VLR-Fc in brain ECs. Anti-rabbit immunogold staining and silver enhancement reveals VLR-Fc localization after IV administration. No immunogold signal is seen in mice injected with negative control VLR-Fc-RBC36. Whereas immunogold signal (black electron dense spheres) shows that VLR-Fc are found binding to the surface of ECs, interacting with invaginating coated pits, and localized inside the ECs. Demonstration of VLR-Fc interacting with cell surface ligands actively internalizing and localized throughout the ECs including adjacent to the basolateral membrane provides strong evidence for endocytosis and trafficking of the VLR-Fc *in vivo*. EC=endothelial cell, L=lumen, A=Abluminal, Scale bar = 500nm

To investigate if the VLRs recognize established BBB receptors, a competitive binding assay was used to determine if the VLR-Fcs interact with three of the major known targets for brain drug delivery: transferrin receptor (TfR), Insulin receptor (IR), and low

density lipoprotein receptor (LDLR). VLR-Fc were pre-incubated with excess recombinant receptor ectodomains prior to a live MBEC cell surface binding assay. Cell surface binding of all three VLR-Fcs was not altered by any of the competing ligands (Figure 4-9 B). In contrast, competition with the TfR recombinant protein reduced the 8D3 binding signal to ~20% of the non-competition signal, whereas IR or LDLR competition did not inhibit binding, demonstrating the sensitivity and selectivity of the assay. These results suggest that VLR-Fc-11, 30, and 46 do not bind murine TfR, IR, or LDLR. Furthermore, similar competition assays carried out using unlabeled VLR-Fc to compete for binding with biotin-labeled VLR-Fc revealed that none of these clones target the same epitope (data not shown). Finally, the rat and human antigen cross-reactivity of VLR-Fc-11, 30, and 46 was investigated to determine if these clones recognize conserved mammalian epitopes. Rat and human brain samples were labeled with VLR-Fc and tomato lectin (rat brains) or mouse anti-CD31 (human brains) and binding was detected with fluorescent secondary antibodies. All three clones tested bound to both rat and human brain capillary antigens and VLR-Fc-30 also bound parenchymal antigens as was seen in the mouse brain (Figure 4-9 C). Thus, VLR-Fc-11, 30, and 46 are high affinity binders to potentially novel conserved mammalian epitopes.

A

Equilibrium Binding	
VLR-Fc	Affinity nM
11	10.4 ± 2.1
30	5.4 ± 0.3
46	68.2 ± 2.4

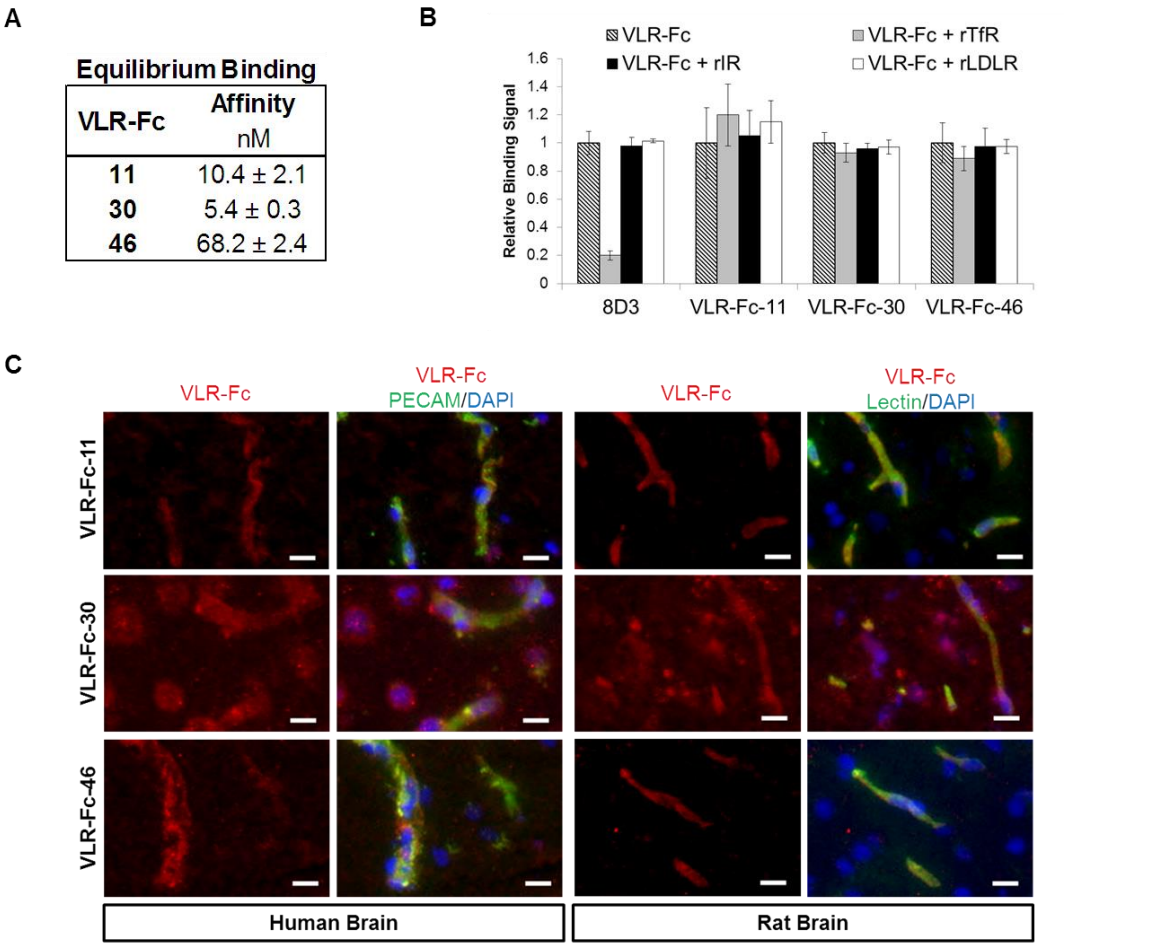

Figure 4-9. Lead VLR-Fc bind with high affinity to potentially novel conserved mammalian epitopes. (A) The equilibrium binding affinity of the VLR-Fc was measured via titration on MBEC cell cultures. The mean equilibrium dissociation constant (K_D) determined from this analysis is listed ± the 95% confidence interval calculated from n=3 independent experiments. (B) Competitive binding assay on MBECs was used to determine whether the lead VLR-Fc target well known RMT proteins. For each antibody the reported relative binding signal was normalized to binding in the absence of competition (hashed bars). Data are the means and error bars the standard deviation calculated from n=3 independent experiments (C) VLR-Fc11, 30, and 46 cross-react with conserved mammalian epitopes as revealed by immunofluorescence staining of human and rat brain cryosections. VLR-Fc signal (red) was found co-localized with capillary markers (green) in all cases. As observed in the mouse, VLR-Fc-30 also recognizes antigens in human and rat brain parenchymal cells. Scale=15 μm

4.4 Discussion

We have generated a panel of VLRs capable of targeting the brain vasculature *in vivo* that complement Ig-based mAbs currently being explored for delivery of drugs to the brain. Lampreys were immunized with PM fractions prepared from freshly isolated mouse brain capillaries to present *in vivo* relevant antigens, which resulted in a robust polyclonal immune response as evidenced by the strong staining of capillary antigens with VLRB from immunized lamprey plasma (Figure 4-1). VLR library construction and YSD screening of both non-immune and immunized libraries has previously been used to select for VLRs that bind to soluble protein and carbohydrate antigens, such as β-gal, cholera toxin subunit B, and human blood group trisaccharides [134, 137]. In separate studies, VLR libraries have been constructed from lampreys immunized with mammalian cells in order to identify novel cell surface markers and potential therapeutic targets; however, these studies used a low-throughput screening approach in which the VLR-containing supernatants of transfected HEK293 cells were screened for binding to target cells [136, 135]. Although these experiments yielded a VLR specific for the idiotype of a leukemia patient's B cell antigen receptor [135] and a VLR that recognizes a novel plasma cell-restricted epitope on human CD38 [136], the screening approach allowed for sampling of only a few hundred clones. Our work, for the first time, combined immunization using mammalian membrane protein antigens with VLR library construction and YSD screening. This enabled millions of clones to be screened, yielded multiple VLRs that bind to brain endothelial cells *in vivo*, and facilitated additional rounds of screening for functional properties such as endocytosis.

The novel multi-tiered screening strategy developed and applied in this study combined the creation of an immunized library with elements of previously reported YSD screening approaches [92–94, 121] in order to rapidly isolate VLRs that target BBB ECs *in vivo*. Previous work carried out in our lab has established the YDIP procedure as a platform for discovery and optimization of antibodies against membrane protein targets through screening of combinatorial YSD libraries using detergent solubilized lysates of cultured cells as sources for antigen binding steps [46, 94, 239]. In this work we have extended the platform by employing detergent-solubilized antigen preparations derived from *ex vivo* mouse brain capillaries increasing the *in vivo* relevance of the antigens presented for binding during screening. This was a vital aspect of the screen design as it is well known that expression profiles are altered when BBB cells are cultured out of their natural environment [102, 103] and therefore screening with antigens derived from in vitro cultured cells alone can yield antibodies against culture artifacts with no *in vivo* relevance [93]. Initial rounds of screening employing a binding step with solubilized BCPM antigens coupled to MACS or FACS sorting were therefore aimed at selectively enriching VLR that recognize membrane protein targets expressed by BBB ECs *in vivo* and de-enriching for culture artifacts which should be present at low levels or absent in the BCPM preparations. This YDIP enrichment procedure was coupled to downstream biopanning screening to enrich for binders to cell surface antigens. YSD biopanning on live MBEC monolayers eliminates the possibility of VLRs interacting with intracellular epitopes of integral membrane proteins or membrane-associated intracellular machinery, ensuring enrichment of clones targeting cell surface exposed epitopes. Furthermore, subtractive binding steps

are a common feature of panning campaigns and can be coupled to subsequent positive binding steps for the removal of unwanted clones in line with the enrichment of desired clones. In this case, each round of biopanning included an initial incubation on decellularized MBEC ECM followed immediately by an MBEC binding incubation with yeast recovered in the non-binding fraction from the ECM plate. The overall coupling of the YDIP procedure for the enrichment of *in vivo*-relevant binders with ECM-/EC+ biopanning for selective enrichment of VLR targeting cell-surface exposed epitopes was quite successful as around 85% of the final pool specifically recognized MBEC cell surface antigens and >60% of *in vitro* binding VLR also bound their target in mouse brain capillaries. In contrast, only <5% of *in vitro* binding antibodies recognized *in vivo* antigens in a previous YSD screening study where biopanning was used alone [93]. As a result of this targeted enrichment there was a high rate of success when translating in vitro cell surface binders to the *in vivo* environment as 3 out of 4 VLR tested were shown to target brain vasculature when administered IV in mice (Figure 4-6). Therefore, the lamprey immunization, screening, and clone selection pipeline presented here (Figure 4-2) represents a robust platform for the identification of cell surface targeting antibodies that can be easily and rapidly translated to relevant animal models. Given numerous examples of the ability to raise VLR against a wide array of protein and glycan antigens [134, 136, 137], this optimized platform could be applied to VLR-based antibody discovery in other fields.

The lead VLR-Fcs identified from the screening platform described above, VLR-Fc-11, 30, and 46, were shown to cross-react with mouse, rat, and human BBB antigens (Figure 4-9 C). One motivation for using VLRs instead of traditional Ig

antibodies was that the much greater phylogenetic distance between the immunized animal and the animal that was the source of antigens could potentially expand the accessible antigen repertoire by avoiding self-tolerance enabling the enrichment of VLR targeting conserved mammalian epitopes not accessible to naturally occurring Ig-based antibodies. A round of whole genome duplication is thought to have occurred in a common ancestor of all jawed vertebrates, but not jawless vertebrates, leading to the expansion of some gene families in the jawed vertebrate lineage. Thus, in addition to sequence divergence between conserved genes in phylogenetically distant jawed and jawless vertebrates, some large gene families are missing from jawless vertebrates, such as major histocompatibility complex class I and II and clustered protocadherins. Furthermore, VLRs have been readily isolated that bind to multiple different mammalian carbohydrate antigens, which implies that many mammalian glycan structures are absent in lampreys. Therefore, the literature supports a wide divergence in the proteome and glycome between lamprey and mammals providing an increased likelihood of immunogenicity when immunizing lamprey with mammalian antigen preparations. While the hypothesis that phylogentic distance allows for recognition of novel mammalian epitopes has not been rigorously tested for the lamprey immune system, several studies suggest that immunizing chickens or sharks with mammalian antigens that are poorly-immunogenic in rodent models produces a robust immune response [282–288]. Furthermore, lampreys immunized with human multiple myeloma yielded a VLR that recognizes a plasma cell-restricted epitope on CD38 that had not been previously found using Ig-based antibodies [136]. In the current study VLR selected against murine antigens were found to cross-react with both rat and human

antigens suggesting they target conserved mammalian epitopes. In addition, competition assays showed that the lead VLRs do not target three established BBB receptors (Figure 4-9 B). Thus, the current evidence in the literature and findings in this report motivate future antigen identification and epitope mapping studies to gain definitive insight into the novelty of the targets.

In addition to phylogenetic distance, there are also several practical advantages of lamprey VLRs and immune VLR libraries. Lamprey larvae are small, low-maintenance animals that require relatively low doses of antigen for immunization (10-100 µg/larvae). The organization of the VLR genomic locus allows for PCR amplification of the entire repertoire with a single pair of primers, which greatly simplifies library construction relative to Ig gene libraries. Lampreys have on the order of 10^7 VLRB lymphocytes making it feasible to display the entire VLRB repertoire on yeast. This combination of ease of library construction and repertoire size makes it practical to construct immune VLR YSD libraries for each immunogen, rather than relying on one large non-immune library. The immune libraries have the advantage of facile and rapid enrichment for antigen-specific clones due to antigen-driven clonal expansion of lymphocytes *in vivo*. For instance, typically ~0.1-1% of VLR clones in an immune YSD library bind to antigen before sorting, whereas binders are not detectable above background before sorting on non-immune libraries. Finally, screening of the immunized BBBVLR library yielded VLR with affinities in the range of typical Ig-based BBB targeting reagents. The lead VLR-Fc were found to have low nanomolar equilibrium dissociation constants (Figure 4-9 A), which agrees favorably with affinities of Ig-based

antibodies and VLR isolated from both non-immune and immunized libraries typically ranging from low nanomolar to micromolar dissociation constants [65, 66, 134, 137].

VLR-Fc-11, 30, and 46, were initially selected based on their ability to endocytose into MBECs and where subsequently shown to target the BBB and traffic *in vivo*. To date, the screening platform of choice for the identification of antibodies capable of endocytosis has been phage display as the small size of phage particles is amenable to packaging in vesicles [66]. However, phage display screens designed to identify internalizing antibodies and peptides have typically yielded low clonal diversity due in part to expression bias and imposition of restrictive screening pressures [66, 67, 79, 110]. Yeast display screens are not hindered by the same extent of expression bias while, given the large size of yeast cells, internalization cannot be included directly as a screening pressure. Thus, we chose to use downstream internalization assays to screen for VLR capable of endocytosis. Through a non-exhaustive sampling of around 200 binding clones from the library we identified 16 out of 33 unique VLR that bound to *in vivo* relevant cell surface antigens and 4 of these clones had endocytosis capability in at least one of the *in vitro* internalization assays (Figure 4-5). This compares favorably with previous biopanning experiments where approximately 25% of unique cell-surface binders were found to endocytose [93]. Importantly, identification of *in vitro* internalization behavior was predictive of internalization *in vivo* as endocytosis and trafficking of IV administered VLR-Fc-11, 30, and 46 was confirmed through confocal (Figure 4-7) and EM (Figure 4-8) analysis. Although the antigens recognized by the 16 unique VLRs have not yet been identified, cell surface binding, intracellular localization, brain section staining patterns (Figure 4-4), and sequence diversity of the VLR clones

(data not shown) suggests that they recognize a varied set of BBB antigens. The diversity of these VLRs implies that the BBBVLR library has not been exhaustively screened and deeper sampling is likely to yield additional unique VLR capable of target engagement and trafficking *in vivo*.

Given their ability to engage target and traffic within mouse brain capillary endothelial cells after IV administration as well as their broad mammalian cross-reactivity, the lead VLRs identified here have potential for BBB targeting applications. However, work remains to further characterize their pharmacokinetics, biodistribution, and ability to deliver drug payloads to the brain. While the *in vivo* data demonstrate that these VLR-Fc are capable of endocytosis and trafficking at the BBB, the extent of transcytosis was not investigated. If transcytosis proves minimal upon further study, engineering of the affinity and avidity of VLR-antigen binding can be pursued to alter intracellular trafficking and enhance brain penetration [41–43, 289, 290] as VLR and VLR-based scaffolds have proven highly amenable to protein engineering techniques aimed at altering binding properties [137, 291]. Furthermore, if these attempts are fruitless, delivery of gene therapies into brain capillary endothelial cells is an attractive drug delivery approach in its own right that does not require transcytosis as the ECs can serve as a local reservoir for production of therapeutic proteins [109, 179]. Although VLR remain unexplored for therapeutic applications, two recent studies have demonstrated that Repebodies [292], consensus designed LRR domain proteins based on VLRs, can mediate therapeutic outcomes in animal models motivating further exploration of VLRs as a novel alternative to traditional Ig-based therapeutics [291,

293]. Thus, given further characterization and optimization as discussed above VLR-Fc-11, 30, and 46 are promising alternatives for brain drug delivery.

Supplemental Figures

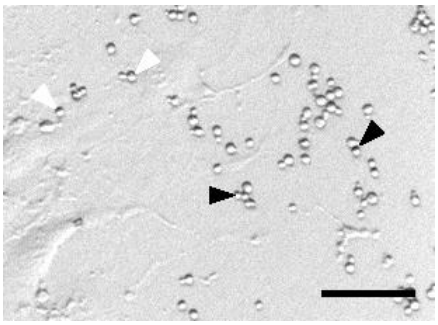

Supplemental Figure 4-S1: Biopanning experiment on sub-confluent MBECs reveals presence of a substantial population of ECM binding VLR in the BBBVLR-FACS library. Yeast (round phase dark cells) are found binding to both MBEC cells (white arrowheads), and ECM (black arrowheads). Scale = 50 µm

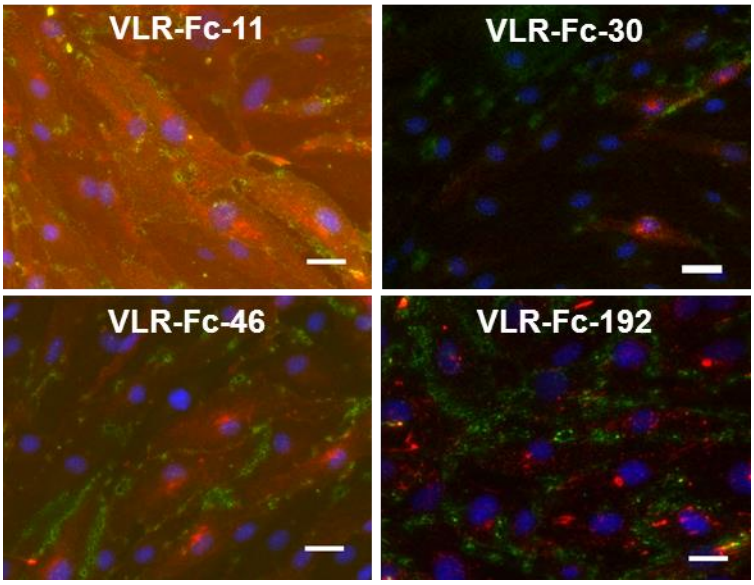

Supplemental Figure 4-S2: Binding and internalization assay with VLR-Fc on MBECs. VLR-Fc-11, 46, and 192 are internalized by the majority of cells. On the other hand, only a small sub-population of MBECs are capable of internalization of VLR-Fc-30 while surface binding signal is seen throughout the plate. Red=internalized VLR-Fc, Green=Surface-bound VLR-Fc, Blue=DAPI. Scale=25 µm

References

1. Xu J, Murphy SL, Kochanek KD, Bastian BA (2016) Deaths: Final Data for 2013. *Natl Vital Stat Rep* 64(2):1–119.

2. World Health Organization. (2006) *Neurological disorders : public health challenges.* (World Health Organization).

3. Palmer AM (2010) The role of the blood-CNS barrier in CNS disorders and their treatment. *Neurobiol Dis* 37:3–12.

4. Alavijeh MS, Chishty M, Qaiser MZ, Palmer AMC-1201315 (2005) Drug metabolism and pharmacokinetics, the blood-brain barrier, and central nervous system drug discovery. *NeuroRx* 2:554–571.

5. Pardridge WM (2005) The blood-brain barrier: bottleneck in brain drug development. *NeuroRx* 2:3–14.

6. Nitta T, et al. (2003) Size-selective loosening of the blood-brain barrier in claudin-5-deficient mice. *J Cell Biol* 161(3):653–60.

7. Pardridge WM (2008) Re-engineering biopharmaceuticals for delivery to brain with molecular Trojan horses. *Bioconjug Chem* 19(7):1327–38.

8. Pardridge WM (2007) Blood-brain barrier delivery. *Drug Discov Today* 12:54–61.

9. Correale J, Villa A (2009) Cellular Elements of the Blood-Brain Barrier. *Neurochem Res* 34:2067–2077.

10. Abbott NJ, Patabendige AAK, Dolman DEM, Yusof SR, Begley DJ (2010) Structure and function of the blood-brain barrier. *Neurobiol Dis* 37(1):13–25.

11. Hartz AMS, Bauer B (2011) ABC transporters in the CNS - an inventory. *Curr Pharm Biotechnol* 12(4):656–73.

12. Nakagawa S, et al. (2009) A new blood-brain barrier model using primary rat brain endothelial cells, pericytes and astrocytes. *Neurochem Int* 54:253–263.

13. Wolburg H, Noell S, Mack A, Wolburg-Buchholz K, Fallier-Becker P (2009) Brain endothelial cells and the glio-vascular complex. *Cell Tissue Res* 335:75–96.

14. Guo X, Geng M, Du G (2005) Glucose transporter 1, distribution in the brain and in neural disorders: its relationship with transport of neuroactive drugs through the blood-brain barrier. *Biochem Genet* 43:175–187.

15. Dauchy S, et al. (2008) ABC transporters, cytochromes P450 and their main transcription factors: expression at the human blood-brain barrier. *J Neurochem* 107:1518–1528.

16. Giri N, et al. (2008) Investigation of the role of breast cancer resistance protein (Bcrp/Abcg2) on pharmacokinetics and central nervous system penetration of abacavir and zidovudine in the mouse. *Drug Metab Dispos* 36:1476–1484.

17. Abbott NJ, Ronnback L, Hansson E (2006) Astrocyte-endothelial interactions at the blood-brain barrier. *Nat Rev Neurosci* 7:41–53.

18. Brasnjevic I, Steinbusch HWM, Schmitz C, Martinez-Martinez P, European NanoBioPharmaceutics R (2009) Delivery of peptide and protein drugs over the blood-brain barrier. *Prog Neurobiol* 87:212–251.

19. Vangilder RL, Rosen CL, Barr TL, Huber JDC-3092634 (2011) Targeting the neurovascular unit for treatment of neurological disorders. *Pharmacol Ther* 130:239–247.

20. Gynther M, et al. (2008) Large neutral amino acid transporter enables brain drug delivery via prodrugs. *J Med Chem* 51(4):932–6.

21. Lajoie JM, Shusta EV (2015) *Targeting receptor-mediated transport for delivery of biologics across the blood-brain barrier* doi:10.1146/annurev-pharmtox-010814-124852.

22. Herz J, Marschang P (2003) Coaxing the LDL receptor family into the fold. *Cell* 112:289–292.

23. Ulbrich K, Knobloch T, Kreuter J (2011) Targeting the insulin receptor: nanoparticles for drug delivery across the blood-brain barrier (BBB). *J Drug Target* 19:125–132.

24. Visser CC, Voorwinden LH, Crommelin DJA, Danhof M, de Boer AG (2004) Characterization and modulation of the transferrin receptor on brain capillary endothelial cells. *Pharm Res* 21:761–769.

25. Hu Y-B, Dammer EB, Ren R-J, Wang G (2015) The endosomal-lysosomal system: from acidification and cargo sorting to neurodegeneration. *Transl Neurodegener* 4:18.

26. Grant BD, Donaldson JG (2009) Pathways and mechanisms of endocytic recycling. *Nat Rev Mol Cell Biol* 10:597–608.

27. Gan Y, McGraw TE, Rodriguez-Boulan E (2002) The epithelial-specific adaptor AP1B mediates post-endocytic recycling to the basolateral membrane. *Nat Cell Biol* 4(8):605–9.

28. Dehouck B, et al. (1997) A new function for the LDL receptor: transcytosis of LDL across the blood-brain barrier. *J Cell Biol* 138(4):877–89.

29. Candela P, et al. (2008) Physiological pathway for low-density lipoproteins across the blood-brain barrier: transcytosis through brain capillary endothelial cells in vitro. *Endothelium* 15(5-6):254–64.

30. Chung NS, Wasan KM (2004) Potential role of the low-density lipoprotein receptor family as mediators of cellular drug uptake. *Adv Drug Deliv Rev* 56(9):1315–34.

31. Descamps L, Dehouck MP, Torpier G, Cecchelli R (1996) Receptor-mediated transcytosis of transferrin through blood-brain barrier endothelial cells. *Am J Physiol* 270(4 Pt 2):H1149–58.

32. Jefferies WA, et al. Transferrin receptor on endothelium of brain capillaries. *Nature* 312(5990):162–3.

33. Friden PM, et al. (1991) Anti-transferrin receptor antibody and antibody-drug conjugates cross the blood-brain barrier. *Proc Natl Acad Sci U S A* 88(11):4771–5.

34. Jones AR, Shusta E V (2007) Blood-brain barrier transport of therapeutics via receptor-mediation. *Pharm Res* 24:1759–1771.

35. Kurzrock R, et al. (2012) Safety, pharmacokinetics, and activity of GRN1005, a novel conjugate of angiopep-2, a peptide facilitating brain penetration, and paclitaxel, in patients with advanced solid tumors. *Mol Cancer Ther* 11(2):308–16.

36. Drappatz J, et al. (2013) Phase I study of GRN1005 in recurrent malignant glioma. *Clin Cancer Res* 19(6):1567–76.

37. Kelaita D (2016) ArmaGen Pipeline. Available at: http://www.armagen.com/pipeline [Accessed September 3, 2014].

38. Ueno M, et al. (2010) Transporters in the brain endothelial barrier. *Curr Med Chem* 17(12):1125–38.

39. Couch JA, et al. (2013) Addressing safety liabilities of TfR bispecific antibodies that cross the blood-brain barrier. *Sci Transl Med* 5(183):183ra57, 1–12.

40. Ohshima-Hosoyama S, et al. (2012) A monoclonal antibody-GDNF fusion protein is not neuroprotective and is associated with proliferative pancreatic lesions in parkinsonian monkeys. *PLoS One* 7(6):e39036.

41. Yu YJ, et al. (2011) Boosting brain uptake of a therapeutic antibody by reducing its affinity for a transcytosis target. *Sci Transl Med* 3(84):84ra44.

42. Bien-Ly N, et al. (2014) Transferrin receptor (TfR) trafficking determines brain uptake of TfR antibody affinity variants. *J Exp Med*. doi:10.1084/jem.20131660.

43. Niewoehner J, et al. (2014) Increased Brain Penetration and Potency of a Therapeutic Antibody Using a Monovalent Molecular Shuttle. *Neuron* 81(1):49–60.

44. Raub TJ, Newton CR (1991) Recycling kinetics and transcytosis of transferrin in primary cultures of bovine brain microvessel endothelial cells. *J Cell Physiol* 149(1):141–51.

45. Mayle KM, Le AM, Kamei DT (2012) The intracellular trafficking pathway of transferrin. *Biochim Biophys Acta-General Subj* 1820:264–281.

46. Tillotson BJ, Goulatis LI, Parenti I, Duxbury E, Shusta E V (2015) Engineering an Anti-Transferrin Receptor ScFv for pH-Sensitive Binding Leads to Increased Intracellular Accumulation. *PLoS One* 10(12):e0145820.

47. Clark AJ, Davis ME (2015) Increased brain uptake of targeted nanoparticles by adding an acid-cleavable linkage between transferrin and the nanoparticle core. *Proc Natl Acad Sci* 112(40):12486–12491.

48. Li JY, Boado RJ, Pardridge WM (2001) Blood-brain barrier genomics. *J Cereb Blood Flow Metab* 21(1):61–8.

49. Li JY, Boado RJ, Pardridge WM (2002) Rat Blood – Brain Barrier Genomics . II. *J Cereb blood flow Metab* 22:1319–1326.

50. Shusta E V, Boado RJ, Mathern GW, Pardridge WM (2002) Vascular genomics of the human brain. *J Cereb Blood Flow Metab* 22(3):245–52.

51. Enerson BE, Drewes LR (2006) The rat blood-brain barrier transcriptome. *J Cereb Blood Flow Metab* 26(7):959–73.

52. Daneman R, et al. (2010) The Mouse Blood-Brain Barrier Transcriptome: A New Resource for Understanding the Development and Function of Brain Endothelial Cells. *PLoS One* 5. doi:e13741 10.1371/journal.pone.0013741.

53. Tam SJ, et al. (2012) Death Receptors DR6 and TROY Regulate Brain Vascular Development. *Dev Cell* 22:403–417.

54. Zhang Y, et al. (2014) An RNA-Sequencing Transcriptome and Splicing Database of Glia, Neurons, and Vascular Cells of the Cerebral Cortex. *J Neurosci* 34(36):11929–47.

55. Nolan DJ, et al. (2013) Molecular signatures of tissue-specific microvascular endothelial cell heterogeneity in organ maintenance and regeneration. *Dev Cell* 26(2):204–19.

56. Zamore PD, Haley B (2005) Ribo-gnome: the big world of small RNAs. *Science* 309(5740):1519–24.

57. Järvelin AI, Noerenberg M, Davis I, Castello A (2016) The new (dis)order in RNA regulation. *Cell Commun Signal* 14:9.

58. Kamiie J, et al. (2008) Quantitative atlas of membrane transporter proteins: development and application of a highly sensitive simultaneous LC/MS/MS method combined with novel in-silico peptide selection criteria. *Pharm Res* 25(6):1469–83.

59. Uchida Y, et al. (2011) Quantitative targeted absolute proteomics of human blood-brain barrier transporters and receptors. *J Neurochem* 117(2):333–45.

60. Lu Q, et al. (2008) Analysis of mouse brain microvascular endothelium using immuno-laser capture microdissection coupled to a hybrid linear ion trap with Fourier transform-mass spectrometry proteomics platform. *Electrophoresis* 29(12):2689–95.

61. Chun HB, et al. (2011) The proteome of mouse brain microvessel membranes and basal lamina. *J Cereb Blood Flow Metab* 31(12):2267–81.

62. Agarwal N, Shusta E V (2009) Multiplex expression cloning of blood-brain barrier membrane proteins. *Proteomics* 9:1099–1108.

63. Agarwal N, Lippmann ES, Shusta E V (2010) Identification and expression profiling of blood-brain barrier membrane proteins. *J Neurochem* 112(3):625–35.

64. Zuchero YJY, et al. (2015) Discovery of Novel Blood-Brain Barrier Targets to Enhance Brain Uptake of Therapeutic Antibodies. *Neuron* 89(1):70–82.

65. Feldhaus MJ, et al. (2003) Flow-cytometric isolation of human antibodies from a

nonimmune Saccharomyces cerevisiae surface display library. *Nat Biotechnol* 21:163–170.

66. Poul MA, Becerril B, Nielsen UB, Morisson P, Marks JD (2000) Selection of tumor-specific internalizing human antibodies from phage libraries. *J Mol Biol* 301:1149–1161.

67. Muruganandam A, Tanha J, Narang S, Stanimirovic D (2002) Selection of phage-displayed llama single-domain antibodies that transmigrate across human blood-brain barrier endothelium. *FASEB J* 16(2):240–2.

68. Rakestraw JA, Aird D, Aha PM, Baynes BM, Lipovsek D (2011) Secretion-and-capture cell-surface display for selection of target-binding proteins. *Protein Eng Des Sel* 24(6):525–30.

69. Rhiel L, et al. (2014) REAL-Select: full-length antibody display and library screening by surface capture on yeast cells. *PLoS One* 9(12):e114887.

70. Ponsel D, Neugebauer J, Ladetzki-Baehs K, Tissot K (2011) High affinity, developability and functional size: the holy grail of combinatorial antibody library generation. *Molecules* 16(5):3675–700.

71. Prassler J, et al. (2011) HuCAL PLATINUM, a synthetic Fab library optimized for sequence diversity and superior performance in mammalian expression systems. *J Mol Biol* 413(1):261–78.

72. Merkenschlager J, et al. (2016) Stepwise B-cell-dependent expansion of T helper clonotypes diversifies the T-cell response. *Nat Commun* 7:10281.

73. Song H, Nie X, Basu S, Cerny J (1998) Antibody feedback and somatic mutation in B cells: regulation of mutation by immune complexes with IgG antibody. *Immunol Rev* 162:211–8.

74. Stavnezer J (2011) Complex regulation and function of activation-induced cytidine deaminase. *Trends Immunol* 32(5):194–201.

75. Krumpe LRH, Mori T (2006) The Use of Phage-Displayed Peptide Libraries to Develop Tumor-Targeting Drugs. *Int J Pept Res Ther* 12(1):79–91.

76. Bradbury ARM, Marks JD (2004) Antibodies from phage antibody libraries. *J Immunol Methods* 290(1-2):29–49.

77. Pande J, Szewczyk MM, Grover AK Phage display: concept, innovations, applications and future. *Biotechnol Adv* 28(6):849–58.

78. Rakonjac J, Bennett NJ, Spagnuolo J, Gagic D, Russel M (2011) Filamentous bacteriophage: biology, phage display and nanotechnology applications. *Curr Issues Mol Biol* 13(2):51–76.

79. Umlauf BJ, Mercedes JS, Chung C-Y, Brown KC (2014) Identification of a novel lysosomal trafficking peptide using phage display biopanning coupled with endocytic selection pressure. *Bioconjug Chem* 25(10):1829–37.

80. Grieger JC, Samulski RJ (2012) Adeno-associated virus vectorology, manufacturing, and clinical applications. *Methods Enzymol* 507:229–54.

81. Bevan AK, et al. (2011) Systemic gene delivery in large species for targeting spinal cord, brain, and peripheral tissues for pediatric disorders. *Mol Ther* 19(11):1971–80.

82. Dominguez E, et al. (2011) Intravenous scAAV9 delivery of a codon-optimized SMN1 sequence rescues SMA mice. *Hum Mol Genet* 20(4):681–93.

83. Adachi K, Nakai H (2010) A new recombinant adeno-associated virus (AAV)-based random peptide dislpay library system: infection-defective AAV1.9-3 as a novel detargeted platform for vector evolution. *Gene Ther Regul* 5(1):31–55.

84. Boder ET, Wittrup KD (1997) Yeast surface display for screening combinatorial polypeptide libraries. *Nat Biotechnol* 15:553–557.

85. Boder ET, Wittrup KD (1998) Optimal screening of surface-displayed polypeptide libraries. *Biotechnol Prog* 14:55–62.

86. Shusta E V, Holler PD, Kieke MC, Kranz DM, Wittrup KD (2000) Directed evolution of a stable scaffold for T-cell receptor engineering. *Nat Biotechnol* 18(7):754–9.

87. Boder ET, Midelfort KS, Wittrup KD (2000) Directed evolution of antibody fragments with monovalent femtomolar antigen-binding affinity. *Proc Natl Acad Sci U S A* 97(20):10701–5.

88. Gai SA, Wittrup KD (2007) Yeast surface display for protein engineering and characterization. *Curr Opin Struct Biol* 17:467–473.

89. Pepper LR, Cho YK, Boder ET, Shusta E V (2008) A decade of yeast surface display technology: Where are we now? *Comb Chem High Throughput Screen* 11:127–134.

90. Boder ET, Wittrup KD (2000) Yeast surface display for directed evolution of protein expression, affinity, and stability. *Appl Chimeric Genes Hybrid Proteins, Pt C* 328:430–444.

91. Kondo A, Ueda M (2004) Yeast cell-surface display - applications of molecular display. *Appl Microbiol Biotechnol* 64:28–40.

92. Wang XX, Shusta E V (2005) The use of scFv-displaying yeast in mammalian cell surface selections. *J Immunol Methods* 304(1-2):30–42.

93. Wang XX, Cho YK, Shusta E V (2007) Mining a yeast library for brain endothelial cell-binding antibodies. *Nat Methods* 4:143–145.

94. Cho YK, Shusta E V (2010) Antibody library screens using detergent-solubilized mammalian cell lysates as antigen sources. *Protein Eng Des Sel* 23:567–577.

95. Stutz CC (2015) Identification of novel scFv that target the blood-brain barrier.

96. Gray SJ, et al. (2010) Directed evolution of a novel adeno-associated virus (AAV) vector that crosses the seizure-compromised blood-brain barrier (BBB). *Mol Ther* 18(3):570–8.

97. Roux F, et al. (1994) Regulation of gamma-glutamyl transpeptidase and alkaline phosphatase activities in immortalized rat brain microvessel endothelial cells. *J Cell Physiol* 159(1):101–13.

98. Williams RL, et al. (1989) Endothelioma cells expressing the polyoma middle T oncogene induce hemangiomas by host cell recruitment. *Cell* 57(6):1053–63.

99. Weksler BB, et al. (2005) Blood-brain barrier-specific properties of a human adult brain endothelial cell line. *FASEB J* 19(13):1872–4.

100. Lippmann ES, et al. (2012) Derivation of blood-brain barrier endothelial cells from human pluripotent stem cells. *Nat Biotechnol* 30(8):783–91.

101. Lippmann ES, Al-Ahmad A, Azarin SM, Palecek SP, Shusta E V (2014) A retinoic acid-enhanced, multicellular human blood-brain barrier model derived from stem cell sources. *Sci Rep* 4:4160.

102. Calabria AR, Shusta E V (2008) A genomic comparison of in vivo and in vitro brain microvascular endothelial cells. *J Cereb Blood Flow Metab* 28(1):135–48.

103. Lyck R, et al. (2009) Culture-induced changes in blood-brain barrier transcriptome: implications for amino-acid transporters in vivo. *J Cereb Blood Flow Metab* 29(9):1491–502.

104. Valadon P, et al. (2006) Screening phage display libraries for organ-specific vascular immunotargeting in vivo. *Proc Natl Acad Sci U S A* 103(2):407–12.

105. Cho YK, Chen I, Wei X, Li LJ, Shusta E V (2009) A yeast display immunoprecipitation method for efficient isolation and characterization of antigens. *J Immunol Methods* 341:117–126.

106. Agarwal N, Shusta E V (2009) Multiplex expression cloning of blood-brain barrier membrane proteins. *Proteomics* 9(4):1099–108.

107. Hong H-Y, et al. (2008) Detection of apoptosis in a rat model of focal cerebral ischemia using a homing peptide selected from in vivo phage display. *J Control Release* 131(3):167–72.

108. Roodink I, et al. (2010) Isolation of targeting nanobodies against co-opted tumor vasculature. *Lab Invest* 90(1):61–7.

109. Chen YH, Chang M, Davidson BL (2009) Molecular signatures of disease brain endothelia provide new sites for CNS-directed enzyme therapy. *Nat Med* 15(10):1215–8.

110. Jones AR, Stutz CC, Zhou Y, Marks JD, Shusta E V (2014) Identifying blood-brain-barrier selective single-chain antibody fragments. *Biotechnol J* 9(5):664–74.

111. Abulrob A, Sprong H, Van Bergen en Henegouwen P, Stanimirovic D (2005) The blood-brain barrier transmigrating single domain antibody: mechanisms of transport and antigenic epitopes in human brain endothelial cells. *J Neurochem* 95(4):1201–14.

112. Farrington GK, et al. (2014) A novel platform for engineering blood-brain barrier-crossing

bispecific biologics. *FASEB J*. doi:10.1096/fj.14-253369.

113. Webster CI, et al. (2016) Brain penetration, target engagement, and disposition of the blood-brain barrier-crossing bispecific antibody antagonist of metabotropic glutamate receptor type 1. *FASEB J*. doi:10.1096/fj.201500078.

114. Abulrob A, Stanimirovic D, Muruganandam A (2007) Blood-brain barrier epitopes and uses thereof.

115. Paulusma CC, et al. (2008) ATP8B1 requires an accessory protein for endoplasmic reticulum exit and plasma membrane lipid flippase activity. *Hepatology* 47(1):268–78.

116. Folmer DE, et al. (2012) Cellular localization and biochemical analysis of mammalian CDC50A, a glycosylated β-subunit for P4 ATPases. *J Histochem Cytochem* 60(3):205–18.

117. Li J, et al. (2011) Targeting the brain with PEG-PLGA nanoparticles modified with phage-displayed peptides. *Biomaterials* 32(21):4943–50.

118. Li J, et al. (2012) Identification of peptide sequences that target to the brain using in vivo phage display. *Amino Acids* 42(6):2373–81.

119. Bowley DR, Labrijn AF, Zwick MB, Burton DR (2007) Antigen selection from an HIV-1 immune antibody library displayed on yeast yields many novel antibodies compared to selection from the same library displayed on phage. *Protein Eng Des Sel* 20(2):81–90.

120. Ackerman M, et al. Highly avid magnetic bead capture: an efficient selection method for de novo protein engineering utilizing yeast surface display. *Biotechnol Prog* 25(3):774–83.

121. Stern LA, et al. (2016) Geometry and expression enhance enrichment of functional yeast-displayed ligands via cell panning. *Biotechnol Bioeng*. doi:10.1002/bit.26001.

122. Zhang X, Wang XX, Shusta E V (2014) Creation and Evaluation of a Single-chain Antibody Tetramer that Targets Brain Endothelial Cells. *AIChE J* 60(4):1245–1252.

123. Zhou H, Zhang Y-L, Lu G, Ji H, Rodi CP (2011) Recombinant antibody libraries and selection technologies. *N Biotechnol* 28(5):448–52.

124. Pelat T, Hust M, Thullier P (2009) Obtention and engineering of non-human primate (NHP) antibodies for therapeutics. *Mini Rev Med Chem* 9(14):1633–8.

125. Finstad J, Good RA (1964) Immunologic responses in the lamprey. *J Exp Med* 120(6):1151–1168.

126. Linthicum DS, Hildemann WH (1970) Immunologic responses of Pacific hagfish. 3. Serum antibodies to cellular antigens. *J Immunol* 105(4):912–8.

127. Pancer Z, et al. (2004) Somatic diversification of variable lymphocyte receptors in the agnathan sea lamprey. *Nature* 430(6996):174–80.

128. Herrin BR, et al. (2008) Structure and specificity of lamprey monoclonal antibodies. *Proc*

Natl Acad Sci U S A 105(6):2040–5.

129. Herrin BR, Cooper MD (2010) Alternative adaptive immunity in jawless vertebrates. *J Immunol* 185(3):1367–74.

130. Kasahara M, Sutoh Y (2014) Two forms of adaptive immunity in vertebrates: similarities and differences. *Adv Immunol* 122:59–90.

131. Velikovsky CA, et al. (2009) Structure of a lamprey variable lymphocyte receptor in complex with a protein antigen. *Nat Struct Mol Biol* 16(7):725–30.

132. Han BW, Herrin BR, Cooper MD, Wilson IA (2008) Antigen recognition by variable lymphocyte receptors. *Science* 321(5897):1834–7.

133. Luo M, et al. (2013) Recognition of the Thomsen-Friedenreich pancarcinoma carbohydrate antigen by a lamprey variable lymphocyte receptor. *J Biol Chem* 288(32):23597–606.

134. Hong X, et al. (2013) Sugar-binding proteins from fish: selection of high affinity “lambodies” that recognize biomedically relevant glycans. *ACS Chem Biol* 8(1):152–60.

135. Nakahara H, et al. (2013) Chronic lymphocytic leukemia monitoring with a Lamprey idiotope-specific antibody. *Cancer Immunol Res* 1(4):223–8.

136. Yu C, et al. (2016) Identification of human plasma cells with a lamprey monoclonal antibody. *JCI Insight* 1(3). doi:10.1172/jci.insight.84738.

137. Tasumi S, et al. (2009) High-affinity lamprey VLRA and VLRB monoclonal antibodies. *Proc Natl Acad Sci U S A* 106(31):12891–6.

138. Daneman R (2012) The blood-brain barrier in health and disease. *Ann Neurol* 72(5):648–72.

139. Ohtsuki S, Terasaki T (2007) Contribution of carrier-mediated transport systems to the blood-brain barrier as a supporting and protecting interface for the brain; importance for CNS drug discovery and development. *Pharm Res* 24(9):1745–58.

140. Begley DJ (2004) ABC transporters and the blood-brain barrier. *Curr Pharm Des* 10:1295–1312.

141. Hartz AMS, Miller DS, Bauer B (2010) Restoring blood-brain barrier P-glycoprotein reduces brain amyloid-beta in a mouse model of Alzheimer’s disease. *Mol Pharmacol* 77(5):715–23.

142. Kumagai AK, Eisenberg JB, Pardridge WM (1987) Absorptive-mediated endocytosis of cationized albumin and a beta-endorphin-cationized albumin chimeric peptide by isolated brain capillaries. Model system of blood-brain barrier transport. *J Biol Chem* 262(31):15214–15219.

143. Poduslo JF, Curran GL (1996) Polyamine modification increases the permeability of proteins at the blood-nerve and blood-brain barriers. *J Neurochem* 66(4):1599–609.

144. Poduslo JF, Curran GL, Gill JS (1998) Putrescine-modified nerve growth factor: bioactivity, plasma pharmacokinetics, blood-brain/nerve barrier permeability, and nervous system biodistribution. *J Neurochem* 71(4):1651–60.

145. Hervé F, Ghinea N, Scherrmann J-M (2008) CNS delivery via adsorptive transcytosis. *AAPS J* 10(3):455–72.

146. Duffy KR, Pardridge WM (1987) Blood-brain barrier transcytosis of insulin in developing rabbits. *Brain Res* 420(1):32–38.

147. Golden PL, Maccagnan TJ, Pardridge WM (1997) Human blood-brain barrier leptin receptor. Binding and endocytosis in isolated human brain microvessels. *J Clin Invest* 99(1):14–8.

148. Parkar NS, et al. (2009) Vesicle formation and endocytosis: function, machinery, mechanisms, and modeling. *Antioxid Redox Signal* 11(6):1301–12.

149. Rodriguez-Boulan E, Kreitzer G, Müsch A (2005) Organization of vesicular trafficking in epithelia. *Nat Rev Mol Cell Biol* 6(3):233–47.

150. Brooks DA (2009) The endosomal network. *Int J Clin Pharmacol Ther* 47 Suppl 1:S9–17.

151. Strazielle N, Ghersi-Egea JF (2013) Physiology of blood-brain interfaces in relation to brain disposition of small compounds and macromolecules. *Mol Pharm* 10(5):1473–91.

152. Pardridge WM, Buciak JL, Friden PM (1991) Selective transport of an anti-transferrin receptor antibody through the blood-brain barrier in vivo. *J Pharmacol Exp Ther* 259(1):66–70.

153. Broadwell RD, BakerCairns BJ, Friden PM, Oliver C, Villegas JC (1996) Transcytosis of protein through the mammalian cerebral epithelium and endothelium .3. Receptor-mediated transcytosis through the blood-brain barrier of blood-borne transferrin and antibody against the transferrin receptor. *Exp Neurol* 142:47–65.

154. Lu JZ, Hui EK-W, Boado RJ, Pardridge WM (2010) Genetic engineering of a bifunctional IgG fusion protein with iduronate-2-sulfatase. *Bioconjug Chem* 21(1):151–6.

155. Gabathuler R (2010) Development of new peptide vectors for the transport of therapeutic across the blood-brain barrier. *Ther Deliv* 1(4):571–86.

156. Daneman R, et al. (2010) The mouse blood-brain barrier transcriptome: a new resource for understanding the development and function of brain endothelial cells. *PLoS One* 5(10):e13741.

157. Moos T, Morgan EH (2000) Transferrin and transferrin receptor function in brain barrier systems. *Cell Mol Neurobiol* 20(1):77–95.

158. Sharma G, et al. (2013) Cell penetrating peptide tethered bi-ligand liposomes for delivery to brain in vivo: Biodistribution and transfection. *J Control Release* 167(1):1–10.

159. Staquicini FI, et al. (2011) Systemic combinatorial peptide selection yields a non-canonical iron-mimicry mechanism for targeting tumors in a mouse model of human

glioblastoma. *J Clin Invest* 121(1):161–173.

160. Hajitou A, et al. (2006) A hybrid vector for ligand-directed tumor targeting and molecular imaging. *Cell* 125(2):385–98.

161. Hajitou A, et al. (2007) Design and construction of targeted AAVP vectors for mammalian cell transduction. *Nat Protoc* 2(3):523–31.

162. Qian ZM, Li HY, Sun HZ, Ho K (2002) Targeted drug delivery via the transferrin receptor-mediated endocytosis pathway. *Pharmacol Rev* 54:561–587.

163. Boado RJ, Zhang Y, Wang Y, Pardridge WM (2009) Engineering and expression of a chimeric transferrin receptor monoclonal antibody for blood-brain barrier delivery in the mouse. *Biotechnol Bioeng* 102(4):1251–8.

164. Sumbria RK, et al. (2013) Pharmacokinetics and brain uptake of an IgG-TNF decoy receptor fusion protein following intravenous, intraperitoneal, and subcutaneous administration in mice. *Mol Pharm* 10(4):1425–31.

165. Zhou Q-H, Boado RJ, Hui EK-W, Lu JZ, Pardridge WM (2011) Brain-penetrating tumor necrosis factor decoy receptor in the mouse. *Drug Metab Dispos* 39(1):71–6.

166. Zhou Q-H, et al. (2011) Neuroprotection with a brain-penetrating biologic tumor necrosis factor inhibitor. *J Pharmacol Exp Ther* 339(2):618–23.

167. Zhou Q-H, Hui EK-W, Lu JZ, Boado RJ, Pardridge WM (2011) Brain penetrating IgG-erythropoietin fusion protein is neuroprotective following intravenous treatment in Parkinson's disease in the mouse. *Brain Res* 1382:315–20.

168. Fu A, et al. (2010) Intravenous treatment of experimental Parkinson's disease in the mouse with an IgG-GDNF fusion protein that penetrates the blood-brain barrier. *Brain Res* 1352:208–13.

169. Zhang Y, Pardridge WM (2009) Near complete rescue of experimental Parkinson's disease with intravenous, non-viral GDNF gene therapy. *Pharm Res* 26(5):1059–63.

170. Boado RJ, Zhou Q-H, Lu JZ, Hui EK-W, Pardridge WM (2010) Pharmacokinetics and brain uptake of a genetically engineered bifunctional fusion antibody targeting the mouse transferrin receptor. *Mol Pharm* 7(1):237–44.

171. Sumbria RK, Hui EK-W, Lu JZ, Boado RJ, Pardridge WM (2013) Disaggregation of amyloid plaque in brain of Alzheimer's disease transgenic mice with daily subcutaneous administration of a tetravalent bispecific antibody that targets the transferrin receptor and the abeta amyloid Peptide. *Mol Pharm* 10(9):3507–13.

172. Zhou Q-H, et al. (2011) Receptor-mediated abeta amyloid antibody targeting to Alzheimer's disease mouse brain. *Mol Pharm* 8(1):280–5.

173. Lee HJ, Engelhardt B, Lesley J, Bickel U, Pardridge WM (2000) Targeting rat anti-mouse transferrin receptor monoclonal antibodies through blood-brain barrier in mouse. *J Pharmacol Exp Ther* 292:1048–1052.

174. Zhang Y, Wang Y, Boado RJ, Pardridge WM (2008) Lysosomal enzyme replacement of the brain with intravenous non-viral gene transfer. *Pharm Res* 25(2):400–6.

175. Karatas H, et al. (2009) A nanomedicine transports a peptide caspase-3 inhibitor across the blood-brain barrier and provides neuroprotection. *J Neurosci* 29(44):13761–9.

176. Crowe A, Morgan EH (1992) Iron and transferrin uptake by brain and cerebrospinal fluid in the rat. *Brain Res* 592(1-2):8–16.

177. Roberts R, Sandra A, Siek GC, Lucas JJ, Fine RE (1992) Studies of the mechanism of iron transport across the blood-brain barrier. *Ann Neurol* 32 Suppl:S43–50.

178. Banks W a, Jaspan JB, Huang W, Kastin a J (1997) Transport of insulin across the blood-brain barrier: saturability at euglycemic doses of insulin. *Peptides* 18(9):1423–9.

179. Bickel U, Yoshikawa T, Pardridge WM (2001) Delivery of peptides and proteins through the blood-brain barrier. *Adv Drug Deliv Rev* 46(1-3):247–79.

180. Pardridge WM, Kang YS, Buciak JL, Yang J (1995) Human insulin receptor monoclonal antibody undergoes high affinity binding to human brain capillaries in vitro and rapid transcytosis through the blood-brain barrier in vivo in the primate. *Pharm Res* 12(6):807–16.

181. Boado RJ, Zhang Y, Zhang Y, Pardridge WM (2007) Humanization of anti-human insulin receptor antibody for drug targeting across the human blood-brain barrier. *Biotechnol Bioeng* 96(2):381–91.

182. Boado RJ, et al. (2008) Genetic engineering of a lysosomal enzyme fusion protein for targeted delivery across the human blood-brain barrier. *Biotechnol Bioeng* 99(2):475–84.

183. Boado RJ, Pardridge WM (2010) Genetic engineering of IgG-glucuronidase fusion proteins. *J Drug Target* 18(3):205–11.

184. Lu JZ, Boado RJ, Hui EK-W, Zhou Q-H, Pardridge WM (2011) Expression in CHO cells and pharmacokinetics and brain uptake in the Rhesus monkey of an IgG-iduronate-2-sulfatase fusion protein. *Biotechnol Bioeng* 108(8):1954–64.

185. Wang D, et al. (2013) Engineering a lysosomal enzyme with a derivative of receptor-binding domain of apoE enables delivery across the blood-brain barrier. *Proc Natl Acad Sci U S A* 110(8):2999–3004.

186. Boado RJ, Hui EK-W, Lu JZ, Pardridge WM (2009) AGT-181: expression in CHO cells and pharmacokinetics, safety, and plasma iduronidase enzyme activity in Rhesus monkeys. *J Biotechnol* 144(2):135–41.

187. Boado RJ, Hui EK-W, Lu JZ, Pardridge WM (2012) Glycemic control and chronic dosing of rhesus monkeys with a fusion protein of iduronidase and a monoclonal antibody against the human insulin receptor. *Drug Metab Dispos* 40(10):2021–5.

188. Boado RJ, Zhang Y, Zhang Y, Xia C-F, Pardridge WM (2007) Fusion antibody for Alzheimer's disease with bidirectional transport across the blood-brain barrier and abeta fibril disaggregation. *Bioconjug Chem* 18(2):447–55.

189. Boado RJ, Lu JZ, Hui EK-W, Pardridge WM (2010) IgG-single chain Fv fusion protein therapeutic for Alzheimer's disease: Expression in CHO cells and pharmacokinetics and brain delivery in the rhesus monkey. *Biotechnol Bioeng* 105(3):627–35.

190. Boado RJ, Zhang Y, Zhang Y, Wang Y, Pardridge WM (2008) GDNF fusion protein for targeted-drug delivery across the human blood-brain barrier. *Biotechnol Bioeng* 100(2):387–96.

191. Boado RJ, Pardridge WM (2009) Comparison of blood-brain barrier transport of glial-derived neurotrophic factor (GDNF) and an IgG-GDNF fusion protein in the rhesus monkey. *Drug Metab Dispos* 37(12):2299–304.

192. Hui EK-W, Boado RJ, Pardridge WM Tumor necrosis factor receptor-IgG fusion protein for targeted drug delivery across the human blood-brain barrier. *Mol Pharm* 6(5):1536–43.

193. Boado RJ, Hui EK-W, Lu JZ, Zhou Q-H, Pardridge WM (2010) Selective targeting of a TNFR decoy receptor pharmaceutical to the primate brain as a receptor-specific IgG fusion protein. *J Biotechnol* 146(1-2):84–91.

194. Boado RJ, Hui EK-W, Lu JZ, Pardridge WM (2010) Drug targeting of erythropoietin across the primate blood-brain barrier with an IgG molecular Trojan horse. *J Pharmacol Exp Ther* 333(3):961–9.

195. Boado RJ, Zhang Y, Zhang Y, Wang Y, Pardridge WM IgG-paraoxonase-1 fusion protein for targeted drug delivery across the human blood-brain barrier. *Mol Pharm* 5(6):1037–43.

196. Boado RJ, Hui EK-W, Lu JZ, Pardridge WM (2011) CHO cell expression, long-term stability, and primate pharmacokinetics and brain uptake of an IgG-paroxonase-1 fusion protein. *Biotechnol Bioeng* 108(1):186–96.

197. Demeule M, et al. (2002) High transcytosis of melanotransferrin (P97) across the blood-brain barrier. *J Neurochem* 83(4):924–33.

198. Benchenane K, et al. (2005) Tissue-type plasminogen activator crosses the intact blood-brain barrier by low-density lipoprotein receptor-related protein-mediated transcytosis. *Circulation* 111(17):2241–9.

199. Pan W, et al. (2004) Efficient transfer of receptor-associated protein (RAP) across the blood-brain barrier. *J Cell Sci* 117(Pt 21):5071–8.

200. Chung NS, Wasan KM (2004) Potential role of the low-density lipoprotein receptor family as mediators of cellular drug uptake. *Adv Drug Deliv Rev* 56:1315–1334.

201. Stefansson S, Chappell DA, Argraves KM, Strickland DK, Argraves WS (1995) Glycoprotein 330/low density lipoprotein receptor-related protein-2 mediates endocytosis of low density lipoproteins via interaction with apolipoprotein B100. *J Biol Chem* 270(33):19417–21.

202. Boren J, et al. (1998) Identification of the low density lipoprotein receptor-binding site in apolipoprotein B100 and the modulation of its binding activity by the carboxyl terminus in

familial defective apo-B100. *J Clin Invest* 101(5):1084–93.

203. Zensi A, et al. (2009) Albumin nanoparticles targeted with Apo E enter the CNS by transcytosis and are delivered to neurones. *J Control Release* 137(1):78–86.

204. Wagner S, et al. (2012) Uptake mechanism of ApoE-modified nanoparticles on brain capillary endothelial cells as a blood-brain barrier model. *PLoS One* 7:e32568.

205. Sorrentino NC, et al. (2013) A highly secreted sulphamidase engineered to cross the blood-brain barrier corrects brain lesions of mice with mucopolysaccharidoses type IIIA. *EMBO Mol Med* 5(5):675–90.

206. Spencer B, et al. (2011) Peripheral delivery of a CNS targeted, metalo-protease reduces aβ toxicity in a mouse model of Alzheimer's disease. *PLoS One* 6(1):e16575.

207. Herweijer H, Wolff JA (2007) Gene therapy progress and prospects: hydrodynamic gene delivery. *Gene Ther* 14(2):99–107.

208. Demeule M, et al. (2008) Identification and design of peptides as a new drug delivery system for the brain. *J Pharmacol Exp Ther* 324(3):1064–72.

209. Kounnas MZ, et al. (1995) LDL receptor-related protein, a multifunctional ApoE receptor, binds secreted beta-amyloid precursor protein and mediates its degradation. *Cell* 82(2):331–40.

210. Régina A, et al. (2008) Antitumour activity of ANG1005, a conjugate between paclitaxel and the new brain delivery vector Angiopep-2. *Br J Pharmacol* 155(2):185–97.

211. Thomas FC, et al. (2009) Uptake of ANG1005, a novel paclitaxel derivative, through the blood-brain barrier into brain and experimental brain metastases of breast cancer. *Pharm Res* 26(11):2486–94.

212. Demeule M, et al. (2008) Involvement of the low-density lipoprotein receptor-related protein in the transcytosis of the brain delivery vector angiopep-2. *J Neurochem* 106(4):1534–44.

213. Angiochem (2014) Angiochem Products. Available at: http://angiochem.com/products.

214. Ke W, et al. (2009) Gene delivery targeted to the brain using an Angiopep-conjugated polyethyleneglycol-modified polyamidoamine dendrimer. *Biomaterials* 30(36):6976–85.

215. Demeule M, et al. (2014) Conjugation of a brain-penetrant peptide with neurotensin provides antinociceptive properties. *J Clin Invest*. doi:10.1172/JCI70647.

216. Stutz CC, Zhang X, Shusta E V (2014) Combinatorial approaches for the identification of brain drug delivery targets. *Curr Pharm Des* 20(10):1564–76.

217. Haqqani AS, et al. (2013) Multiplexed evaluation of serum and CSF pharmacokinetics of brain-targeting single-domain antibodies using a NanoLC-SRM-ILIS method. *Mol Pharm* 10(5):1542–56.

218. Kumar P, et al. (2007) Transvascular delivery of small interfering RNA to the central

nervous system. *Nature* 448(7149):39–43.

219. Lentz TL (1990) Rabies virus binding to an acetylcholine receptor alpha-subunit peptide. *J Mol Recognit* 3(2):82–8.

220. Liu Y, et al. (2013) Targeting caspase-3 as dual therapeutic benefits by RNAi facilitating brain-targeted nanoparticles in a rat model of Parkinson's disease. *PLoS One* 8(5):e62905.

221. Record M, Subra C, Silvente-Poirot S, Poirot M (2011) Exosomes as intercellular signalosomes and pharmacological effectors. *Biochem Pharmacol* 81(10):1171–82.

222. El Andaloussi S, Lakhal S, Mäger I, Wood MJA (2013) Exosomes for targeted siRNA delivery across biological barriers. *Adv Drug Deliv Rev* 65(3):391–7.

223. Alvarez-Erviti L, et al. (2011) Delivery of siRNA to the mouse brain by systemic injection of targeted exosomes. *Nat Biotechnol* 29(4):341–5.

224. Moos T, Morgan EH (2001) Restricted transport of anti-transferrin receptor antibody (OX26) through the blood-brain barrier in the rat. *J Neurochem* 79(1):119–29.

225. Gosk S, Vermehren C, Storm G, Moos T (2004) Targeting anti-transferrin receptor antibody (OX26) and OX26-conjugated liposomes to brain capillary endothelial cells using in situ perfusion. *J Cereb Blood Flow Metab* 24(11):1193–204.

226. Paris-Robidas S, Emond V, Tremblay C, Soulet D, Calon F (2011) In vivo labeling of brain capillary endothelial cells after intravenous injection of monoclonal antibodies targeting the transferrin receptor. *Mol Pharmacol* 80(1):32–9.

227. Alata W, Paris-Robidas S, Emond V, Bourasset F, Calon F (2014) Brain uptake of a fluorescent vector targeting the transferrin receptor: a novel application of in situ brain perfusion. *Mol Pharm* 11(1):243–53.

228. Manich G, et al. (2013) Study of the transcytosis of an anti-transferrin receptor antibody with a Fab' cargo across the blood-brain barrier in mice. *Eur J Pharm Sci* 49(4):556–64.

229. Atwal JK, et al. (2011) A therapeutic antibody targeting BACE1 inhibits amyloid-β production in vivo. *Sci Transl Med* 3(84):84ra43.

230. Bohrmann B, et al. (2012) Gantenerumab: a novel human anti-Aβ antibody demonstrates sustained cerebral amyloid-β binding and elicits cell-mediated removal of human amyloid-β. *J Alzheimers Dis* 28(1):49–69.

231. Wiley DT, Webster P, Gale A, Davis ME (2013) Transcytosis and brain uptake of transferrin-containing nanoparticles by tuning avidity to transferrin receptor. *Proc Natl Acad Sci U S A* 110(21):8662–7.

232. Mayle KM, Le AM, Kamei DT (2012) The intracellular trafficking pathway of transferrin. *Biochim Biophys Acta* 1820(3):264–81.

233. Widera A, Norouziyan F, Shen W-C (2003) Mechanisms of TfR-mediated transcytosis and sorting in epithelial cells and applications toward drug delivery. *Adv Drug Deliv Rev*

55(11):1439–66.

234. Muro S (2003) A novel endocytic pathway induced by clustering endothelial ICAM-1 or PECAM-1. *J Cell Sci* 116(8):1599–1609.

235. Papademetriou J, et al. (2013) Comparative binding, endocytosis, and biodistribution of antibodies and antibody-coated carriers for targeted delivery of lysosomal enzymes to ICAM-1 versus transferrin receptor. *J Inherit Metab Dis* 36(3):467–77.

236. Jevnikar AM, et al. (1990) Differing regulation and function of ICAM-1 and class II antigens on renal tubular cells. *Kidney Int* 38(3):417–25.

237. Boder ET, Raeeszadeh-Sarmazdeh M, Price JV (2012) Engineering antibodies by yeast display. *Arch Biochem Biophys* 526(2):99–106.

238. Tillotson BJ, Cho YK, Shusta E V (2013) Cells and cell lysates: A direct approach for engineering antibodies against membrane proteins using yeast surface display. *Methods* 60:27–37.

239. Tillotson BJ, de Larrinoa IF, Skinner CA, Klavas DM, Shusta E V (2013) Antibody affinity maturation using yeast display with detergent-solubilized membrane proteins as antigen sources. *Protein Eng Des Sel* 26:101–112.

240. Lajoie J, Herrin BR, Shusta E V (2016) Creation and screening of a blood-brain barrier immunized library yields lamprey antibodies that target the brain vasculature in vivo. *Submitted*.

241. Stynen B, Tournu H, Tavernier J, Van Dijck P (2012) Diversity in genetic in vivo methods for protein-protein interaction studies: from the yeast two-hybrid system to the mammalian split-luciferase system. *Microbiol Mol Biol Rev* 76(2):331–82.

242. Carneiro DG, Clarke T, Davies CC, Bailey D (2016) Identifying novel protein interactions: Proteomic methods, optimisation approaches and data analysis pipelines. *Methods* 95:46–54.

243. Lajoie JM, Shusta E V (2015) Targeting receptor-mediated transport for delivery of biologics across the blood-brain barrier. *Annu Rev Pharmacol Toxicol* 55:613–31.

244. Preston JE, Joan Abbott N, Begley DJ (2014) Transcytosis of macromolecules at the blood-brain barrier. *Adv Pharmacol* 71:147–63.

245. Owen DJ (2004) Linking endocytic cargo to clathrin: structural and functional insights into coated vesicle formation. *Biochem Soc Trans* 32(1):1.

246. McMahon HT, Boucrot E (2011) Molecular mechanism and physiological functions of clathrin-mediated endocytosis. *Nat Rev Mol Cell Biol* 12(8):517–33.

247. Lidinsky WA, Drewes LR (1983) Characterization of the Blood-Brain Barrier: Protein Composition of the Capillary Endothelial Cell Membrane. *J Neurochem* 41(5):1341–1348.

248. Chao G, et al. (2006) Isolating and engineering human antibodies using yeast surface display. *Nat Protoc* 1:755–768.

249. Bonifacino JS, Traub LM (2003) Signals for sorting of transmembrane proteins to endosomes and lysosomes. *Annu Rev Biochem* 72:395–447.

250. Heissler SM, Manstein DJ (2013) Nonmuscle myosin-2: mix and match. *Cell Mol Life Sci* 70(1):1–21.

251. Hein MY, et al. (2015) A Human Interactome in Three Quantitative Dimensions Organized by Stoichiometries and Abundances. *Cell* 163(3):712–723.

252. Goel M, Sinkins W, Keightley A, Kinter M, Schilling WP (2005) Proteomic analysis of TRPC5- and TRPC6-binding partners reveals interaction with the plasmalemmal Na(+)/K(+)-ATPase. *Pflugers Arch* 451(1):87–98.

253. Humphries JD, et al. (2009) Proteomic analysis of integrin-associated complexes identifies RCC2 as a dual regulator of Rac1 and Arf6. *Sci Signal* 2(87):ra51.

254. Utech M, et al. (2005) Mechanism of IFN-gamma-induced endocytosis of tight junction proteins: myosin II-dependent vacuolarization of the apical plasma membrane. *Mol Biol Cell* 16(10):5040–52.

255. Rey M, et al. (2007) Myosin IIA is involved in the endocytosis of CXCR4 induced by SDF-1alpha. *J Cell Sci* 120(Pt 6):1126–33.

256. Davis TA, Loos B, Engelbrecht A-M (2014) AHNAK: the giant jack of all trades. *Cell Signal* 26(12):2683–93.

257. De Seranno S, et al. (2006) Identification of an AHNAK binding motif specific for the Annexin2/S100A10 tetramer. *J Biol Chem* 281(46):35030–8.

258. Rezvanpour A, Santamaria-Kisiel L, Shaw GS (2011) The S100A10-annexin A2 complex provides a novel asymmetric platform for membrane repair. *J Biol Chem* 286(46):40174–83.

259. Jolly C, Winfree S, Hansen B, Steele-Mortimer O (2014) The Annexin A2/p11 complex is required for efficient invasion of Salmonella Typhimurium in epithelial cells. *Cell Microbiol* 16(1):64–77.

260. Deribe YL, et al. (2009) Regulation of epidermal growth factor receptor trafficking by lysine deacetylase HDAC6. *Sci Signal* 2(102):ra84.

261. Li J, et al. (2013) Perturbation of the mutated EGFR interactome identifies vulnerabilities and resistance mechanisms. *Mol Syst Biol* 9:705.

262. Stasi M, De Luca M, Bucci C (2015) Two-hybrid-based systems: powerful tools for investigation of membrane traffic machineries. *J Biotechnol* 202:105–17.

263. Garrido-Urbani S, et al. (2016) Proteomic peptide phage display uncovers novel interactions of the PDZ1-2 supramodule of syntenin. *FEBS Lett* 590(1):3–12.

264. Zhou Y, Zhao L, Marks JD (2012) Selection and characterization of cell binding and internalizing phage antibodies. *Arch Biochem Biophys* 526(2):107–13.

265. Pasqualini R, Ruoslahti E (1996) Organ targeting in vivo using phage display peptide libraries. *Nature* 380(6572):364–6.

266. Rangel R, et al. (2012) Combinatorial targeting and discovery of ligand-receptors in organelles of mammalian cells. *Nat Commun* 3:788.

267. Roux KJ, Kim DI, Raida M, Burke B (2012) A promiscuous biotin ligase fusion protein identifies proximal and interacting proteins in mammalian cells. *J Cell Biol* 196(6):801–10.

268. Rhee H-W, et al. (2013) Proteomic mapping of mitochondria in living cells via spatially restricted enzymatic tagging. *Science* 339(6125):1328–31.

269. Ma X, Adelstein RS (2014) The role of vertebrate nonmuscle Myosin II in development and human disease. *Bioarchitecture* 4(3):88–102.

270. Gentil BJ, et al. (2005) Specific AHNAK expression in brain endothelial cells with barrier properties. *J Cell Physiol* 203(2):362–71.

271. Ivanov AI, et al. (2007) A unique role for nonmuscle myosin heavy chain IIA in regulation of epithelial apical junctions. *PLoS One* 2(7):e658.

272. Naydenov NG, et al. (2016) Nonmuscle Myosin IIA Regulates Intestinal Epithelial Barrier in vivo and Plays a Protective Role During Experimental Colitis. *Sci Rep* 6:24161.

273. von Boxberg Y, et al. (2006) Spinal cord injury-induced up-regulation of AHNAK, expressed in cells delineating cystic cavities, and associated with neoangiogenesis. *Eur J Neurosci* 24(4):1031–41.

274. Ivanov AI, McCall IC, Parkos CA, Nusrat A (2004) Role for actin filament turnover and a myosin II motor in cytoskeleton-driven disassembly of the epithelial apical junctional complex. *Mol Biol Cell* 15(6):2639–51.

275. Yu YJ, et al. (2014) Therapeutic bispecific antibodies cross the blood-brain barrier in nonhuman primates. *Sci Transl Med* 6(261):261ra154–261ra154.

276. Silber PM, Gandolfi AJ, Brendel K (1986) Adaptation of a gamma-glutamyl-transferase transpeptidase assay to microtiter plates. *Anal Biochem* 158:68–71.

277. Alder MN, et al. (2008) Antibody responses of variable lymphocyte receptors in the lamprey. *Nat Immunol* 9(3):319–27.

278. Kumar P, et al. (2015) Macromolecularly crowded in vitro microenvironments accelerate the production of extracellular matrix-rich supramolecular assemblies. *Sci Rep* 5:8729.

279. Castaldo C, et al. (2013) Cardiac fibroblast-derived extracellular matrix (biomatrix) as a model for the studies of cardiac primitive cell biological properties in normal and pathological adult human heart. *Biomed Res Int* 2013:352370.

280. Harvey A, Yen T-Y, Aizman I, Tate C, Case C (2013) Proteomic analysis of the extracellular matrix produced by mesenchymal stromal cells: implications for cell therapy mechanism. *PLoS One* 8(11):e79283.

281. Iacopetta BJ, Morgan EH (1983) The kinetics of transferrin endocytosis and iron uptake from transferrin in rabbit reticulocytes. *J Biol Chem* 258(15):9108–15.

282. Horton JJ, Holden CA, Ward PJ, MacDonald DM, Sanderson AR (1985) Exploitation of phylogenetic distance in cell surface immune labeling: studies with beta 2-microglobulin. *J Invest Dermatol* 84(2):96–9.

283. Gassmann M, Thömmes P, Weiser T, Hübscher U (1990) Efficient production of chicken egg yolk antibodies against a conserved mammalian protein. *FASEB J* 4(8):2528–32.

284. Camenisch G, et al. (1999) General applicability of chicken egg yolk antibodies: the performance of IgY immunoglobulins raised against the hypoxia-inducible factor 1alpha. *FASEB J* 13(1):81–8.

285. Abdiche YN, et al. Assessing kinetic and epitopic diversity across orthogonal monoclonal antibody generation platforms. *MAbs* 8(2):264–77.

286. Müller MR, et al. (2012) Generation and isolation of target-specific single-domain antibodies from shark immune repertoires. *Methods Mol Biol* 907:177–94.

287. Camacho-Villegas T, Mata-Gonzalez T, Paniagua-Solis J, Sanchez E, Licea A Human TNF cytokine neutralization with a vNAR from Heterodontus francisci shark: a potential therapeutic use. *MAbs* 5(1):80–5.

288. Zielonka S, et al. (2014) Structural insights and biomedical potential of IgNAR scaffolds from sharks. *MAbs*. doi:10.4161/19420862.2015.989032.

289. Gadkar K, et al. (2016) Mathematical PKPD and safety model of bispecific TfR/BACE1 antibodies for the optimization of antibody uptake in brain. *Eur J Pharm Biopharm* 101:53–61.

290. Calderon AJ, et al. (2011) Optimizing endothelial targeting by modulating the antibody density and particle concentration of anti-ICAM coated carriers. *J Control Release* 150(1):37–44.

291. Lee J-J, et al. (2014) A high-affinity protein binder that blocks the IL-6/STAT3 signaling pathway effectively suppresses non-small cell lung cancer. *Mol Ther* 22(7):1254–65.

292. Lee S-C, et al. (2012) Design of a binding scaffold based on variable lymphocyte receptors of jawless vertebrates by module engineering. *Proc Natl Acad Sci U S A* 109(9):3299–304.

293. Hwang D-E, et al. (2016) Anti-Human VEGF Repebody Effectively Suppresses Choroidal Neovascularization and Vascular Leakage. *PLoS One* 11(3):e0152522.